INVESTIGATION OF RELATIONSHIP BETWEEN AGGREGATE SHAPE PARAMETERS AND CONCRETE STRENGTH USING IMAGING TECHNIQUES

A THESIS SUBMITTED TO
THE GRADUATE SCHOOL OF NATURAL AND APPLIED SCIENCES
OF
MIDDLE EAST TECHNICAL UNIVERSITY

BY

MURAT ÖZEN

IN PARTIAL FULFILLMENT OF THE REQUIREMENTS
FOR
THE DEGREE OF MASTER OF SCIENCE
IN
CIVIL ENGINEERING

APRIL 2007

Approval of the Graduate School of Natural and Applied Sciences

Prof. Dr. Canan ÖZGEN
Director

I certify that this thesis satisfies all the requirements as a thesis for the degree of Master of Science.

Prof. Dr. Güney ÖZCEBE
Head of Department

This is to certify that we have read this thesis and that in our opinion it is fully adequate, in scope and quality, as a thesis for the degree of Master of Science.

Assoc. Prof. Dr. İ. Özgür YAMAN
Co-Supervisor

Asst. Prof. Dr. Murat GÜLER
Supervisor

Examining Committee Members

Prof. Dr. Mustafa TOKYAY (METU, CE)

Asst. Prof. Dr. Murat GÜLER (METU, CE)

Assoc. Prof. Dr. İ. Özgür YAMAN (METU, CE)

Inst. Dr. Osman ACAR (METU, CE)

Dr. Korhan ERDOĞDU (Ash Plus Yapı Malz. San. ve Tic. A. Ş.)

I hereby declare that all information in this document has been obtained and presented in accordance with academic rules and ethical conduct. I also declare that, as required by these rules and conduct, I have fully cited and referenced all material and results that are not original to this work.

Name, Surname: Murat ÖZEN

Signature:

ABSTRACT

INVESTIGATION OF RELATIONSHIP BETWEEN AGGREGATE SHAPE PARAMETERS AND CONCRETE STRENGTH USING IMAGING TECHNIQUES

Özen, Murat
M. S., Department of Civil Engineering
Supervisor : Asst. Prof. Dr. Murat GÜLER
Co-Supervisor: Assoc. Prof. Dr. İ. Özgür YAMAN

April 2007, 152 pages

In this study, relationships between aggregate shape parameters and compressive strength of concrete were investigated using digital image processing and analysis methods. The study was conducted based on three mix design parameters, gradation type, aggregate type and maximum aggregate size, at two levels. A total of 40 cubic concrete specimens were prepared at a constant water-cement ratio. After the compressive strength tests were performed, each specimen was cut into 4 equal pieces in order to obtain the digital images of cross sections using a digital flatbed scanner. A number of aggregate shape parameters were then determined from the digital image of the cross sections to investigate their relationships with the compressive strength. The results indicted that even though the aggregate type was found to give strong correlation with the compressive strength, weak correlations, however, exist between the compressive strength and the aggregate shape parameters. The study suggested that the analyses of relationships should be further investigated by including the effects of aggregate distribution within the specimen cross sections.

Keywords: Digital Image, Concrete, Strength, Aggregate, Shape Parameters.

ÖZ

AGREGA ŞEKİL PARAMETRELERİ İLE BETON DAYANIMI ARASINDAKİ İLİŞKİNİN GÖRÜNTÜ YÖNTEMLERİ YARDIMIYLA İNCELENMESİ

Özen, Murat

Yüksek Lisans, İnşaat Mühendisliği Bölümü

Tez Yöneticisi : Yrd. Doç. Dr. Murat GÜLER

Ortak Tez Yöneticisi: Doç. Dr. İ. Özgür YAMAN

Nisan 2007, 152 pages

Bu çalışmada agrega şekil parametreleri ve beton basınç dayanımı arasındaki ilişkiler dijital görüntü işleme ve analizi metotları kullanılarak incelenmiştir. Bu çalışma iki seviyede üç karışım dizayn parametresi kullanılarak gerçekleştirilmiştir. Bu parametreler sırasıyla gradasyon tipi, agrega tipi ve maksimum agrega çapıdır. Toplam 40 adet kubik beton numunesi su-çimento oranı sabit tutularak hazırlanmıştır. Her bir numune kesit yüzeylerinin dijital görüntülerinin elde edilmesi amacıyla basınç dayanımı testinden sonra 4 eşit parçaya kesilmiştir. Bu dijital görüntülerden, basınç dayanımı ile olan ilişkilerinin incelenmesi amacıyla bir çok agrega şekil parametresi hesaplanmıştır. Elde edilen sonuçlara göre, agrega tipi ve basınç dayanımı arasında güçlü bir korelasyon görülmesine karşın, agrega şekil parametreleri ve basınç dayanımı arasında zayıf korelasyonlar bulunmuştur. Bu çalışma agrega şekil parametreleri ve beton dayanımı arasındaki ilişkilerin agregaların numune kesit yüzeyi içerisindeki dağılımlarının yaratacağı etkilerin de göz önüne alınarak tekrar incelenmesini önermektedir.

Anahtar Kelimeler: Dijital Görüntü, Beton, Dayanım, Agrega, Şekil Parametreleri.

To My Family

ACKNOWLEDGMENTS

I would like to express my gratitude to my supervisor Asst. Prof. Dr. Murat GÜLER and co-supervisor Assoc. Prof. Dr. İ. Özgür YAMAN for their guidance, advice, criticism, encouragement and insight throughout this research and preparation of the thesis.

This work owes endless thanks to my family for their support and encouragement during my thesis study.

I would like to expand my thanks to Mr. Hasan KESER for his advice during preparation of the thesis.

Thanks are also due to Construction Laboratory and Transportation Laboratory stuff for their assistance with laboratory work.

And last but not least, I am also grateful to Mrs. Özgül ULUTAŞ for her help, support and motivation throughout this study.

TABLE OF CONTENTS

LIST OF TABLES

TABLE

LIST OF FIGURES

FIGURES

CHAPTER 1

INTRODUCTION

1.1 Background

Aggregate particles occupy approximately 70 to 80% volume of concrete and hence their characteristics significantly affect the performance of both fresh and hardened concrete. Aggregates have also an impact on the cost effectiveness of concrete, as they are one of the inexpensive components of a typical portland cement concrete. Past experiences indicate that while aggregate overall shape characteristics, surface texture and its particle size distribution influence the workability, pumpability, bleeding, finishability and segregation resistance of fresh concrete, they also affect strength, stiffness, shrinkage, density, creep, durability and permeability of hardened concrete (Mindess et al., 2003; Quiroga and Fowler, 2003).

Previous studies showed that there is an obvious relationship between overall shape, surface texture, gradation and the packing characteristics of aggregates in a certain volume. Generally, flaky, elongated, angular and poorly graded particles result in looser packing hence larger inter-particle voids (Dewar, 1999).

As aggregate overall shape characteristics and surface texture have significant effects on the properties of concrete, it becomes necessary that the shape properties should be efficiently measured and evaluated. The measurement of aggregate shape properties can be achieved either by direct or indirect means.

For instance, geologists developed a sophisticated system that involves physical measurements of aggregates, however, the methods used by engineers rest mainly on visual classification and index tests for overall shape, angularity and surface texture. It should be emphasized that none of the index tests developed by engineers can separately quantify the overall shape, angularity and surface texture. Generally, these characteristics are grouped together as geometric irregularities (Janoo, 1998).

Recently, researchers have started using digital imaging processing (DIP) techniques for automated aggregate shape characterization. Digital imaging techniques can be used to investigate particles' shape at different scales. They can offer powerful tools to distinguish among different shape properties and to quantify a number of geometric and distribution specific variables that are effective for the properties of concrete. According to Das (2006) the DIP methods have the following advantages:

- It is a rapid method that can be applied in real-time for quality control in aggregate quarries and sieving plants,
- Since it is an automated method, it is free from subjectivity associated with human errors,
- Since a large number of aggregates can be evaluated in one time, the statistical reliability is generally enhanced,
- With the application of this technique, various geometrical features of aggregates, i.e., area, perimeter, cross section, perimeter of ellipses or rectangles with equivalent areas, convex perimeters, particle count, size distribution, shortest and longest dimensions, orientation which may not be easily measured by physical means can be analyzed.

1.2 Research Objectives and Scope

In this study, it is hypothesized that the compressive strength of hardened concrete is affected by the shape parameters of aggregates. To prove the proposed hypothesis, an experimental program was performed, based on laboratory testing of 40 cubical concrete specimens. The specimens were prepared in 5 replicates for two maximum aggregate size levels (1 in. and $\frac{1}{2}$ in.), two gradation types (well gradation and gap gradation), and two aggregate types (crushed and natural) obtained from the same source. Thus, a total of 8 concrete mixtures and 40 specimens were prepared. The fresh state properties that were determined are the slump and the unit weight of concrete mixes. The hardened state property that was tested is the compressive strength. After the compressive strength tests, each specimen was cut into 4 pieces of equal thickness parallel to the applied load direction. This process resulted in 6 cross sectional surfaces for each specimen. The gray color digital pictures of these surfaces were obtained by utilizing a digital flatbed scanner at 150 dpi resolution level. Subsequently, only 3 images within the non-overlapping cut planes were selected to determine various aggregate shape parameters of each specimen. Finally, statistical analysis of variance was conducted to determine the effects of design variables on the compressive strength of the concrete specimens. Statistical analyses of relationships between the shape parameters of aggregates and the compressive strength were also investigated.

The layout of the study presented in this thesis is given as follows: In Chapter 2, the scope of digital image processing is presented. In Chapter 3, a summary of literature survey on the computer based aggregate shape characterization methods is given and a discussion of aggregate shape parameters and their effects on performance of fresh and hardened concrete are presented. Chapter 4 presents the experimental program and the procedures used for testing laboratory specimens. Chapter 5 summarizes the procedures used for determining aggregate shape parameters and statistical analysis methods to investigate possible relationship between concrete strength and the measured shape parameters.

In Chapter 6, the effects of experimental design parameters on the compressive strength are presented and possible relationships between particle shape parameters and the compressive strength were demonstrated. Finally, the findings of the investigation and suggestions for further studies are presented in Chapter 7.

CHAPTER 2

DIGITAL IMAGE PROCESSING

2.1 Introduction

Gonzalez and Woods (2001) define image as a two dimensional function f(x,y) where x and y are the spatial coordinates within the image frame. The amplitude of f at any pair of coordinates (x,y), is called intensity or gray level of the image at that point.

A digital image differs from a continuous image in that both spatial coordinates and amplitude of f(x,y) are discrete. Thus, an image function, f(x,y), must be digitized in both spatial domain and amplitude levels in order to be converted into a digital form before processing by computer. Digitization of the spatial coordinates, x and y, is called image sampling and amplitude digitization is called gray level quantization (McAndrew, 2004; Efford, 2000).

Figure 2.1 illustrates how a rectangular array of numbers can represent a physical image. The physical image is divided into regions called picture elements, or pixels. The most common subdivision scheme is the rectangular sampling grid as shown in Figure 2.1. The image is divided into horizontal lines of adjacent pixels. The number inserted into the digital image at each pixel location reflects the brightness of the actual image at the corresponding point. This conversion process is called digitization, and a common form is illustrated in Figure 2.2. At each pixel location, the brightness of the image is sampled and quantized. This step generates, for each pixel, an integer representing the brightness or darkness of the image at that point. When it is done for all pixels, the image is represented by a rectangular array of integers.

Each pixel has an integer location and an integer value called gray level or intensity. This array of digital data can be utilized for processing the image through computers (Castleman, 1996).

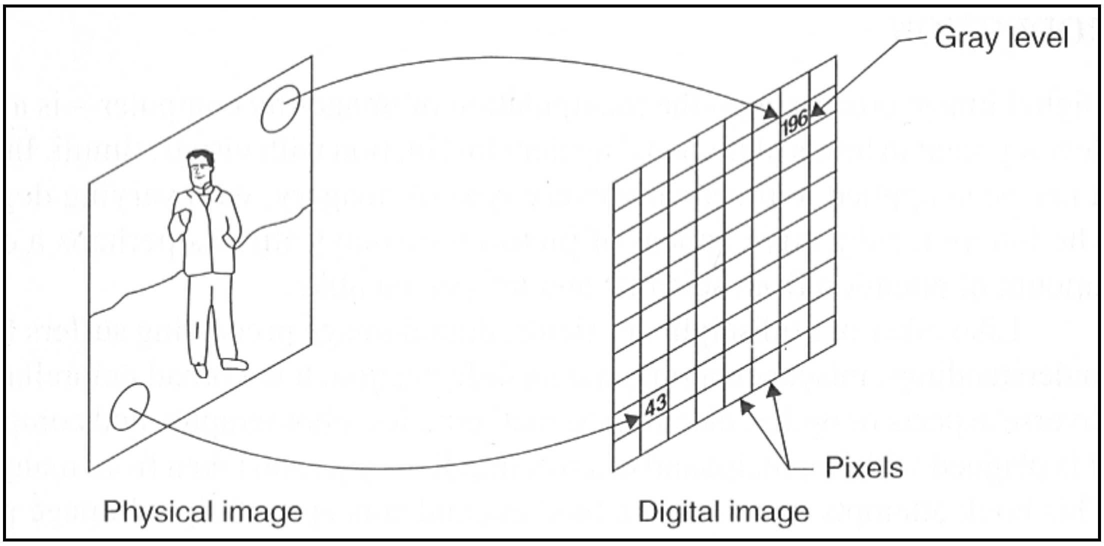

Figure 2.1 A physical image and its corresponding digital image (After Castleman, 1996).

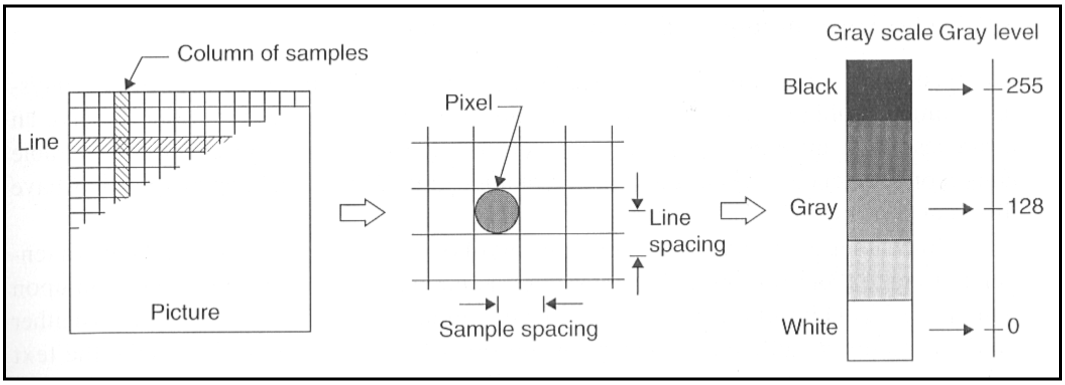

Figure 2.2 Digitizing an image (After Castleman, 1996).

According to Castleman (1996), the restricted definition of digital image is that, *digital image is sampled, quantized function of two dimensions that has been generated by optical means, sampled in an equally spaced rectangular grid pattern, and generated in equal intervals of amplitude.* Thus, a digital image can be considered as a two dimensional array of quantized sample values.

Figure 2.3 illustrates the coordinate convention used for representing the digital images. As seen in the figure, the same notation is used as for matrices. The first index, m, and the second index, n, are used to denote the position of row and column of a pixel, respectively. If the image sampled into M rows and N columns, the digital image contains M x N pixels and called the image of size of M x N. Generally, the position of the first element of the array is denoted by (m,n) = (0,0) and the index of row, m, ranges from 0 to M-1, and the index of column, n, from 0 to N-1 (Jähne, 2005).

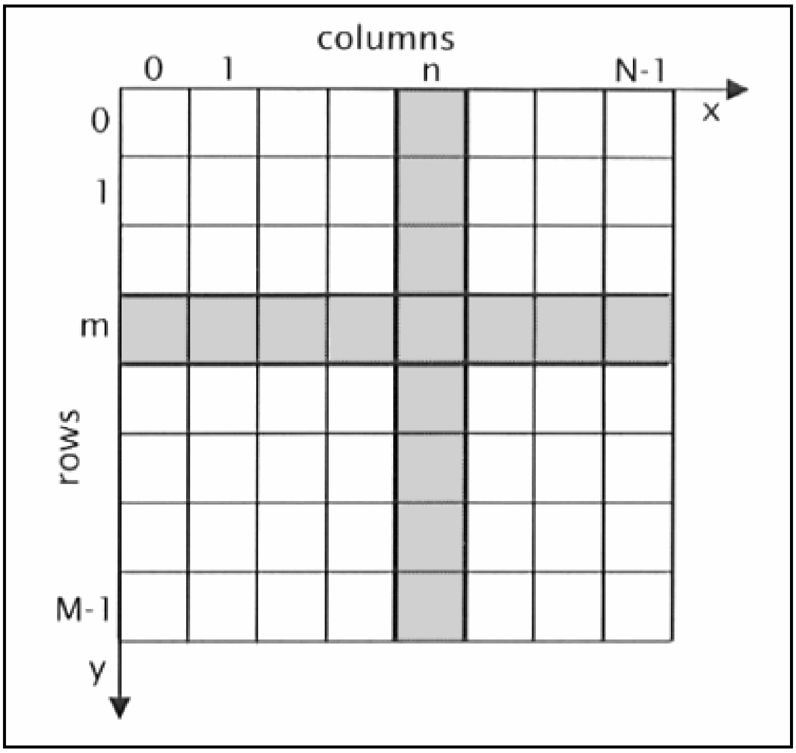

Figure 2.3 Representation of digital image by arrays of discrete points on a rectangular grid (Jähne, 2005).

The area represented by a single pixel is called spatial resolution. Figure 2.4 shows an identical image represented with a different number of pixels. Figure 2.4(a) shows a 1024 x 1024, 256 level digital image of a rose. Figures 2.4(b-f) show the results of reducing the spatial resolution from N = 1024 to N = 512, 256, 128, 64, and 32, respectively. As seen from Figure 2.4(a), and Figure 2.4(b), dense sampling points produces a high resolution image in which there are many pixels, each representing relatively smaller area of the picture. It is almost impossible to tell whether these two images are visually apart and the level of details lost by reducing the spatial resolution is not discernible at the selected scales. On the other hand, as shown in Figure 2.4(c-f), coarse sampling produces low resolution image in which there are relatively fewer number of pixels, each represents relatively large spatial area. In the case of low resolution, pixel edges start to appear and cause checkerboard effect. As it is noticed, the 256 x 256 image in Figure 2.4(c) shows fine checkerboard pattern in the edges and more pronounced graininess throughout the image. These behaviors are more visible in the 128 x 128 image in Figure 2.4(d), and they become completely noticeable in the 64 x 64 and 32 x 32 images in Figure 2.4(e) and Figure 2.4(f), respectively (Gonzalez and Woods, 2001).

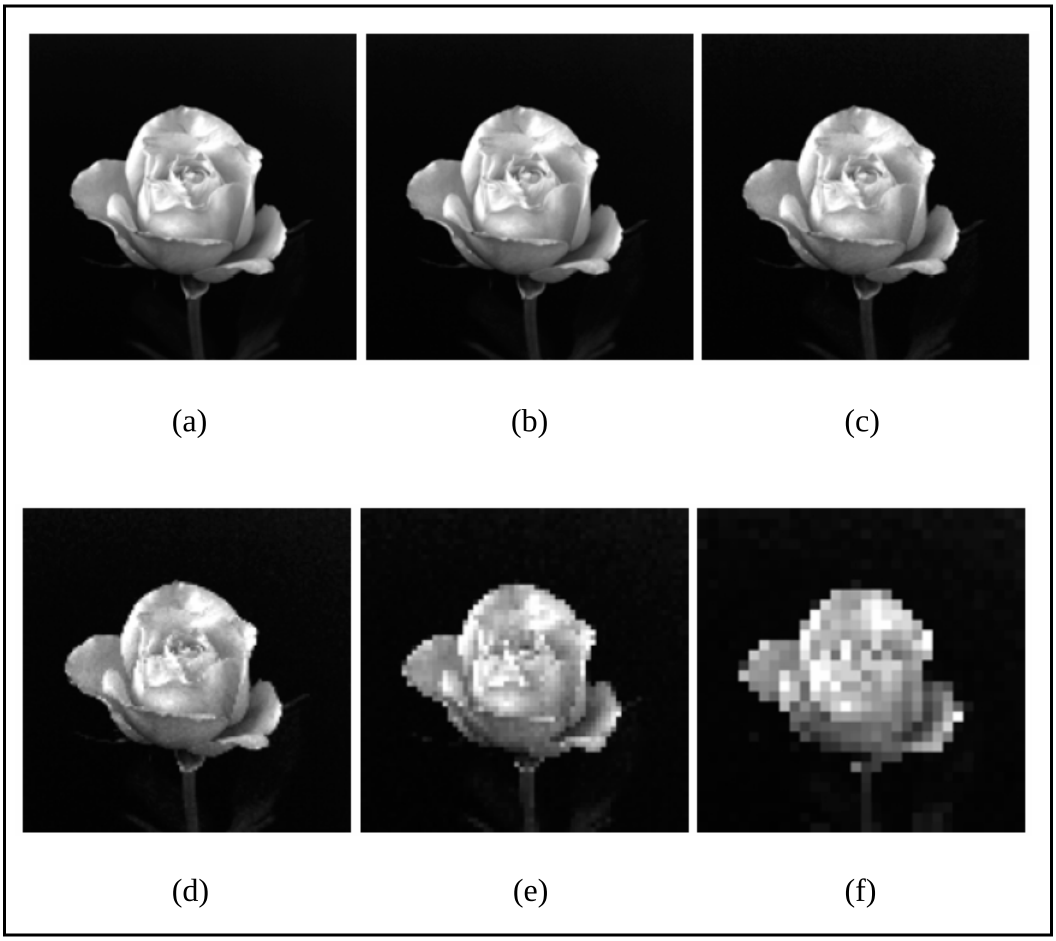

Figure 2.4 Effects of reducing spatial resolution (After Gonzalez and Woods, 2001).

As stated previously, the process of transforming the continuous image function, f(x,y) into a digital equivalent is called gray level quantization. The more quantization level is used, the more accuracy is obtained to reflect variations in the image function, f(x,y). The number of gray levels used to represent brightness of each pixel is determined as follows:

$$n = 2^{b} \tag{2.1}$$

where n = the number of quantization levels; b = the number of bits allocated to store each pixel.

The number of n quantization levels includes the integers 0, 1, 2, ..., n-1, in which 0 represents the black and n-1 represents the white. In general, each pixel is stored by 8 bits, but some 4 and 6 bits per pixels are also used by some systems. In case of 8 bits, 256 quantization levels ranging from 0 (black) to 255 (white) is used. The number of bits required to store a digitized image is computed by Equation 2.2.

$$b = nMN \tag{2.2}$$

where b = the number of bits to store a digitized image; M and N = the number of rows and columns in the digitized image, respectively (Efford, 2000).

Figures 2.5 illustrate the effect of reducing the number of bits used to represent the number of quantization levels in an image. Figure 2.5(a) shows the 452 x 374, 8 bit original image used in the preceding discussion. Figure 2.5(b–h) shows the effects of reducing number of bits from 7 to 1, while keeping the spatial resolution constant. The 256, 128, and 64 level images are visually identical for all practical purposes. However, the 32 level image shown in Figure 2.5(d) has almost imperceptible set of very fine structures in areas of smooth gray levels particularly in the skull that start to appear. This effect caused by the use of insufficient number of gray levels in smooth areas of the images, is called false countering. False countering has more pronounced effect in images displayed using 16 or less uniformly spaced gray levels and makes it very difficult to recognize objects that show slow spatial variation in gray values, as the images in Figure 2.5(e) through Figure 2.5(h) show (Gonzalez and Woods, 2001).

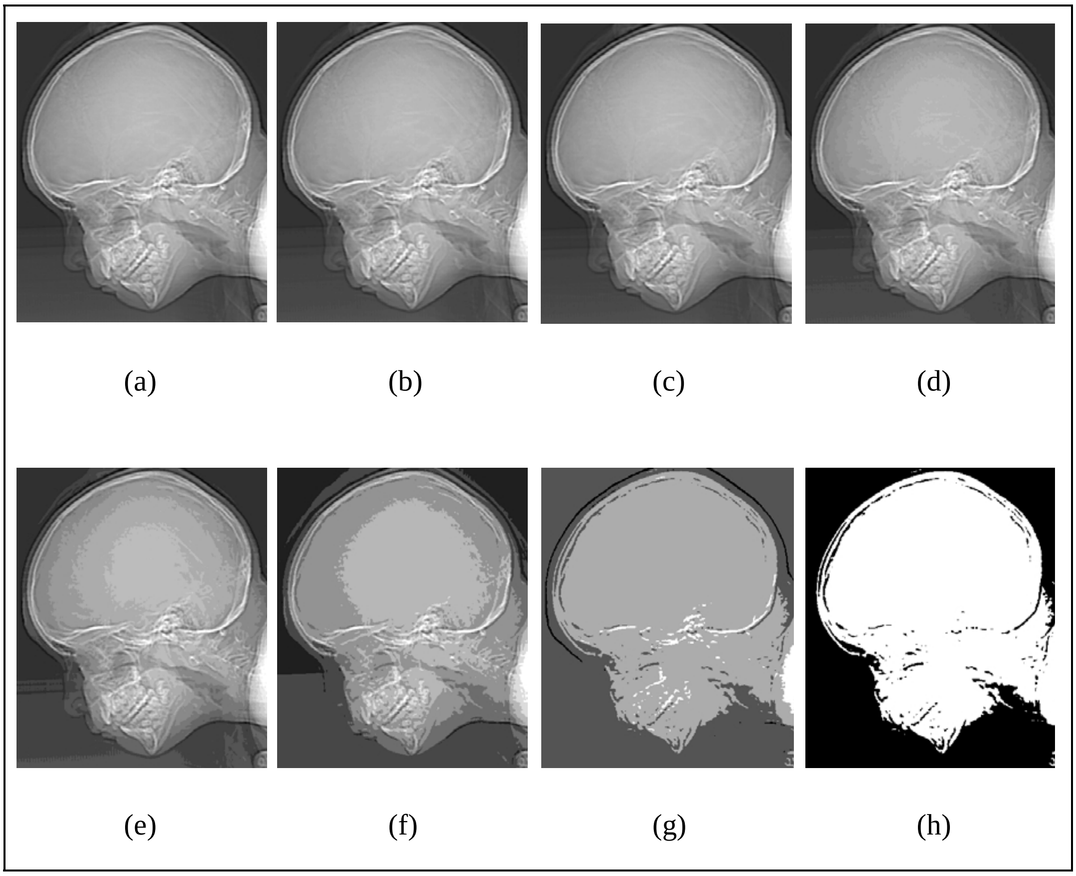

Figure 2.5 A 452 x 374 image displayed in 256, 128, 64, 32, 16, 8, 4 and 2 levels, respectively (After Gonzalez and Woods, 2001).

2.2 Terminology of Digital Image Processing

The term “processing” refers to act of subjecting to a process. A process is a series of operations or actions performed upon an object in order to achieve the desired result. Therefore, digital image processing can be defined as subjecting a digital image to a series of operations in order to obtain a desired result. In case of pictures, the processing changes their form to make them more desirable or attractive, or to achieve some other predefined goals (Castleman, 1996).

Efford (2000) defines the digital image processing as the series of operations performed in order to modify and manipulate the nature of images. The principal application areas of the digital image processing comprise the improvement of the pictorial information of images for human interpretation or processing the image data for autonomous computer perception (McAndrew, 2004). For instance, in Figure 2.6(a), a car is shown with an unreadable number plate and blurred details. However, after application of logarithmic contrast enhancement the number plate and details become more visible, as shown in Figure 2.6(b).

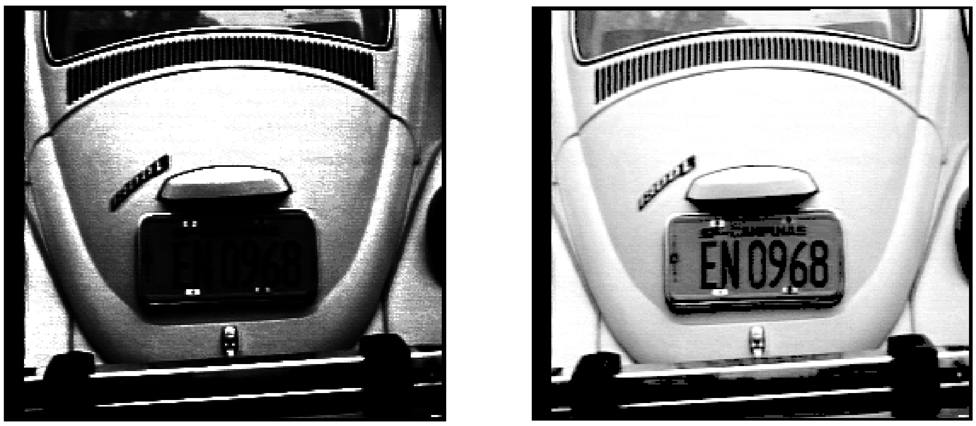

(a) (b)

Figure 2.6 Contrast enhancement. (a) Image of car with unreadable number plate. (b) Result of logarithmic contrast enhancement (After Lerner, 2005).

Digital image processing starts with one image and produces a modified version of the same image. It is, therefore, a process that transforms an input image into an output image. Digital image analysis refers to a process through which a desired information is derived from a digital image, such as a set of measurement data or a decision. For example, if a digital image contains a number of objects, a program might analyze the image and extract the measurements of the objects. However, the term digital image processing is loosely used to cover both image processing and analysis (Castleman, 1996).

2.3 Application Areas of Digital Image Processing

The rapid developments in the computer technology have provided the implementation of the digital image processing and analysis techniques in diverse range of fields like material science, agriculture, industry, and law enforcement. Figure 2.7 illustrates some of the emerging application areas of the digital image processing.

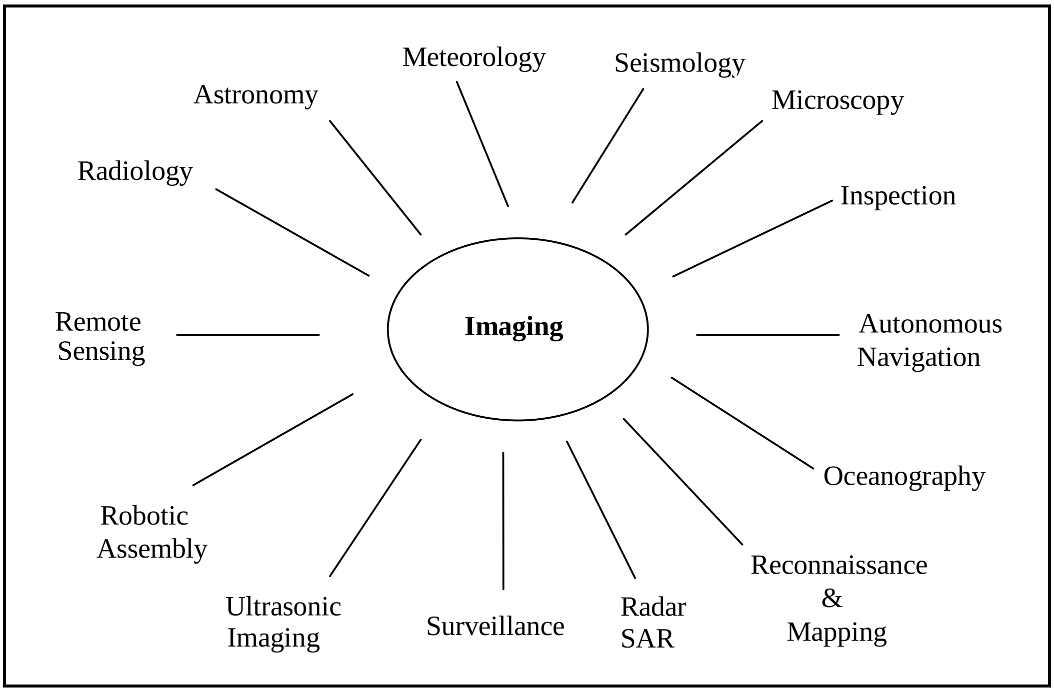

Figure 2.7 Emerging application areas of digital image processing (After Shah, 2005).

In civil engineering, digital image processing have been implemented in the detection and analysis of pavement distress, study of microstructure of concrete, assessment of structural conditions, sediment transport in streams, soil deformation, particle size distribution and particle shape analysis. In previous years, manual and time consuming procedures were used to perform the aforementioned applications; however, with the help of imaging techniques, these are now being carried out more efficiently and precisely (Kwan et al., 1999).

Digital image processing has also been utilized to quantify the spatial and directional distributions of granular material microstructure. These distributions are used to develop computer simulations of the microstructure and to compare their response to experimental measurements. Another application of the imaging techniques is to measure displacements and strain localization of civil engineering materials using geometrical correlations between the undeformed and deformed microstructures. The advantage of this approach is to conduct the measurements without taking any contact with the materials under consideration. These measurements can be used in the verification of model predictions and to obtain material properties to be used in theoretical models (Masad et al., 2004).

These examples show that the continuing progress in the computer technology will encourage new application fields for imaging techniques in civil engineering and material science.

2.4 Fundamental Steps of Digital Image Processing

Figure 2.8 shows the fundamental steps of digital image processing to produce a result from a problem domain. These steps are image acquisition, preprocessing, segmentation, representation and description, and, recognition and interpretation, respectively. In the below sections, each operation is discussed briefly.

As shown in Figure 2.8, knowledge about a problem domain is coded into an image processing system from a knowledge database. This knowledge could be as simple as detailing regions of an image where the information of interest is known, therefore, limiting the search efforts for the desired information. The knowledge base could be also quite complex, such as an interrelated list of all major possible defects in a materials inspection problem or an image database containing high resolution satellite images of a region in connection with the change detection applications (Gonzalez and Woods, 2001).

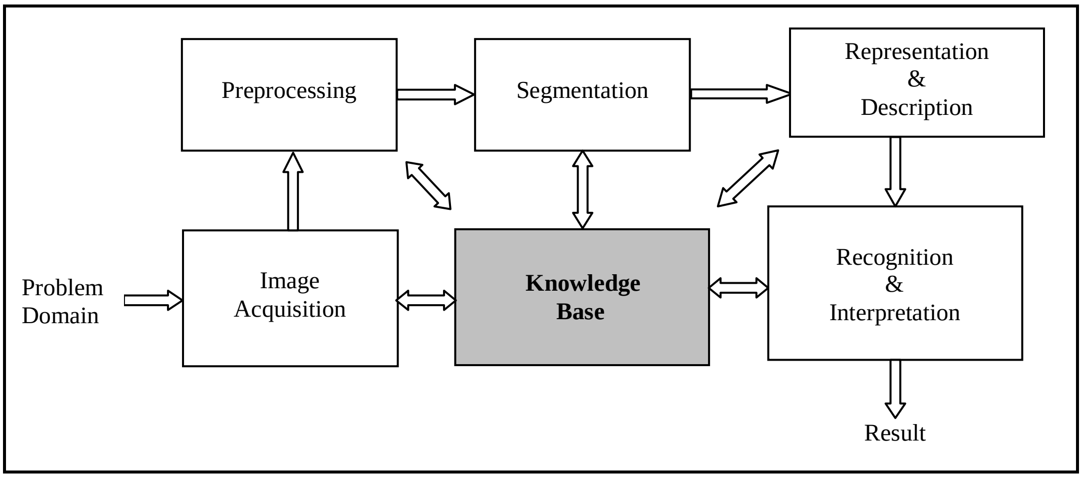

Figure 2.8 Fundamental steps in digital image processing (After Gonzalez and Woods, 1992).

2.4.1 Image Acquisition

Image acquisition is the first step to transform a scene into a digital form that can be processes by a computer. The image acquisition requires two essential components: an image acquisition system called an imaging sensor and a frame grabber which digitizes the signal produced by the sensor (Gonzalez and Woods, 2001).

The image acquisition system could be a CCD camera or a flatbed scanner. CCD stands for "charge-coupled device". Figure 2.9 shows the architecture of a simple full frame CCD. A CCD sensor is an array of light sensitive imaging elements or photosites manufactured from silicon. Each photosite produces electrical charge proportional to the light intensity and the time of incident illumination falling on it. Colors are obtained by red, green and blue filters. In addition, each photosite has a capacity of about 10^6 charge carriers which is the upper limit for the brightness of the object to be captured. CCDs are preferred for most of the digital cameras, as they can achieve high resolution and produce very good results without being effected from noise and geometric distortions (McAndrew, 2004; Efford, 2000).

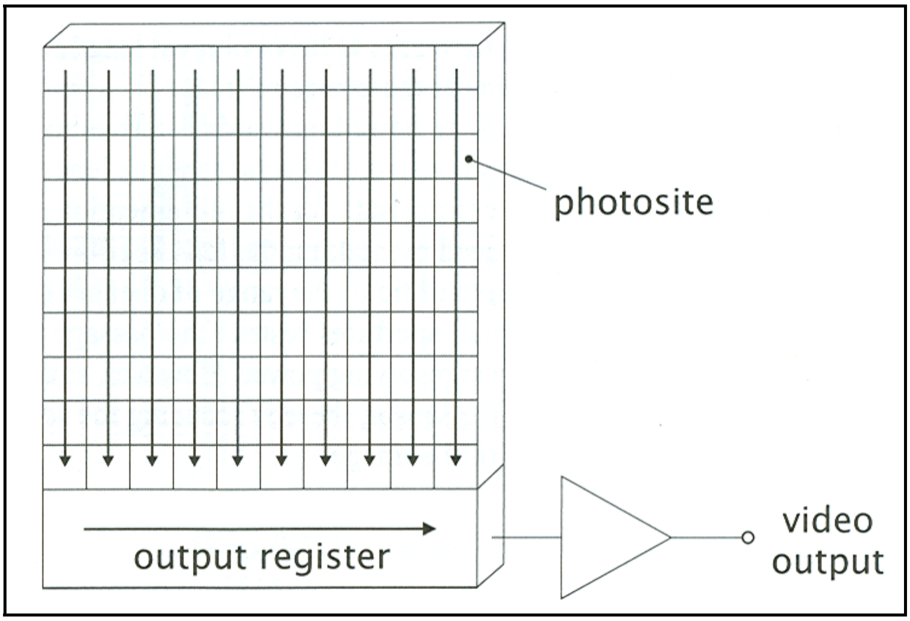

Figure 2.9 Architecture of a CCD sensor (After Efford, 2000).

The imaging sensor could also be a line-scene camera that produces a single image line at a time. In this case, single row of photosites is moved across the image, capturing it row by row as it moves through the image, instead of capturing the entire image at once on a large array. This process is schematically shown in Figure 2.10 (McAndrew, 2004).

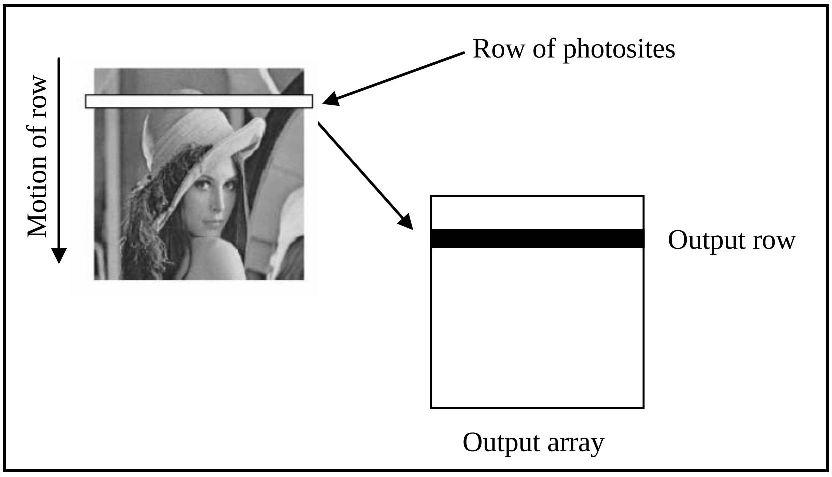

Figure 2.10 Capturing an image with a CCD scanner (After McAndrew, 2004).

The device frame grabber converts the electrical signal produced by the imaging sensor into a digital image that can be stored and processed by the computer. Today, computers do not require any special hardware for image display and processing. Gray scale image with 256 intensity level (8 bit) and true colors images with about 16 million colors (3 channels with 8 bits for each) can be displayed with inexpensive PC graphic display systems. Consequently, modern frame grabber devices do not require a specialized image display unit. It only needs circuits to digitize the electrical signal sent from the imaging sensor and store it in the memory of the computer (Jähne, 2005).

2.4.2 Preprocessing

After an image has been obtained, the next step is to preprocess the image. The key function of preprocessing is to improve the image so that further processing applications can be successfully implemented. The preprocessing operations may involve enhancement of the specific image features, noise removal, or elimination of the image features which are not related to the region of interest operations (Gonzalez and Woods, 2001).

2.4.3 Segmentation

Segmentation subdivides an image into its constituent regions or object. Generally, autonomous segmentation is one of the difficult tasks in the digital image processing applications. Segmentation operation produces a binary image in which the object pixels are represented by 1 and the others by zero. After segmentation, it is known which pixel belongs to object of interest. As the image is parted into regions, the discontinuities of the boundaries between regions can be recognized. After segmentation, shape of the object can also be analyzed (Jähne, 2005).

Gray level thresholding is the one of the most important approaches to image segmentation. The simplest gray level thresholding can be implemented by partitioning the image histogram by using threshold value, T, or values, T_1, T_2, T_3, ..., T_n, as illustrated in Figure 2.11. Segmentation is carried out by scanning the image pixel by pixel and labeling each as object or background depending on whether the gray level is greater or less than the selected threshold value(s). Consequently, the success of gray level thresholding depends entirely on how well the histogram is partitioned.

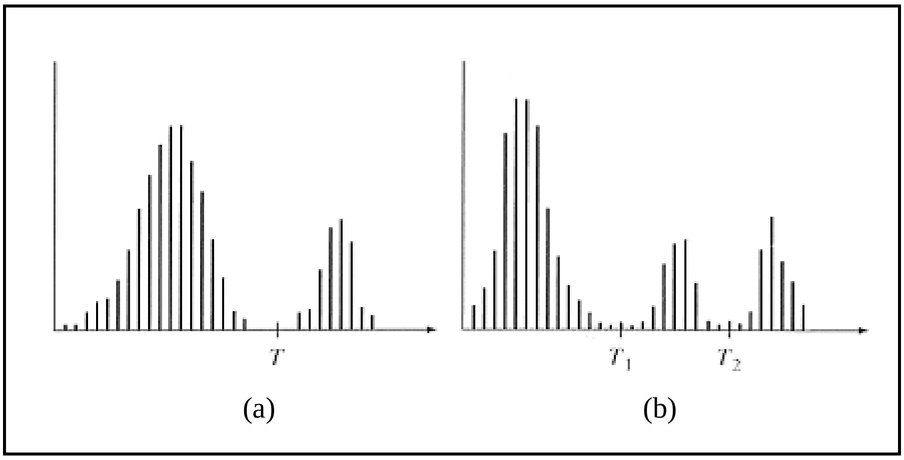

Figure 2.11 Gray level histograms that can be partitioned by (a) single threshold and (b) multiple thresholds (After Gonzalez and Woods, 2001).

For the images with bimodal histograms (i.e. with two major modes, Figure 2.11(a)), single threshold, T, can be selected for separating the existing modes. The thresholded image is then:

$$g(x,y) = \begin{cases} 0, & f(x,y) < T \\ 1, & f(x,y) \geq T \end{cases} \tag{2.3}$$

where T = selected global threshold value; g(x,y) = binary level of point (x,y) in the segmented image; f(x,y) = gray level of point (x,y) in the original image.

For images with three and more dominant modes as shown in Figure 2.11(b), multilevel thresholding approach may be performed. This approach uses two or more thresholding values, T_1, T_2, T_3, ..., T_{n-1}. In this case, the thresholded image becomes:

$$g(x,y) = \begin{cases} 0, & f(x,y) < T_1 \\ 1, & T_1 \leq f(x,y) < T_2 \\ 2, & T_2 \leq f(x,y) < T_3 \\ 3, & T_3 \leq f(x,y) < T_4 \\ . & . \\ . & . \\ n-1, & T_{n-1} \leq f(x,y) < T_n \end{cases} \tag{2.4}$$

where n = number of modes; T_n = maximum gray level value and f(x,y) is the gray level of point (x,y) in the original image.

If the image consists of two types of light objects on the dark background, Equation 2.4 classifies the image as belonging to the first object class if $T_1 \leq f(x,y) < T_2$, to the other object class if $f(x,y) > T_2$, and to the background if $f(x,y) < T_1$ (Figure 2.11(b)).

However, multilevel thresholding approach has less accuracy than the single thresholding, since it is difficult to select thresholding values especially if the image consists of more than three major modes (Gonzalez and Woods, 2001).

2.4.4 Representation and Description

The output of the segmentation step generally is row pixel data consisting either the boundary or the region-wise information of the selected region of interest. In the representation and description phase, the row data is generally converted into a suitable form to derive specific characteristics of image through further processing.

The first decision that must be made is whether the data should be represented as a boundary, or as a complete region. Boundary representation focuses on external shape characteristics, such as corners and inflections. Regional representation focuses on internal characteristics, such as color and texture. Sometimes both external and internal representations are used together in character recognition applications, which often require algorithms based on boundary shape as well as skeletons and other internal properties.

Choosing a representation scheme is only the first step of the necessary tasks for making the data usable by computer. The next step is the description of the data based on the chosen representation so that objects of interest are highlighted. Description is also called feature selection and copes with extracting features that result in some quantitative information of interest or features that are basic for differentiating one class objects from another. For instance, the region represented by its boundary may be described by features such as its length, orientation of the straight line joining its extreme points or the number of concavities it contains (Gonzalez and Woods, 2001).

2.4.5 Recognition and Interpretation

Recognition is the process of assigning a label to an object based on the information provided by its descriptors. Interpretation involves assigning meaning to an ensemble of the recognized objects (Gonzalez and Woods, 2001).

2.5 Color Models for Digital Images

2.5.1 True Color or RGB

RGB stands for Red-Green-Blue and indicates that each pixel is represented by a red, green and blue level. The RGB color model can be represented by a cartesian coordinate system as shown in Figure 2.12. Each axis of the cube denotes the values of red, green, or blue in the range of 0 to 255. The red, green and blue axes, labeled as R, G, B, show the associated color scales.

The origin of the cube, or 0^R 0^G 0^B, corresponds to the total absence of color, which is a full black. The far corner from the origin is the sum of the highest intensities of red, green, and blue, or 255^R 255^G 255^B which produces a full white color.

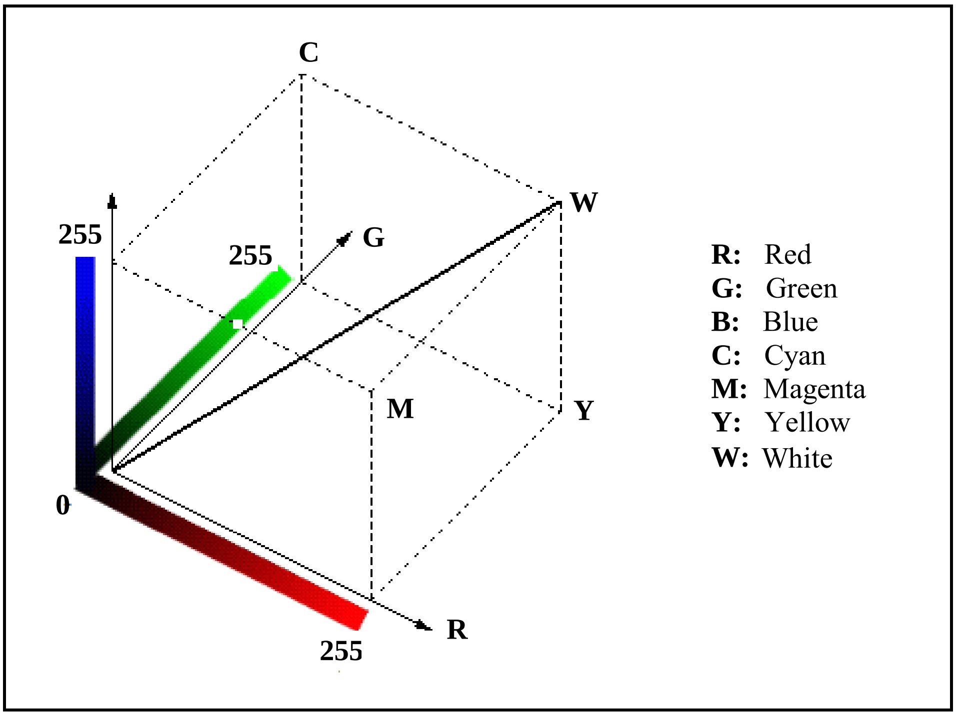

Figure 2.12 The RGB color cube (After Gimp-Savvy.com, 2006).

The corners of the cube correspond to red, green, blue, and their complementary colors, cyan, magenta, and yellow, respectively. The colors act like vectors and can be combined by addition and subtraction to obtain other colors. From Figure 2.12, it is seen that adding 255 red to 255 green makes $255^R\ 255^G\ 0^B$ or yellow, adding 255 red to 255 blue makes $255^R\ 0^G\ 255^B$ or magenta, and adding 255 green to 255 blue makes $0^R\ 255^G\ 255^B$ or cyan.

As shown in Figure 2.13, a RGB image can be considered as a stack of three matrices representing the red, green, and blue values for each pixel. This means that for every pixel, there are three corresponding color values.

RGB images are also called 24 bit color images, since each of the three components (red, green, blue) is quantized using 8 bits. Therefore, more than 16 million (256 x 256 x 256) colors are available in a 24-bit image (Gimp-Savvy.com, 2006).

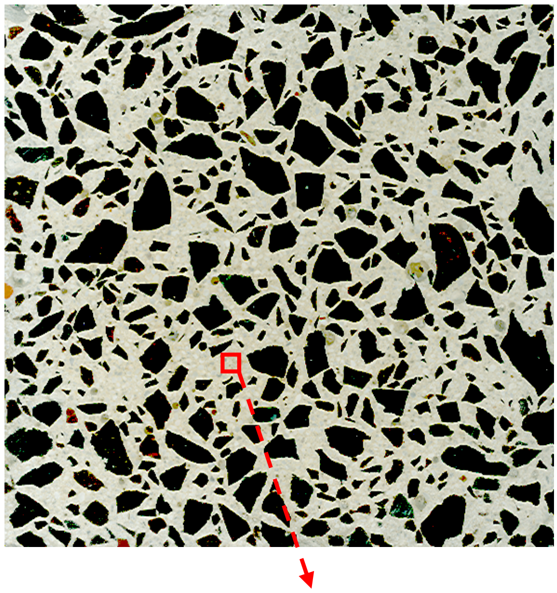

Pixel values in highlighted region

161	161	170	162	167
164	156	160	161	160
171	163	154	152	151
167	163	158	155	148
177	162	158	154	155

Red

157	156	163	15	161
159	152	153	154	153
164	153	149	150	146
164	158	154	149	142
177	147	153	174	151

Green

68	59	89	2	86
63	25	38	40	14
134	125	49	52	13
152	51	62	42	5
163	109	44	15	50

Blue

Figure 2.13 A true color (RGB) image.

2.5.2 Gray Scale

Gray scale model is represented by the main diagonal of the RGB cube as illustrated in Figure 2.12 through the line drawn between the origin (0, 0, 0) and the farthest corner (255, 255, 255). This line represents the colors in the RGB cube that consist of equal amounts of red, green, and blue. All the points on this line are the shades of gray colors. The closer to the origin, the darker the gray level and the closer to the farthest corner, the lighter the gray level. The range between 0 and 255 means that each pixel is represented by 8 bits, or exactly 1 byte. Figure 2.14 represents a gray scale image.

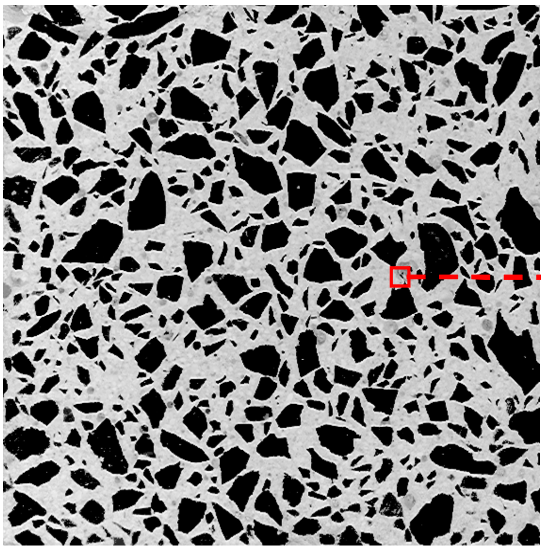

Pixel values in highlighted region

180	173	194	241	171
208	197	194	210	194
179	173	195	200	225
141	131	201	203	215
199	194	205	232	212

Figure 2.14 A gray scale image.

2.5.3 Binary

Binary model consists of pixels that are quantized using only two values 0 and 1, or often 0 and 255, representing the full black and the full white colors, respectively. Since there are only two possible values for each pixel, it requires 1 bit per pixel. Binary images can therefore be very efficient in terms of storage and processing. Images for which a binary representation may be suitable include fingerprints, architectural plans and printed or handwriting texts (McAndrew, 2004).

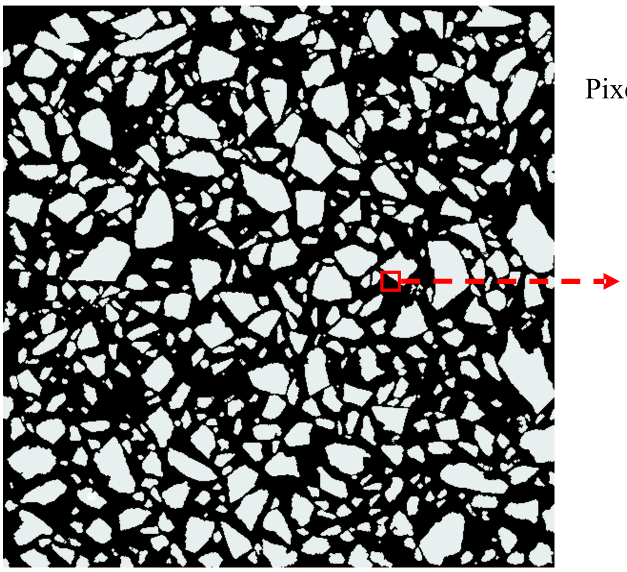

Pixel values in highlighted region

0	1	1	1	1
0	0	1	1	1
0	0	0	1	1
0	0	0	0	1
0	0	0	0	0

Figure 2.15 A binary image.

CHAPTER 3

LITERATURE REVIEW

3.1 Introduction

This chapter presents a review of literature on the definition of aggregates shape parameters and computer based particle shape characterization methods used in digital image analysis. Effects of aggregate shape and texture, gradation, and maximum aggregate size on properties of fresh and hardened portland cement concrete are also discussed.

3.2 Fundamental Particle Geometry Measurements

Area, perimeter, feret diameters and pixel coordinates are the fundamental particle shape properties measured by most of the image analysis systems. The particle area, perimeter, and feret diameters are classified as the size measurements, whereas the pixel coordinates fall into the group of position measurements (Kuo and Freeman, 2000). Figure 3.1 illustrates the geometry of an aggregate cross section in plane Cartesian coordinates. As shown in the figure, the major axis of aggregate cross section connects the two points which are the farthest apart on the boundary of the aggregate cross section, and corresponds closely to the particle length. Major axis is also commonly termed as the maximum Feret diameter (e.g. Russ, 1999). The minor axis is the longest line that can be drawn from one boundary point to another so as to be perpendicular to the major axis, and corresponds to the particle width (Yue, 1995).

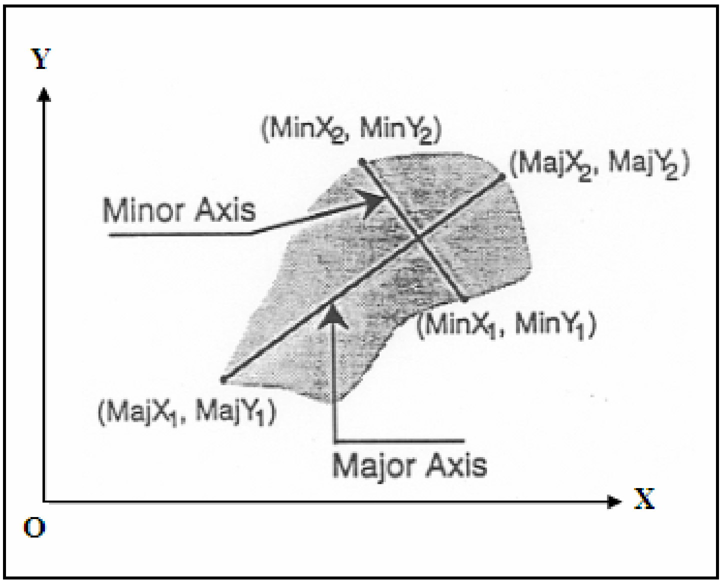

Figure 3.1 An aggregate cross section in plane Cartesian coordinates (After Yue, 1995).

In image analysis, area of a particle is the summation of pixels present within the aggregate boundary.

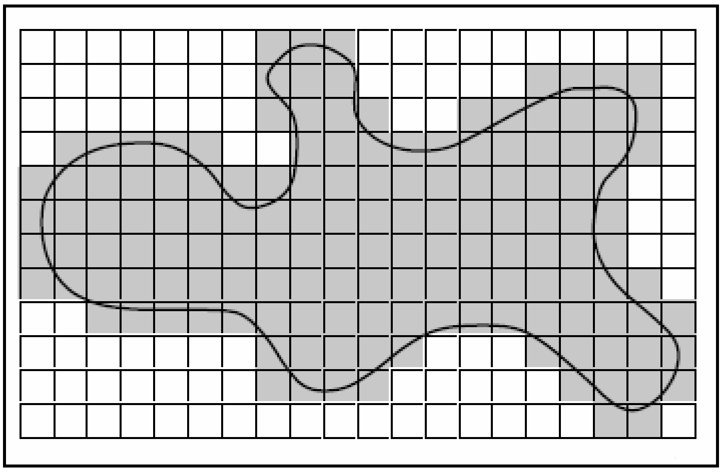

Figure 3.2 Particle area calculated through the image analysis (After Janoo, 1998).

Particle area is often expressed in terms of equivalent circular diameter. It is the diameter of fictitious circle that has the same area as the particle and defined in the following form:

$$\text{Equivalent Circular Diameter} = \sqrt{\frac{4}{\pi}\text{Area}} \tag{3.1}$$

where Area = particle area calculated by the summation of interior pixels.

The perimeter is the summation of all pixels forming the boundary of an aggregate cross section.

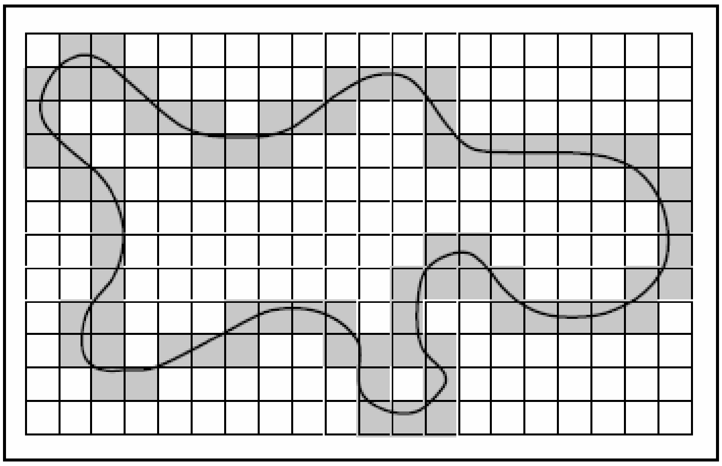

Figure 3.3 Particle perimeter calculated through image analysis (After Janoo, 1998).

The bounding polygon around the particle approximates the particle boundary while eliminating particle surface texture details. Figure 3.4 shows an irregular particle with its maximum Feret diameter, bounding polygon and equivalent circular diameter (Russ, 1999).

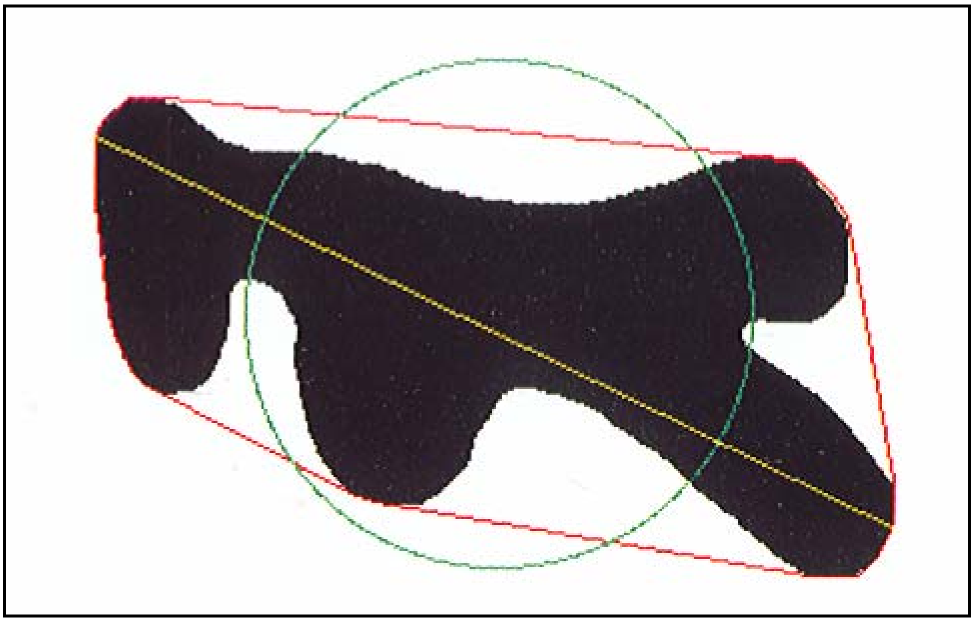

Figure 3.4 An irregular particle with its maximum Feret diameter, bounding polygon and equivalent circular diameter (Russ, 1999).

3.3 Definitions of Particle Shape Properties

Barrett (1980) suggested that the shape of a rock particle can be expressed in terms of form (overall shape), roundness (angularity or large scale smoothness), and surface texture (roughness or small scale smoothness). Form, roundness and surface texture are the geometrically independent properties of a particle shape although there might be natural correlation between them due to the common physical factors (Figure 3.5).

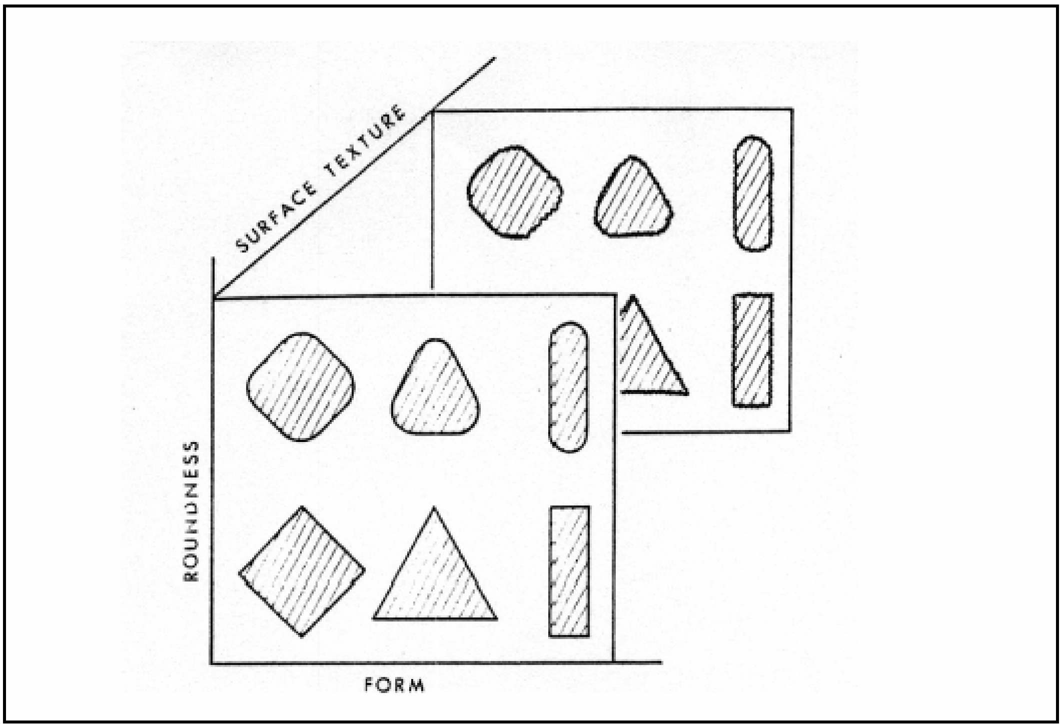

Figure 3.5 A simplified representation of form, roundness and surface texture by three linear dimensions to illustrate their independence (After Barrett, 1980).

Alternatively, aggregate particle shape might also be assessed in terms of sensual (visually or by touching) observations of the particles. Visually, these types of observations classify particles such as equidimensional, flat or elongated. By manually inspecting surface characteristics, particles may also be classified in accordance with their surfaces as smooth or rough or combination of them in the case of partially crushed particles (Erdoğan and Fowler, 2005). Figure 3.6 suggested by Quiroga and Fowler (2003) can provide two comparable charts for such a visual assessment of particle shapes. This type of visual assessments of particles only gives an idea about the particle shape, however, do not indicate any idea about the fine surface characteristics.

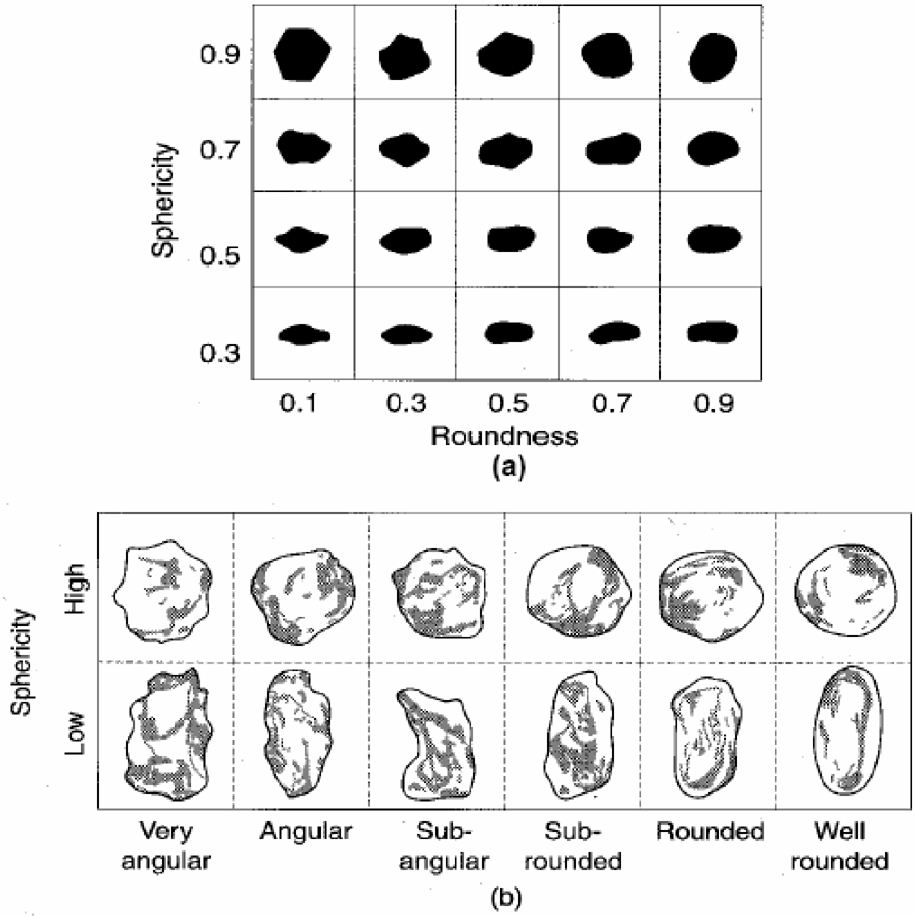

Figure 3.6 Visual assessment of particle shape (a) Derived from measurements of sphericity and roundness, (b) Based upon morphological observations (After Quiroga and Fowler, 2003).

There are a number of particle shape parameters defined to describe particle shape and surface characteristics. Some of these parameters are elongation ratio, flatness ratio, shape factor, angularity, formfactor, compactness, convexity ratio, fullness ratio and roughness.

However, in the literature there is a lack of consensus on the definitions of particle shape parameters. For instance, different researchers have used:

- different particle shape parameters to indicate the same shape attribute e.g., circularity of aggregate cross section by formfactor and compactness as proposed by Kuo and Freeman (2000) and Yue et al. (1995), respectively,
- different definitions and formulations for the same particle shape parameters e.g., several different formulations for elongation ratio as proposed by Kuo et al. (1998) and Barksdale et al. (1991),
- different names assigned to the same particle shape parameter e.g., the same formulation for formfactor by Kuo and Freeman, (2000) and for shape factor by Yue et al. (1995).

In the subsequent sections, various particle shape parameters that are used in previous studies are introduced and the similarities and differences between the parameters are discussed in detail.

3.3.1 Parameters for Particle Form

Form is a first order property that reflects variations in overall shape of a particle (Barrett, 1980).

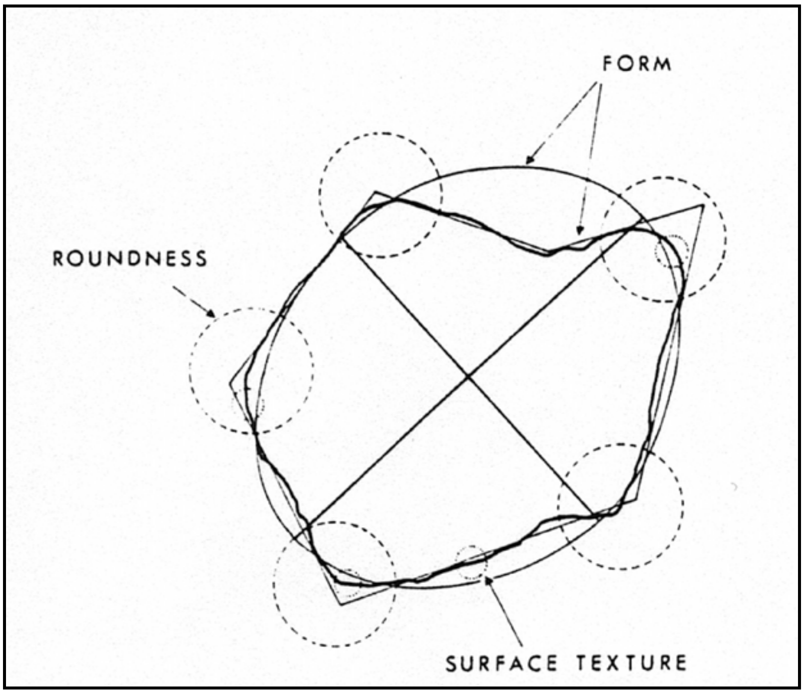

Figure 3.7 Particle outline (heavy solid line) with its component elements of form (light solid lines, two approximations shown), roundness (dashed circles) and texture (dotted circles) identified (After Barrett, 1980).

Almost all parameters of particle form measures the relation between the three principal axes of the particle as shown in Figure 3.8.

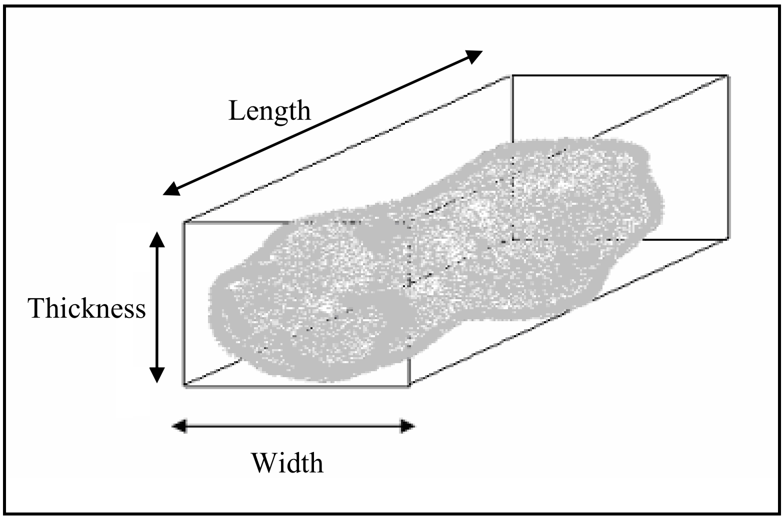

Figure 3.8 The principal dimensions of an aggregate particle (After Erdoğan and Fowler, 2005).

Two fundamental parameters defined by Kuo et al. (1998) in order to describe the particle form are the elongation ratio, defined as the ratio of the particle maximum dimension (length) to the maximum dimension in the plane perpendicular to the length (width), and flatness ratio, defined as the ratio of the particle width to the maximum dimension perpendicular to length and width (thickness). These terms are explained in below equations where L, W and T represent the length, width and thickness of a particle, respectively.

$$\text{Elongation Ratio} = \frac{L}{W} \tag{3.2}$$

$$\text{Flatness Ratio} = \frac{W}{T} \tag{3.3}$$

Elongation ratio and flatness ratio were called as aspect ratio by Kuo and Freeman (2000) and flakiness ratio by Mora and Kwan (2000), respectively. In addition, some researchers used the inverse of Equation 3.2 and Equation 3.3 as elongation and flatness parameters (Barksdale et al., 1991; Aschenbrenner, 1956; Erdoğan and Fowler, 2005).

ASTM D 2488-00 "Standard Practice for Description and Identification of Soils (Visual - Manual Procedure)" describes the shape of aggregates as either flat or elongated or flat and elongated using the criteria shown in Table 3.1.

Table 3.1 Criteria for describing particle shape according to ASTM D 2488-00.

Shape	Description
Flat	Particles with width/thickness >3
Elongated	Particles with length/width >3
Flat and Elongated	Particles that meet criteria both flat and elongated

Similarly, the British Standard BS 812:1975 classifies particles as flaky if its thickness is small relative to the other two dimensions, as elongated if its length is considerably larger than the other two dimensions, and as flaky and elongated if particle's length is considerably larger than the width, and the width is considerable larger than the thickness.

Among the first order particle shape descriptors used, formfactor is one of the most widely used to measure the degree of circularity of the particle surface. Its formulation defined by Kuo and Freeman (2000) is given in Equation 3.4.

$$\text{Formfactor} = \frac{4\pi\text{Area}}{\text{Perimeter}^2} \tag{3.4}$$

where Area = area of particle; Perimeter = perimeter of particle.

Formfactor has a maximum value of 1.0 for a perfect circle, and takes smaller values for shapes departing from the perfect circle. The formfactor formulation in the above Equation 3.4 is called as shape factor by Yue et al. (1995) and as roundness index by Janoo (1998).

However, according to Kuo and Freeman (2000) such definition for formfactor is sensitive to changes in aggregate form, roundness and surface texture.

Another first order particle shape parameter, compactness, proposed by Yue et al. (1995) is an alternative method to measure how nearly circular an aggregate cross section is, and formulated in Equation 3.5. A perfect circle has a compactness value of 4π and a line that of infinity.

$$\text{Compactness} = \frac{\text{Perimeter}^2}{\text{Area}} \tag{3.5}$$

Shape factor is also a commonly used particle parameter to describe the overall particle shape by Mora and Kwan (2000). Researchers have proposed various shape factor definitions in order to express different features of particle form. For instance, Aschenbrenner (1956) defined the shape factor in Equation 3.6 whereas Barksdale et al. (1991), Yue et al. (1995) and Kuo et al. (1996) all used Equation 3.7.

$$\text{Shape Factor (F)} = \frac{\text{Elongation Ratio}}{\text{Flatness Ratio}} = \frac{\text{TL}}{\text{W}^2} \tag{3.6}$$

where elongation ratio and flatness ratio are the inverse of the Equation 3.2 and Equation 3.3, respectively.

By Aschenbrenner's (1956) definition, a round or cubical particle has a shape factor equal to 1.0. Shape factor is less than 1.0 for elongated and thin particles whereas it is greater than 1.0 for blade shaped particles.

$$\text{Shape Factor} = \frac{\text{T}}{\sqrt{\text{WL}}} \tag{3.7}$$

Sphericity is another parameter that is proposed to measure the particle form. Harr (1977) defines the sphericity as a particle property that varies with the following factors:

- ratio of the surface area of particle to its volume,
- relative lengths of its principal axes or those of circumscribing rectangular prism,
- relative settling velocity,
- ratio of the volume of particle to that of the circumscribing sphere.

Sphericity has also been defined by Quiroga and Fowler (2003) as a measure of how the three principal axes of a particle are close to each other. In the current literature, various different mathematical definitions have been proposed for sphericity. For instance, according to Wadell (1932), most exact shape expression of sphericity is the ratio of the surface area of sphere having the same volume of particle to the actual surface area of particle and formulated as follows:

$$\text{Degree of True Sphericity} = \frac{s}{S} \tag{3.8}$$

where s = surface area of a sphere of the equivalent volume particle; S = actual surface area of particle.

By the above definition, 1.00 is the maximum value obtained by the shape of a sphere and it is 0.81 for a cube.

Wadell (1933) proposed a more simplistic approach to determine the sphericity as formulated by Equation 3.9, however, the method proposed by Wadell (1932) requires three dimensional shape analysis of particle surface area.

$$\text{Operational Sphericity} = \sqrt[3]{\frac{V_P}{V_{CS}}} \tag{3.9}$$

where V_P= volume of particle; V_{CS}= volume of circumscribing sphere.

Another definition of sphericity proposed by Aschenbrenner (1956) is based on the flatness and elongation ratio.

$$\text{Sphericity } (\psi) = \frac{12.8(\sqrt[3]{p^2 q})}{1 + p(1+q) + 6\sqrt{1 + p^2(1+q^2)}} \tag{3.10}$$

where ψ is the Aschenbrenner sphericity; q and p are the elongation and flatness ratios determined by inverse of the Equation 3.2 and Equation 3.3, respectively. The Aschenbrenner sphericity (ψ) can vary from 0.0 to 1.0 for a perfect sphere.

The elongation ratio, q, the flatness ratio, p, the shape factor, F (Equation 3.6), and the sphericity, ψ, are combined in the Figure 3.9 which classifies aggregates as disc, equidimensional, and blade or rod shaped particles.

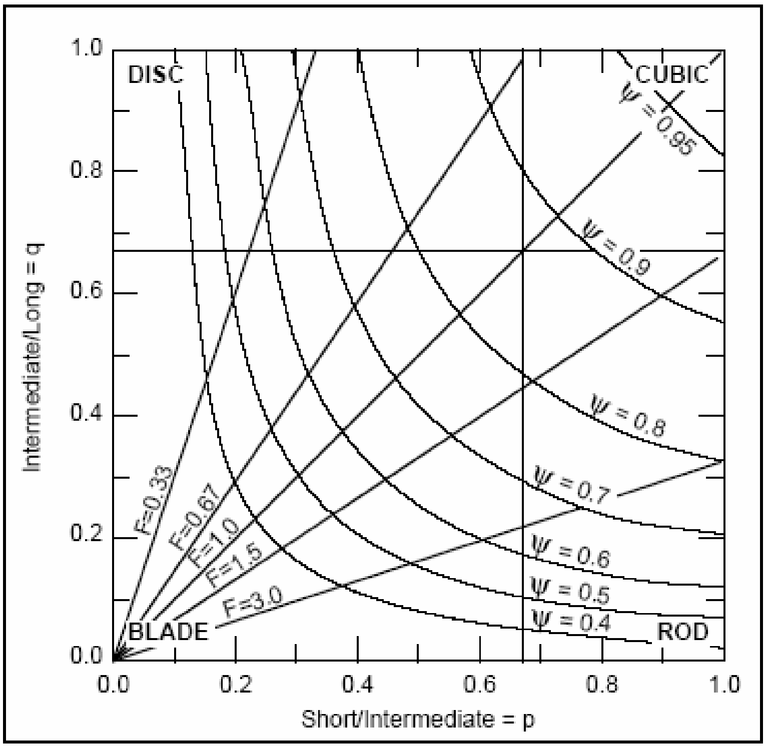

Figure 3.9 Aggregate classification chart (After Aschenbrenner, 1956).

Definitions for disc, equidimensional, blade, and rod shaped particles based on the descriptions of several authors are presented by Lees (1964) and Barksdale and Itani (1989) in Table 3.2.

Table 3.2 Descriptions of aggregate shape (Janoo, 1998).

Aggregate Shape	Description
Disc	Slabby in appearance, but not elongated
Equidimensional	Neither slabby appearance nor elongated
Blade	Slabby appearance
Rod	Elongated, but not slabby in appearance

Krumbein (1941) proposed the product of principal dimensions to approximate sphericity as follows:

$$\text{Sphericity} = \sqrt[3]{\left(\frac{WT}{L^2}\right)} \qquad (3.11)$$

where L, W, T are the principal dimensions of particle as described in Figure 3.8.

A more "natural" measure of sphericity is developed by Krumbein (1942) which takes into account the hydraulic behavior of particles. It can be formulated as follows:

$$\text{Maximum Projection Sphericity} = \psi_p = \sqrt[3]{\frac{T^2}{WL}} \qquad (3.12)$$

Sneed and Folk (1958) developed a triangular sphericity-form diagram by combining maximum projection sphericity and form of particle as shown in Figure 3.10 (The notation I and S are used instead of W and T, respectively).

In order to determine the form and sphericity of a particle from Figure 3.10, the ratio S/L (shown on the left side of the triangle) should first be computed. Next, (L-I)/(L-S) should be determined and plotted along the lines converging toward the apex. The point determined by the intersection of these two quantities may then be used to obtain sphericity of particle by interpolating between isosphericity contours curving down to the right. Ten form classes are defined by heavy solid lines and designated by the following initials: C, *Compact;* CP, *Compact-Platy*; CB, *Compact-Bladed*; CE, *Compact-Elongate*; P, *Platy;* B, *Bladed*; E, *Elongate*; VP, *Very Platy*; VE, *Very Elongate*.

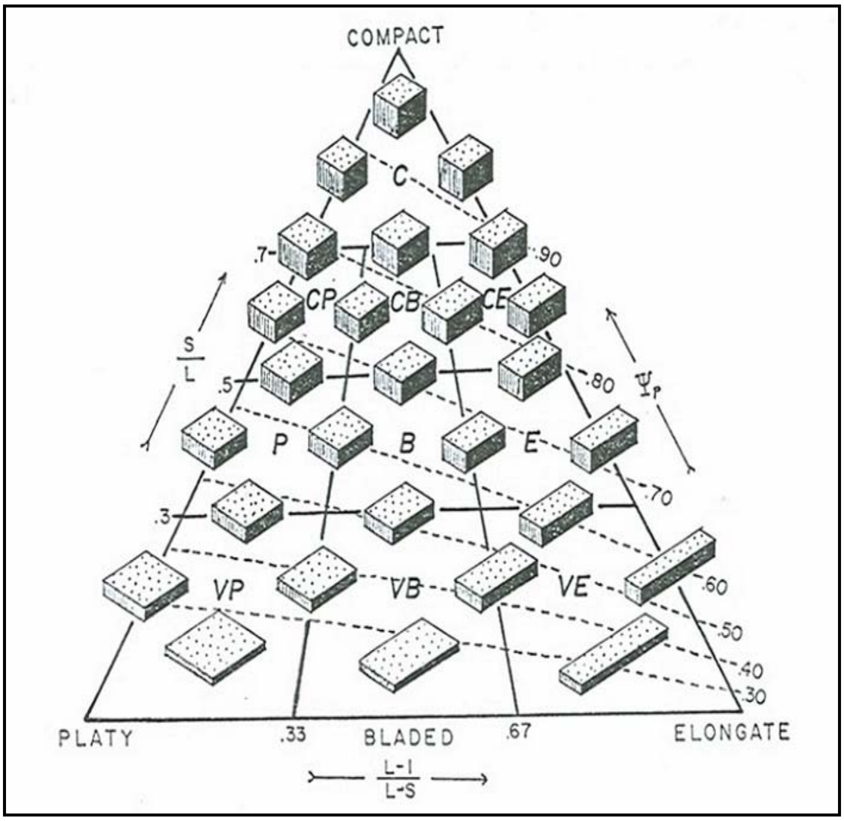

Figure 3.10 Sphericity-form diagram (After Sneed and Folk, 1958).

An advanced method was developed by Masad et al. (2001) in order to evaluate the particle form as the summation of changes in particle radius, as given in Equation 3.6.

$$\text{Form Index (FI)} = \sum_{\theta = 0}^{\theta = 360-\Delta\theta} \frac{\left| R_{\theta+\Delta\theta} - R_{\theta} \right|}{R_{\theta}} \tag{3.13}$$

where R_θ = the radius of particle at an angle of θ; $\Delta\theta$ = incremental difference in the angle. It can be concluded by examining Equation 3.13 that the form index for a perfect circle would be zero. The advantage of this parameter is that it considers the changes in particle dimension in all directions rather than in three dimensions as done in shape factor or sphericity parameters.

3.3.2 Parameters for Particle Roundness

Roundness is a second order shape property that reflects variations at particle corners (Barrett, 1980) (see Figure 3.7). According to Popovics (1992), roundness can be defined numerically for a particle as the ratio of the average radius of curvature of the corners and edges of the particle to the radius of the maximum inscribed circle. However, following descriptive terms of ASTM D 2488-00 are commonly used.

Table 3.3 Criteria for describing angularity of coarse-grained particles according to ASTM D 2488-00 (see Figure 3.11).

Shape	Description
Rounded	Particles have smoothly curved sides and no edges
Angular	Particles have sharp edges and relatively plane sides with unpolished surfaces
Subrounded	Particles have nearly plane sides but have well-rounded corners and edges
Subangular	Particles are similar to angular description but have rounded edges.

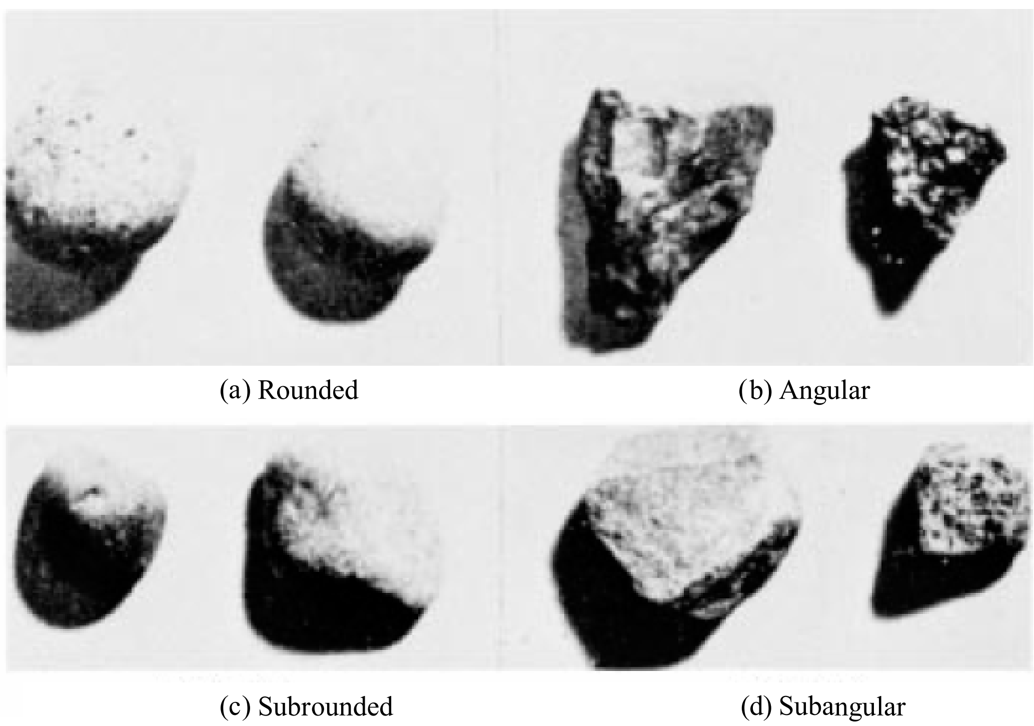

Figure 3.11 Typical angularity of bulky grains (After ASTM D 2488-00).

Wadell (1932) defines the roundness of particle as the arithmetic mean roundness of the individual corners in the same plane.

$$\text{Degree of Roundness of Particle in a Plane} = \frac{\sum\left(r/R\right)}{N} \qquad (3.14)$$

where r = radius of curvature of a corner within the particle surface; R = radius of the maximum inscribed circle within the projected plane; $\sum(r/R)$ = summation of the roundness values of the corners and N = number of corners of particle.

By this roundness definition, a sphere has a roundness value of 1.0. A cylinder capped with two hemispheres also has a roundness of 1.0, and spheres with right-angled corners have a roundness of 0.0 because of their infinitely small radius of curvature at the corners.

According to Mora and Kwan (2000), even though particle roundness can be best displayed by a sphere, it is not a measure of sphericity. It is an independent property apart from the particle form and can be separated into two aspects, namely the roundness of the corners (important for abrasive properties of particles), and the roundness of the outline of the particle (also called overall roundness and more important for the interlocking ability and packing density of particles) which is generally measured in terms of convexity.

Angularity is also an important second order particle shape parameter. It is defined as the square of the ratio of the convex perimeter of particle to the perimeter of fictitious equivalent ellipse having the same area and the aspect ratio of aggregate particle. It can be formulated as follows:

$$\text{Angularity} = \left(\frac{\text{Perimeter}_{\text{convex}}}{\text{Perimeter}_{\text{ellipse}}} \right)^2 \tag{3.15}$$

where $\text{Perimeter}_{\text{convex}}$ = perimeter of the minimum convex boundary circumscribing the particle; $\text{Perimeter}_{\text{ellipse}}$ = perimeter of an fictitious ellipse that has the same area and the aspect ratio as the original particle.

The perimeter of the equivalent ellipse can be expressed in terms of the aspect ratio and the equivalent circular perimeter as:

$$\text{Perimeter}_{\text{ellipse}} = \sqrt{\frac{1+\text{Aspect Ratio}^2}{2\ \text{Aspect Ratio}}}\ \text{Perimeter}_{\text{circle}} \tag{3.16}$$

where Aspect Ratio = particle maximum dimension (length) to the maximum dimension in the plane perpendicular to the length (width); $\text{Perimeter}_{\text{circle}}$ = perimeter of the fictitious circle that has the same area as the particle.

The aforementioned angularity parameter definition is supposed to be independent from the effects of surface texture and aspect ratio and thus believed to be a good parameter to describe roundness. By this angularity definition, the angularity of either a circle or an ellipse will be 1.0. For angular particles, their angularity will be greater than 1.0 and a larger value indicates a higher degree of angularity (Kuo and Freeman, 2000).

Masad and Button (2000) applied the erosion-dilation technique to evaluate fine aggregate angularity and surface texture. This procedure is based on applying number of erosion cycles followed by the equal number of dilation cycles. The concept of image erosion is well known in image processing, where it is used both as a smoothing technique (Rosenfeld and Kak, 1982) and a shape classifier (Blum, 1967) as cited by Ehrlich et al. (1984). Erosion is the process of eliminating all boundary points from an object, leaving the object smaller in area by one pixel all around its perimeter and can be described as a fire burning inward from the periphery of an object, in order to shrink the object to a skeleton or a point (Castleman, 1996). Figures 3.12(a) and Figure 3.12(b) shows the effect of the erosion operations on an image.

Dilation is the inverse of erosion operation. A layer of pixels is added to the eroded object to form a simplified version of the original object. As shown in Figure 3.12(b) and Figure 3.12(c), applying number of erosion operations followed by dilation operations need not restore the image to its original shape (Calabi and Hartnett, 1968; Duda and Hart, 1973 and Young et al., 1981). In addition, small objects may be lost completely during erosion, leaving no "seed" pixels from which the subsequent dilation can build (Ehrlich et al., 1984). Therefore, it might be stated that the particle area lost during the number of erosion-dilation circles are proportional to the angularity of particle assuming that no objects are lost during the process. Angularity of an aggregate particle may be expressed in terms of the percent area of the original particle lost during erosion-dilation process as formulated in Equation 3.17.

$$\text{Surface Parameter (SP)} = \frac{A_1 - A_2}{A_1} 100\% \qquad (3.17)$$

where A_1 = particle area before the erosion-dilation cycles; A_2 = particle area after the erosion-dilation cycles (see Figure 3.12).

A particle with more angularity is expected to lose more area than smooth one; thus, the surface parameter would be higher. Masad and Button (2000) stated that the surface parameter (SP) is well correlated to angularity of a particle at low resolutions and also to surface texture of a particle at higher resolutions.

Another approach for particle angularity proposed by Masad et al. (2000) is based on fractal approach, and presented in Figure 3.12. Figure 3.12(a-d) shows a number of erosion and dilation operations on the original image. In addition, Figure 3.12(e) shows a combination of the eroded and dilated images using logical XOR operator which removes the black color pixels at the same location on both eroded and dilated images. The retained pixels construct a boundary with a width proportional to the number of applied erosion-dilation cycles and surface angularity. This procedure continues by varying the number of erosion-dilation cycles, and measuring the increase in the effective width of the boundary (total number of pixels divided by boundary length and number of cycles). If the effective width is plotted versus the number of erosion-dilation cycles on a log-log scale, the effective width to number of cycle relationship does not show any trend for a smooth boundary. However, for an angular boundary, the graph shows a negative linear variation whose slope gives the fractal length (FL) of the boundary which increases as the angularity of the particle boundary increases.

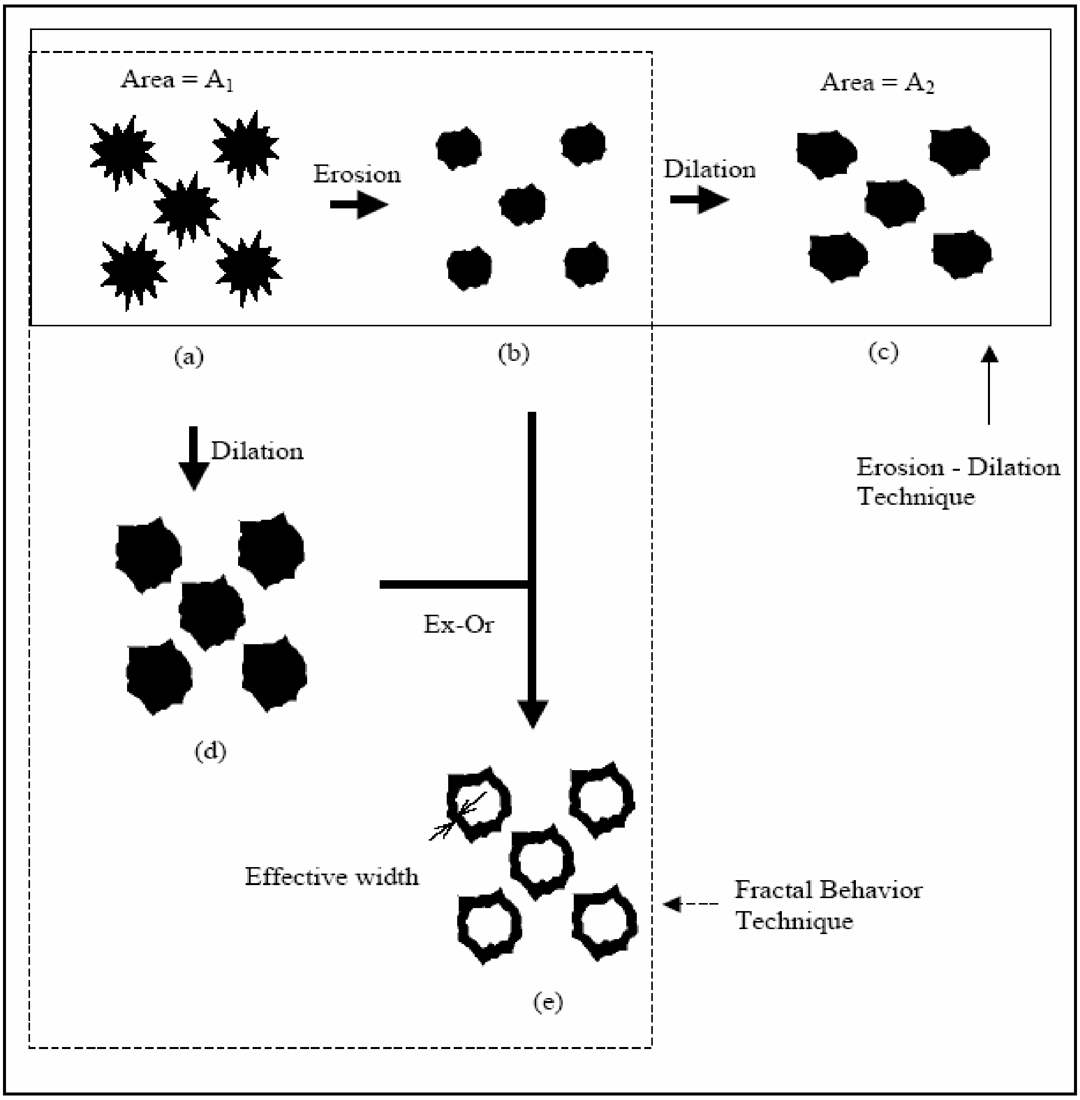

Figure 3.12 Illustration of the erosion-dilation and fractal behavior procedures (After Masad et al., 2000).

Radius method is also proposed by Masad et al. (2001) for the analysis of particle angularity using black and white images. Radius method measures the difference between the particle radius in a certain direction and that of equivalent ellipse. The equivalent ellipse has the same aspect ratio and area as the particle, but no angularity.

Angularity Index (AI) of radius method is expressed as follows:

$$\text{Angularity Index (radius method)} = \sum_{\theta = 0}^{\theta = 355} \frac{\left| R_\theta - R_{EE\theta} \right|}{R_{EE\theta}} \tag{3.18}$$

where R_θ = radius of the particle at an angel of θ, $R_{EE\theta}$ = radius of the equivalent ellipse at an angel of θ.

Chandan et al. (2004) proposed gradient based angularity method. This method has the capability of capturing sharp angular corners of a highly angular particle and assigning almost zero angularity to a rounded particle. Furthermore, it can make fine distinctions between particle shapes. The principle of this method is to measure the magnitude of change in the orientation angles for adjacent points on the particle edges. As shown in Figure 3.13, the change in the angle of gradient vector A (for a rounded object) is much less compared to the change in the angle of gradient vector B (for an angular object). This method calculates the angularity values for all the boundary points and assigns their sum to the angularity index of the aggregate particle.

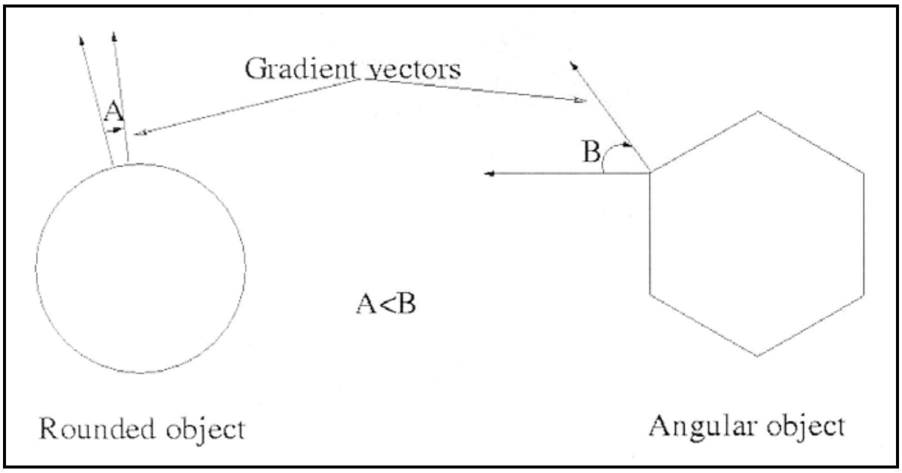

Figure 3.13 Illustration of the difference in gradient between particles (After Chandan, 2004).

The three dimensional angularity index (AI) is proposed by Rao et al. (2002) using UI-AIA aggregate analyzer developed at the University of Illinois Urbana-Champaign for automatic determination of flat and elongated particles, particle angularity, gradation and volume. This approach uses 3 cameras to collect images from the three orthogonal directions. The particles which are to be analyzed are fed on to a conveyor belt system which carries particles one by one towards to the orthogonally placed cameras. Each particle is detected by the cameras as they move into the field of view of cameras. The cameras are synchronized so the pictures from three orthogonal positions are taken at the same time.

Therefore, the angularity index (AI) is determined as the weighed average of angularity values for each images collected from the three orthogonal views:

$$AI_{particle} = \frac{Ang_{front}Area_{front} + Ang_{top}Area_{top} + Ang_{side}Area_{side}}{Area_{top} + Area_{front} + Area_{side}} \tag{3.19}$$

where AI = angularity index for a particle; $Area_{front}$, $Area_{top,}$ $Area_{side}$ = area of the particle from front, top and side views, respectively; and Ang_{front}, $Ang_{top,}$ Ang_{side} = angularity of particle from front, top and side views (a comprehensive computation of angularity value for individual view is provided by Rao et al., 2002, pp. 6-8).

The angularity index (AI) for a sample of aggregate is defined by the weighted angularity index calculated using the angularity index of individual particles. The main advantage of this procedure is that it can give similar angularity index (AI) values irrespective of particle size and orientation.

The particle angularity index (AI) proposed by Rao et al. (2002) has the following advantages. It is:

- independent of the size of particles,
- not sensitive to particle orientations,
- sensitive to changes in particle contours.

The second order particle shape parameters, namely roundness and angularity, are the two complementary parameters which are used interchangeably. Because of this reason, a measure of roundness may also be considered a measure of angularity. Roundness can be considered a more general particle shape definition than angularity. However, angularity might be considered a more general parameter index when it refers to a parameter that is complementary to the roundness of particle corners and edges defining the overall angularity of particle (Mora and Kwan, 2000).

The parameter convexity ratio is defined to further evaluate the particle convexity. Due to the difficulty of performing three dimensional particle geometry analysis, the convexity ratio is often evaluated from the two dimensional projection of particle, as shown in Figure 3.14.

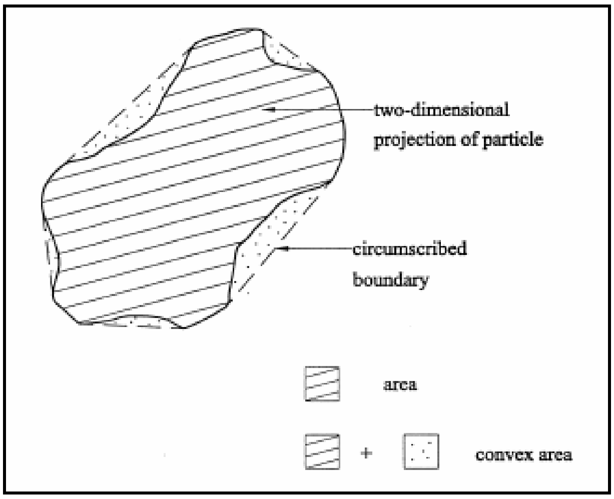

Figure 3.14 Definitions of area and convex area (After Mora and Kwan, 2000).

$$\text{Convexity Ratio} = \frac{\text{Area}}{\text{Convex Area}} \tag{3.20}$$

where Area = two dimensional projection area of particle; Convex Area = area of the minimum convex boundary circumscribing the particle.

Fullness ratio is another measure of convexity that is also evaluated from the two dimensional projection of particle. It is defined by Kuo et al. (1996) in the following formulation:

$$\text{Fullness Ratio} = \sqrt{\frac{\text{Area}}{\text{Convex Area}}} \tag{3.21}$$

The particle convexity indexes aforementioned, namely the convexity ratio and the fullness ratio, are closely related to roundness and angularity. Although they may be used as a measure of angularity, they cannot be considered as complete indicators of angularity, since the sharpness of particle corners is not taken into account (Kwan and Mora, 2001).

3.3.3 Parameters for Particle Surface Texture

Surface texture, the third order shape property (the first and second order properties are form and roundness), is mainly a property of particle surface (Barrett, 1980) (see Figure 3.7). It is independent of form and roundness, and a measure of roughness or smoothness of the particle boundary (Mora and Kwan, 2000). Terzaghi and Peck (1948) defined surface texture as the degree of fineness and uniformity. According to Popovics (1992), surface texture depends on hardness, grain size, porosity, and texture of rock, and the degree to which the forces acting on the particle have roughened or smoothened it. Generally, hard, dense, fine graded materials have smooth surfaces. The British Standard BS 812:1975 has the following descriptive terms for the surface texture of aggregates.

Table 3.4 Surface texture of aggregates according to BS 812:1975.

Surface Texture	Characteristics
Glassy	Conchoidal fracture
Smooth	Waterworn, or smooth due to fracture of laminated or fine graded rock
Granular	Fracture showing more or less uniform rounded grains
Rough	Rough fracture of fine or medium grained rock containing no easily visible crystalline constituents
Crystalline	Containing easily visible crystalline constituents
Honeycombed	With visible pores and cavities

Particle roughness as a measure of surface texture is defined by Kuo and Freeman (2000) as:

$$\text{Roughness} = \left(\frac{\text{Perimeter}}{\text{Perimeter}_{\text{convex}}} \right)^2 \tag{3.22}$$

where Perimeter = perimeter of particle; $\text{Perimeter}_{\text{convex}}$ = perimeter of the minimum convex boundary circumscribing the particle.

For a smooth material, the roughness parameter equals to 1.0. As the roughness increases, so does the roughness factor. An alternative roughness factor definition was proposed by Janoo (1998) as the ratio of the particle perimeter to the particle convex perimeter.

Rao et al. (2003) utilized the erosion–dilation technique to determine the surface texture of coarse aggregates from three orthogonally captured images. As it is mentioned previously, Masad and Button (2000) applied this technique to determine the surface texture of fine aggregates from the two dimensional projections. Similarly, as in the case of weighted angularity index (AI), the weighted surface texture (ST) may also be calculated in a similar way by weighing for the individual particle areas as shown in Equation 3.23.

$$ST_{\text{particle}} = \frac{ST_{\text{front}}\text{Area}_{\text{front}} + ST_{\text{top}}\text{Area}_{\text{top}} + ST_{\text{side}}\text{Area}_{\text{side}}}{\text{Area}_{\text{top}} + \text{Area}_{\text{front}} + \text{Area}_{\text{side}}} \tag{3.23}$$

where ST_{particle} = surface texture of a particle; $\text{Area}_{\text{front}}$, Area_{top}, $\text{Area}_{\text{side}}$ = area of the particle from front, top and side views, respectively; and ST_{front}, ST_{top}, ST_{side} = surface texture of the particle from front, top and side views, respectively as computed according to the following equation:

$$\text{Surface Texture (ST)} = \frac{A_1 - A_2}{A_1} 100\% \qquad (3.24)$$

where ST = surface texture parameter for each view; A_1 = area of the two dimensional projection of the particle in the image and A_2 = area of the two particle after performing a sequence of n cycles of erosion followed by n cycles of dilation (see Figure 3.12).

Particle shape parameters that are mentioned in the above sections are summarized in Table 3.5, Table 3.6 and Table 3.7 for form, roundness and surface texture parameters, respectively.

Table 3.5 Parameters of particle form.

Parameter	Proposed by	Formulation
Elongation Ratio	Kuo et al. (1998)	Elongation Ratio = $\frac{L}{W}$
	Aschenbrenner (1956) Erdoğan and Fowler (2005)	Elongation Ratio = $\frac{W}{L}$
Flatness Ratio	Kuo et al. (1998)	Flatness Ratio = $\frac{W}{T}$
	Aschenbrenner (1956) Erdoğan and Fowler (2005)	Flatness Ratio = $\frac{T}{W}$
Aspect Ratio	Kuo and Freeman (2000)	Aspect Ratio = $\frac{L}{W}$
Flakiness Ratio	Mora and Kwan (2000)	Flakiness Ratio = $\frac{W}{T}$
Formfactor	Kuo and Freeman (2000)	Formfactor = $\frac{4\pi\text{Area}}{\text{Perimeter}^2}$
Shape Factor	Yue et al. (1995)	Shape Factor = $\frac{4\pi\text{Area}}{\text{Perimeter}^2}$
	Aschenbrenner (1956)	Shape Factor = $\frac{TL}{W^2}$
	Barksdale et al. (1991) Yue et al. (1995) Kuo et al. (1996)	Shape Factor = $\frac{T}{\sqrt{WL}}$
Roundness Index	Janoo (1998)	Roundness Index = $\frac{4\pi\text{Area}}{\text{Perimeter}^2}$
Compactness	Yue et al. (1995)	Compactness = $\frac{\text{Perimeter}^2}{\text{Area}}$
Form Index	Masad (2002)	Form Index = $\sum_{Q=0}^{Q=355}\frac{\lvert R_{Q+5} - R_Q\rvert}{R_Q}$
Sphericity	Wadell (1932)	Degree of True Sphericity = $\frac{s}{S}$
	Wadell (1933)	Operational Sphericity = $\sqrt[3]{\frac{V_P}{V_{CS}}}$
	Aschenbrenner (1956)	$\psi = \frac{12.8(\sqrt[3]{p^2q})}{1+p(1+q)+6\sqrt{1+p^2(1+q^2)}}$
	Krumbein (1941)	Sphericity = $\sqrt[3]{(\frac{WT}{L^2})}$
	Krumbein (1942)	Maximum Projection Sphericity = $\sqrt[3]{\frac{T^2}{WL}}$

Table 3.6 Parameters of particle roundness.

Parameter	Proposed by	Formulation
Roundness	Wadell (1932)	$\text{Degree of Roundness of Particle} = \frac{\sum \left(r/R \right)}{N}$
Angularity	Kuo and Freeman (2000)	$\text{Angularity} = \left(\frac{\text{Perimeter}_{\text{convex}}}{\text{Perimeter}_{\text{ellipse}}} \right)^2$
	Masad et al. (2001)	$\text{Angularity Index} = \sum_{\theta=0}^{\theta=355} \frac{\lvert R_Q - R_{EEQ} \rvert}{R_{EEQ}}$
	Rao et al. (2002)	$AI_{\text{particle}} = \frac{\text{Ang}_{\text{front}}\text{Area}_{\text{front}} + \text{Ang}_{\text{top}}\text{Area}_{\text{top}} + \text{Ang}_{\text{side}}\text{Area}_{\text{side}}}{\text{Area}_{\text{top}} + \text{Area}_{\text{front}} + \text{Area}_{\text{side}}}$
Surface Parameter	Masad and Button (2000)	$\text{Surface Parameter} = \frac{A_1 - A_2}{A_1} 100\%$
Convexity Ratio	Mora and Kwan (2000)	$\text{Convexity Ratio} = \frac{\text{Area}}{\text{Convex Area}}$
Fullness Ratio	Mora and Kwan (2000)	$\text{Fullness Ratio} = \sqrt{\frac{\text{Area}}{\text{Convex Area}}}$

Table 3.7 Parameters of particle surface texture.

Parameter	Proposed by	Formulation
Roughness	Kuo and Freeman (2000)	$\text{Roughness} = \left(\frac{\text{Perimeter}}{\text{Perimeter}_{\text{convex}}} \right)^2$
	Janoo (1998)	$\text{Roughness} = \left(\frac{\text{Perimeter}}{\text{Perimeter}_{\text{convex}}} \right)$
Surface Texture	Rao et al. (2003)	$ST_{\text{particle}} = \frac{ST_{\text{front}}\text{Area}_{\text{front}} + ST_{\text{top}}\text{Area}_{\text{top}} + ST_{\text{side}}\text{Area}_{\text{side}}}{\text{Area}_{\text{top}} + \text{Area}_{\text{front}} + \text{Area}_{\text{side}}}$

3.4 Effects of Aggregate Characteristics

Aggregate characteristics may significantly affect the behavior of fresh and hardened concrete. The effects of aggregate characteristics may change as a function of particle sizes. The following classification is generally used to categorize aggregates with respect to particle sizes. Particles retained on the No.4 sieve is considered to be coarse aggregate, particles passing No.4 sieve and retained on the No.200 sieve is considered to be fine aggregate, and particles passing No.200 sieve is considered to be dust or microfines as shown in Table 3.8. Consequently, the impact of aggregate particles on the performance of concrete is different for coarse aggregates, fine aggregates and microfines.

Table 3.8 Classification of aggregates.

Aggregate Fraction	Size Range
Coarse	Retained in No.4
Fine	Passing No.4 - Retained in No.200
Microfines	Passing No.200

There are several aggregate properties affecting performance of fresh and hardened concrete. Shape and texture, maximum aggregate size, and gradation are some of these discussed in the content of this investigation.

3.4.1 Effects of Shape and Texture

First, effects of shape and texture of fine aggregate; secondly, effects of shape and texture of coarse aggregate are discussed in the following sections.

3.4.1.1 Effects of Shape and Texture of Fine Aggregate

Shape and texture of fine aggregate have important effects on workability of fresh concrete as well as strength and durability of hardened concrete. The influence of shape and texture of fine aggregate on the behavior of concrete is generally more important than that of coarse aggregate. This is because of the fact that the shape and texture of fine aggregates have significant effects on the water requirement of fresh mixes (Quiroga and Fowler 2003).

Surface texture affects particle packing efficiency, since rough particles have higher void content. In addition, the impact of surface texture on concrete behavior becomes more important as particles get smaller. In addition, surface texture of fine aggregates also affects the bond between particles and cement paste and influence the water requirement of the mix. Particle shape and texture of fine aggregates also affect the durability of fresh mix (Hudson, 1999).

Generally poorly shaped and angular particles increase the demand for water since they have higher water content; therefore, negatively affects the durability (Neville, 2003; Popovics, 1992). Bleeding is also significantly affected by particle shape and texture. Crushed aggregates have tendency to increase water demand, and, therefore, bleeding. However, this effect may be counterbalanced by proper grading (Washa, 1998 and Kosmatka, 1994 as cited by Quiroga and Fowler 2003).

According to Shilstone (1990), particle shape has a major influence through No.4 and No.8 sieves. Furthermore, mixes containing spherical and equidimensional particle sizes have better pumpability and finishability, and produce consistent higher strengths and lower shrinkage than mixes containing flat and elongated particles.

3.4.1.2 Effects of Shape and Texture of Coarse Aggregate

Although shape and texture for coarse aggregates are not as crucial as for fine aggregates, their influence on the behavior of fresh and hardened concrete should not be underestimated (Quiroga and Fowler, 2003).

Aggregate shape and surface texture are the results of interaction between nature, structure, and texture of rocks. The shape and the surface texture of aggregates influence the properties of fresh concrete more than the hardened concrete. Generally, rough textured, angular, and elongated particles require more cement paste than smooth and rounded particles to produce workable concrete mixture because of higher void contents. In addition, mixtures with rough textured or crushed aggregates have higher strength, especially tensile strength, at early ages than a corresponding concrete with smooth or naturally weathered aggregate of similar mineralogy since they are assumed to produce stronger physical bond with cement. But, at later ages, the effect of surface texture may be reduced because of the chemical interaction starting to take place between the aggregate and the cement paste. Rough surfaces also tend to increase the water requirement to achieve a certain workability level; therefore, the small advantage due to better physical bond may be lost as far as the strength is concerned (Mehta and Monteiro, 2006; Popovics, 1992).

Although rough particles tend to increase the water requirement for a given workability, consequently decrease strength and increase bleeding; workable concrete can be made with well graded crushed aggregates. Furthermore, a satisfactory concrete may be achieved using aggregates having surface texture from very smooth to very rough (Legg, 1998 as cited by Quiroga and Fowler, 2003). Surface texture also affects the stress level to start microcrackings. It may also affect the shape of stress-strain curve of concrete as they influence microcracking in the transition zone (Mindess et al, 2003).

Shilstone (1990) states that, intermediate aggregate particles, between No. $3/8$ and No.8, can contribute to mix harshness and affect the mobility, as they are flaky and elongated. Equidimensional particles are generally preferred against flat and elongated particles since they produce tighter packing and, thus require less water, cement paste or mortar for a given degree of workability. In addition, an excess of poorly shaped particles influence the strength and durability of concrete adversely, since they tend to orientate in one dimension with bleeding water and air voids forming underneath. Poorly shaped particles may also be prone to segregation during handling (Popovics, 1992; Neville, 2003; Mindess et al., 2003).

According to several specifications, there is a limit for the amount of elongated and flaky particles to avoid problems mentioned above. For instance, according to the Spanish Concrete Standard, the percent weight of flaky particles should not be greater than 35 or the shape coefficient (α) determined by Equation 3.24 should not be less than 0.20 (Quiroga and Fowler, 2003).

$$\alpha = \frac{V_1 + V_2 + V_3 + \dots + V_n}{\frac{\pi}{6}(d_1^3 + d_2^3 + d_3^3 + \dots + d_n^3)} \qquad (3.24)$$

where α = particle shape coefficient; V_i = volume of particle i and d_i = size of particle i.

The British Standard BS 882:1992 limits the flakiness index of coarse aggregates to 50 for natural gravel and to 40 for crushed and partially crushed coarse aggregates. Neville (2003) states that the presence of elongated particles more than 10 to 15 percent of the total mass of coarse aggregate is generally considered undesirable.

The effect of shape and texture of coarse aggregates on strength become significant in the case of high strength concrete. In addition, shape and surface texture have more pronounced affect on flexural strength than compressive strength (Neville, 2003). According to Kaplan (1959), surface texture is the most important aggregate property affecting the compressive strength, since rougher surface texture results in greater adhesive forces between cement paste and matrix.

However, the effect of aggregate shape is controversial. Although there is a general agreement that the same strength level of the concrete can be achieved using with different shapes of aggregates for a given cement content, Shilstone (1990) stated that well shaped aggregates are more desirable and produce consistent higher strengths than poorly shaped aggregates.

The influence of shape and texture of coarse aggregate on the strength of concrete varies in magnitude and depends on the water-cement ratio of the mix. It has been found that at low water-cement ratios (below 0.4) the use of crushed aggregate may increase the strength up to 38 percent because of the better mechanical bond. With the increase in the water-cement ratio, the influence of aggregate type decreases since the strength of hydrated cement paste starts to become dominant. For instance, at a water-cement ratio of 0.65, there is no difference between strengths of concretes made with crushed rock and gravel. However, if the mixes with equal workability are considered, the lower water requirement of smooth aggregates lowers the water-cement ratio of the paste, which compensates the effect of lower bond at low water-cement ratios (Neville, 2003, Mindess et al., 2003).

3.4.2 Effects of Maximum Aggregate Size

Maximum size of aggregate has influence on strength, workability, shrinkage and permeability (Quiroga and Fowler, 2003). Change in the maximum size of well graded aggregate of a given mineralogy have two conflicting effect on the strength of concrete. For a given workability and cement content, mixtures with coarser aggregates demand less mixing water, and therefore, the water-cement ratio can be lowered with a consequent increase in the strength because of the decrease in specific surface area (Figure 3.15). However, the amount of water reduction is not linear with the increase in aggregate size. For instance, increasing maximum aggregate size from $3/8$ in. to $2\,1/2$ in. reduces water requirement for a constant workability, the corresponding decrease in water-cement ratio maybe at most 15%. In contrast, with larger aggregate sizes, strengths tend to decrease because of the reduction in bond area and increase in internal stress (Neville, 20003, Mindess et al., 2003).

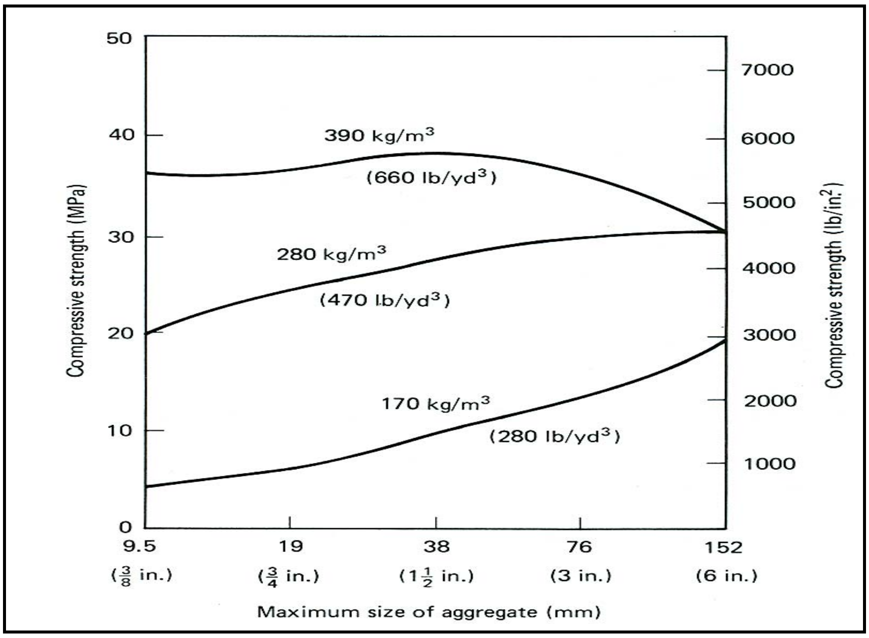

Figure 3.15 Influence of aggregate size on 28-day compressive strength of concretes with different cement contents (After Mindess et al., 2003).

Cordon and Gillespie (1963) investigated the effects of maximum aggregate size, falling between 3 in. and No.4 range with different water-cement ratios of 0.40, 0.55 and 0.70, on the 28 day compressive strengths (see Figure 3.16). The results indicated that the effects of maximum aggregate size are greater at high strength levels for a water-cement ratio of 0.40. In addition, it has noticeable effects at moderate strength levels for a water-cement ratio of 0.55. However, it does not have much effect in the case of low strength level for a water-cement ratio of 0.70. This is because of the fact that at lower water-cement ratios the reduced porosity of interfacial transition zones begins to play an important role in the concrete strength.

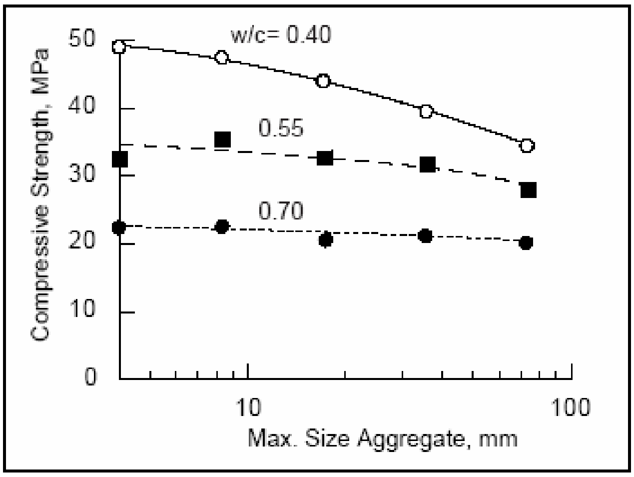

Figure 3.16 Effect of maximum size aggregate on concrete strength for three water-cement ratios (After Cordon and Gillespie, 1963).

Lewis (1961) and Macnaughton (1961) stated that the use of large aggregate sizes have greater advantage at lower strength levels which confirm the results of Cordon and Gillespie (1963).

Lewis (1961) also found the following results for the cylindrical samples for same cement content and slump but varying in maximum aggregate size:

- at the same water-cement ratio, strength decreases as the maximum aggregate size increases,
- provided that the strength level is maintained constant, the water-cement ratio decreases as the maximum aggregate size increases,
- at the same cement content, water-cement ratio decreases hence the strength increases as the maximum size of aggregate increases in the concrete.

3.4.3 Effects of Gradation

Gradation or the particle size distribution also affects some of the characteristics of concrete i.e., packing density, voids content, and consequently, workability, segregation, durability and pumpability (Quiroga and Fowler, 2003).

Tests performed by Shacklock (1954) as cited by Neville (2003) showed that, for a given aggregate-cement and water-cement ratio, mixes with lower fine content in the case of gap-graded aggregate have higher workability then mixes with continuously graded aggregates. However, omission of size fractions can lead to severe segregation problems in mixes of high workability ranges. Therefore, gap grading is recommended primarily for stiff mixes of very low workability which are to be compacted by vibration. In addition, gap graded mixes require close control in handling to prevent segregation (Mindess et al., 2003). There are different opinions for the effects of gradation on the strength of concrete. For instance, Shilstone (1990) and Neville (2003) claim that both well graded and poorly graded mixtures can be used to achieve the same strength level.

Similarly, according to McIntosh (1957), at a fixed aggregate-cement ratio, approximately the same workability and strength can be achieved for gap or continuously graded mixes by adjusting the fine aggregate content. However, Brodda and Weber (1977) as cited by Neville (2003) reported a slight negative influence of gap grading on strength.

CHAPTER 4

EXPERIMENTAL STUDY

4.1 Experimental Program

The objective of this study is to investigate the relationships between aggregate shape parameters and concrete strength using digital imaging techniques. In this respect, two aggregate types of the same source, namely, natural and crushed aggregates were used in preparing concrete specimens. Using these aggregates, well and gap graded mixtures were prepared at two different maximum aggregate sizes. A total of 8 different concrete mix proportions with 5 replicates were prepared. The experimental program resulted in a total of 40 cubic specimens prepared at a selected water-cement (w/c) ratio. After the compressive strength tests, each specimen was cut into 4 pieces of equal thickness along the direction parallel to the applied load. This process resulted in 6 cross sectional surfaces which were numbered from left to right and then converted into a digital form using a digital flatbed scanner. Subsequently, for each specimen three images from the six cross sectional surfaces were used to determine the various aggregate shape parameters. Finally, the relationships between the concrete strength and the aggregate shape parameters for retained No.8 were investigated using various statistical methods.

4.2 Material Properties

This section presents several chemical and physical properties of concrete used in this study.

4.2.1 Cement

The cement used in the mixtures was a typical portland cement CEM I 42.5R which complies with the ASTM Type 1 cement specifications. The physical properties and the chemical composition of the selected cement used in this study are presented in the below tables.

Table 4.1 Physical properties of portland cement.

Property	Value
Specific Gravity	3.18
Blaine Fineness (g/cm^2)	2982
Normal Consistency (%)	27.0
Initial Setting Time (min.)	158
Final Setting Time (min.)	225
Soundness (mm)	0.7

Table 4.2 Chemical composition of portland cement.

Chemical Composition	%
CaO	67.01
SiO_2	18.90
Al_2O_3	4.74
Fe_2O_3	3.03
MgO	1.76
SO_3	2.88
K_2O	0.70
Na_2O	0.51

4.2.2 Aggregates

Aggregates used in this investigation were obtained from Erişsan Ready Mix Concrete Company. Blended aggregates obtained had a maximum size of 1-2 inches, and were used in their present condition after sieving. These aggregates were termed as *natural* throughout this investigation. The other aggregate set was cobbles from the same source having around 3-4 in. size. These aggregates were crushed in the laboratory into smaller sizes before forming the necessary gradation and were termed as *crushed* aggregates.

The natural aggregates were separated into size fractions which consist of 4 coarse aggregate sizes and one fine aggregate size as tabulated in Table 4.3.

Table 4.3 Size fractions of natural aggregates.

Passing From	Retained on	Type
1 in.	$\frac{3}{4}$ in.	Coarse
$\frac{3}{4}$ in.	$\frac{1}{2}$ in.	Coarse
$\frac{1}{2}$ in.	$\frac{3}{8}$ in.	Coarse
$\frac{3}{8}$ in.	No.4	Coarse
No.4	No.8	Fine

Subsequently, specific gravity and water absorption (ASTM C 127-88 and C 128-88) values for each size fraction were determined according to the relevant standards. The results are presented in Table 4.4.

Table 4.4 Specific gravity and absorption of natural aggregates.

Property	Aggregate Size Fractions				
	1 in. - $\frac{3}{4}$ in.	$\frac{3}{4}$ in. - $\frac{1}{2}$ in.	$\frac{1}{2}$ in. - $\frac{3}{8}$ in.	$\frac{3}{8}$ in. – No.4	No.4 - No.8
Specific Gravity	2.63	2.62	2.62	2.58	2.52
Absorption (%)	1.81	2.09	2.52	2.94	3.56

The resistance against abrasion for natural aggregates was tested by performing Los Angeles Abrasion Test in accordance with ASTM C 131-89. C type sample of ASTM C 131-89 procedure was selected for testing. The particle size distribution of C type sample is presented in Table 4.5.

Table 4.5 Particle size distribution of C type sample according to ASTM C 131- 89.

Amount (kg)	Passing from	Retaining on
2.5	$\frac{3}{8}$ in.	$\frac{1}{4}$ in.
2.5	$\frac{1}{4}$ in.	No.4

After the Los Angeles test, the loss after 500 revolutions was determined as 26%. In addition, the ratio of the loss after 100 revolutions to the loss after 500 revolution was found as 0.208, which indicates that the natural aggregates have uniform hardness according to ASTM C 131-89 as the ratio did not exceed 0.200 significantly.

As mentioned previously, the crushed aggregates were produced by crushing big aggregates into smaller sizes using the laboratory mechanical crusher. The mechanical crusher used is shown in Figure 4.1.

Figure 4.1 Laboratory mechanical crusher used for crushing aggregates.

After the crushing operation, it was observed that most of the crushed aggregates produced by the mechanical crusher were flaky and elongated. These particles were crushed again by the Standard Marshall Compactor to reduce the percent of elongated and flaky particles. Subsequently, the crushed aggregates were sieved into the same size fractions as used for the natural aggregates. Similar to the procedure used for natural aggregates, specific gravity and water absorption of the each size fraction of the crushed aggregates were determined. The results are given in Table 4.6.

Table 4.6 Specific gravity and absorption of crushed aggregates.

Property	Aggregate Size Fractions				
	1 in. - $\frac{3}{4}$ in.	$\frac{3}{4}$ in. - $\frac{1}{2}$ in.	$\frac{1}{2}$ in. - $\frac{3}{8}$ in.	$\frac{3}{8}$ in. – No.4	No.4 - No.8
Specific Gravity	2.80	2.80	2.79	2.79	2.76
Absorption (%)	0.88	0.84	1.01	1.52	1.50

As it was performed for natural aggregates, Los Angeles Abrasion Test was also conducted in order to obtain the abrasion resistance of the crushed aggregates. The C type sample procedure was again preferred and the loss after 500 revolutions was determined as 16% (see Table 4.5). The ratio of the loss after 100 revolutions to loss after 500 revaluations was determined as 0.213. As the aggregate is assumed to have a uniform hardness if the above ratio does not greatly exceed 0.200 according to ASTM C 131-89, the natural aggregates under consideration were also accepted to have a uniform hardness.

4.2.3 Mixing Water

The mixing water obtained from the laboratory was assumed to be free from oil, organic materials and alkaline.

4.2.4 Crushed Marble

Crushed marble (mosaic) was used for the portion of fine aggregates passing No.8 sieve in all the prepared mixtures. Samples used to determine the properties of crushed marble were obtained according to ASTM C 702-87. Particle size distribution (ASTM C 136-92), specific gravity and water absorption characteristics (ASTM C 128-88) were determined according to their relevant standards. The results are given in the tabular form in Table 4.7 and Table 4.8.

Table 4.7 Sieve analysis of crushed marble.

Sieve Size	Cumulative Percentage Passing
No.8	100
No.16	59.5
No.30	10.5
No.50	6.8
No.100	4.6
< No.100	0

Table 4.8 Specific gravity and absorption of crushed marble.

Property	Determined as
Specific Gravity	2.64
Absorption (%)	1.16

4.2.5 Limestone Powder

Limestone powder (LP) was used as a fine material (5 µm average diameter) in all the mixes. Limestone powder is a by product of marble extraction with a CaCO3 content of 98%. The physical properties and chemical analysis result are presented in Table 4.9 and Table 4.10, respectively. Figure 4.2 also shows the particle size distribution of the limestone powder used in this study.

Table 4.9 Physical properties of limestone powder.

Property	Determined as
Specific Gravity	2.70
Specific SA (sq.m/g)	1.60

Table 4.10 Chemical composition of limestone powder.

Chemical Composition	%
CaO	54.97
SiO_2	0.01
Al_2O_3	0.02
Fe_2O_3	0.05
MgO	0.64
Loss on Ignition	44.31

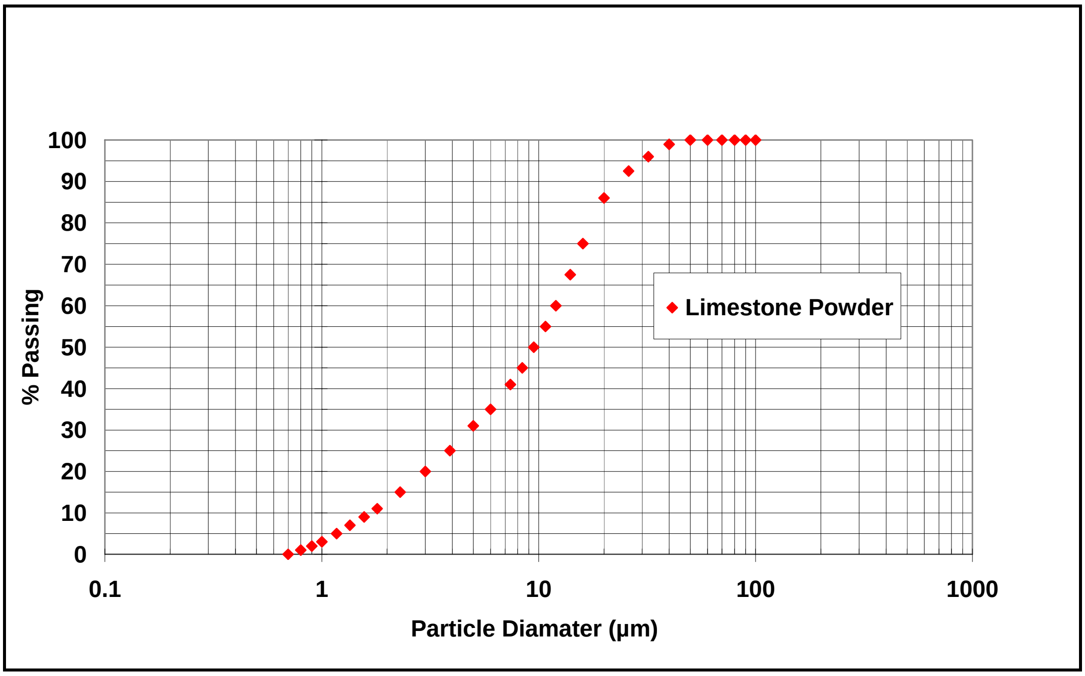

Figure 4.2 Particle size distribution of limestone powder.

4.3 Mix Design

As it can be seen in Table 4.11, 8 different concrete mix proportions of the same water-cement ratio were prepared at two levels of maximum aggregate size, (d_{max}), gradations (*well* and *gap*), and aggregate types (*natural* and *crushed*). The water-cement ratio of the mixes was selected as 0.80 in order to maintain a certain workability level. The d_{max} levels were selected 1 inch and ½ inch. Each mix proportion was studied with five replicates, as a result, a total of 40 specimens were prepared.

The specimens were coded with three indexes referring to their aggregate types, gradations and d_{max} values as shown in Table 4.11.

- The first index corresponds to aggregate type (C for *crushed* and N for *natural*).
- The second index corresponds to gradation type (W for *well gradation* and G for *gap gradation*).
- The third index corresponds to d_{max} value (25 for d_{max} *of 1 in.* and 13 for d_{max} *of ½ in.*).

Table 4.11 Concrete mix properties.

Mixture Code	Aggregate Type	Gradation Type	d_{max} (inch)
CG13	Crushed	Gap Gradation	½
CW13	Crushed	Well Gradation	½
CG25	Crushed	Gap Gradation	1
CW25	Crushed	Well Gradation	1
NG13	Natural	Gap Gradation	½
NW13	Natural	Well Gradation	½
CG25	Natural	Gap Gradation	1
CW25	Natural	Well Gradation	1

The same gradations were used for the same d_{max} aggregates regardless of the aggregate types. Hence, the following 4 different gradations were obtained from 8 different mixes:

- d_{max} of 1 inch with well gradation,
- d_{max} of 1 inch with gap gradation,
- d_{max} of ½ inch with well gradation,
- d_{max} of ½ inch with gap gradation.

Well graded mixes were constructed by fitting the gradation curves to the Fuller's maximum density curve as much as possible. Fuller's maximum density curve was proposed in order to obtain ideal gradation for the maximum density. The equation for Fuller's maximum density curve is:

$$P = 100(\frac{d}{D})^{0.5} \tag{4.2}$$

where P = % finer than the sieve size; d = aggregate size being considered and D = maximum aggregate size to be used.

The gap graded mixes were produced by eliminating the intermediate sizes during the preparation of gradations. The omitted particles were the sizes between No.4 and No. $\frac{3}{4}$ for d_{max} of 1 inch and No.4 and No. $\frac{3}{8}$ for d_{max} of $\frac{1}{2}$ inch.

The particle size distribution of the well and gap graded mixes, and the Fuller's maximum density curve for d_{max} of 1 in. and $\frac{1}{2}$ in. are illustrated in Figure 4.3 and Figure 4.4, respectively.

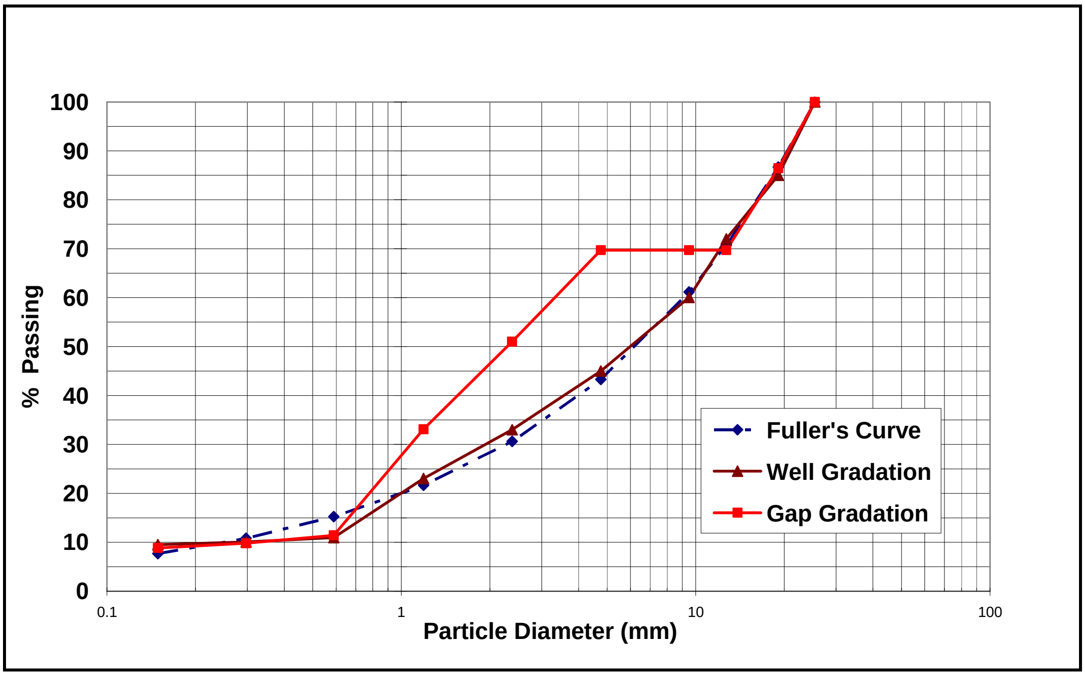

Figure 4.3 Particle size distributions for the well and gap graded mixtures, and the Fuller's maximum density curve at d_{max} = 1 inch.

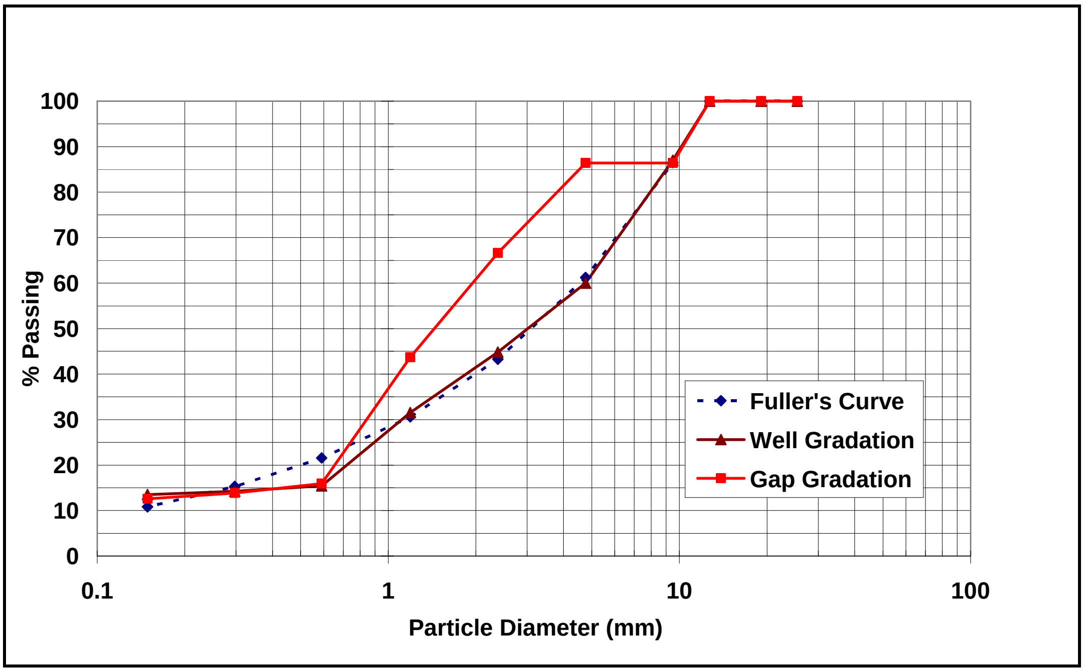

Figure 4.4 Particle size distributions for the well and gap graded mixtures, and the Fuller's maximum density curve at d_{max} = ½ inch.

4.4 Preparation of Concrete Specimens

The mixes for concrete specimens were prepared in accordance with the ASTM C 192-90a using a mechanical mixer. The ambient temperature during mixing ranged from 18Cº - 22Cº. Slump test were performed according to the ASTM C 143-90a. The mixes used in slump test were returned to the original batches and remixed thoroughly to maintain their uniformity. The mixes were than cast into 15x15 cm cubes for subsequent curing. Furthermore, the unit weight of mixes was determined according to ASTM C 138-92. Fresh concrete properties of the mixes are shown in Table 4.12. Mixture proportions used are shown in Table 4.13 and Table 4.14.

Table 4.12 Fresh properties of concrete mixtures.

Mixture Code	Slump (cm)	Unit Weight (kg/m^3)
CG13	0.5	2305
CW13	2.5	2382
CG25	5	2335
CW25	13.5	2406
NG13	1	2222
NW13	6	2264
NG25	15	2246
NW25	17	2325

According to fresh properties of the mixtures the following observations can be made:

- well graded mixtures increased the slump,
- as the maximum aggregate size increases, slump also increases,
- natural aggregates increased the slump of mixtures when compared to crushed aggregates.

Table 4.13 Mixture proportions at d_{max} = 1 inch.

Material	Well Graded Mixtures			Gap Graded Mixtures		
	Aggregate Ratio	S.S.D Weight (kg/m^3)		Aggregate Ratio	S.S.D Weight (kg/m^3)	
		Crushed	Natural		Crushed	Natural
1 in.	0.15	296.7	278.7	0.14	267.8	251.5
¾ in.	0.13	257.1	241.5	0.17	331.6	311.5
½ in.	0.12	235.6	221.2	0.00	0.0	0.0
⅜ in.	0.15	296.6	274.2	0.00	0.0	0.0
No.4	0.12	234.0	213.5	0.19	364.6	332.6
Crushed Marble	0.25	459.3	459.3	0.44	824.7	824.7
LP	0.08	157.8	157.8	0.07	127.8	127.8
Cement	-	250.0	250.0	-	250.0	250.0
Water	-	200.0	200.0	-	200.0	200.0

Table 4.14 Mixture proportions at d_{max} = ½ inch.

Material	Well Graded Mixtures			Gap Graded Mixtures		
	Aggregate Ratio	S.S.D Weight (kg/m³)		Aggregate Ratio	S.S.D Weight (kg/m³)	
		Crushed	Natural		Crushed	Natural
½ in.	0.13	256.2	240.6	0.14	275.9	259.1
⅜ in.	0.27	532.1	492.1	0.00	0.0	0.0
No.4	0.15	295.8	269.9	0.20	386.2	352.4
Crushed Marble	0.33	612.4	612.4	0.57	1055.9	1055.9
LP	0.12	226.2	226.2	0.10	188.6	188.6
Cement	-	250.0	250.0	-	250.0	250.0
Water	-	200.0	200.0	-	200.0	200.0

4.5 Compressive Strength Tests

Compressive strength tests were carried out by universal testing machine of 200 ton capacity. Because of the sample preparation and the instrumentation process, the compressive strength tests were scheduled at the 80th day of curing. In this study, the curing time of the specimens was not considered as significant experimental variable. Hence, it was assumed that testing all the specimens under the same conditions and the time of curing could not affect possible relationships between the compressive strength and the aggregate shape properties. The compressive strengths of the specimens, mean and coefficient of variation values for mixtures are tabulated in Table 4.15.

Table 4.15 Compressive strength test results of the specimens.

Mixture	Specimen	Compressive Strength (MPa)	Mixture	Specimen	Compressive Strength (MPa)
CG13	CG13-1	29.5	NG13	NG13-1	23.8
	CG13-1	32.6		NG13-2	24.8
	CG13-3	30.2		NG13-3	24.9
	CG13-4	31.9		NG13-4	24.6
	CG13-5	29.4		NG13-5	23.5
	Mean	*30.7*		*Mean*	*24.4*
	C.O.V.	*0.05*		*C.O.V.*	*0.03*
CW13	CW13-1	32.0	NW13	NW13-1	26.9
	CW13-2	32.2		NW13-2	28.0
	CW13-3	30.8		NW13-3	28.5
	CW13-4	31.6		NW13-4	28.3
	CW13-5	32.3		NW13-5	26.0
	Mean	*31.8*		*Mean*	*27.5*
	C.O.V.	*0.02*		*C.O.V.*	*0.04*
CG25	CG25-1	26.5	NG25	NG25-1	26.7
	CG25-2	26.9		NG25-2	24.9
	CG25-3	26.6		NG25-3	24.7
	CG25-4	25.6		NG25-4	26.1
	CG25-5	25.2		NG25-5	24.6
	Mean	*26.2*		*Mean*	*25.4*
	C.O.V.	*0.03*		*C.O.V.*	*0.04*
CW25	CW25-1	30.1	NW25	NW25-1	22.9
	CW25-2	29.8		NW25-2	25.9
	CW25-3	28.6		NW25-3	28.0
	CW25-4	29.9		NW25-4	28.3
	CW25-5	26.0		NW25-5	27.6
	Mean	*28.9*		*Mean*	*26.6*
	C.O.V.	*0.06*		*C.O.V.*	*0.08*

4.6 Preparation of Specimens for Image Processing

After the compressive strength tests, each specimen was cut into 4 equal pieces parallel to the applied load direction using a circular diamond saw as shown in Figure 4.5.

Figure 4.5 Process of cutting of the specimens by diamond saw.

As depicted in Figure 4.6, the cutting process produced 6 cross sectional surfaces for each test specimen. These cross sectional surfaces were numbered from left to right. An HP flatbed scanner was used to acquire digital image of each cross sectional surface. The resolution of the scanner was set to 150 dpi in order to keep the file size moderate for further processing and analysis. The digital images were stored in gray scale colors in which every pixel has a color depth ranging from 0 to 255.

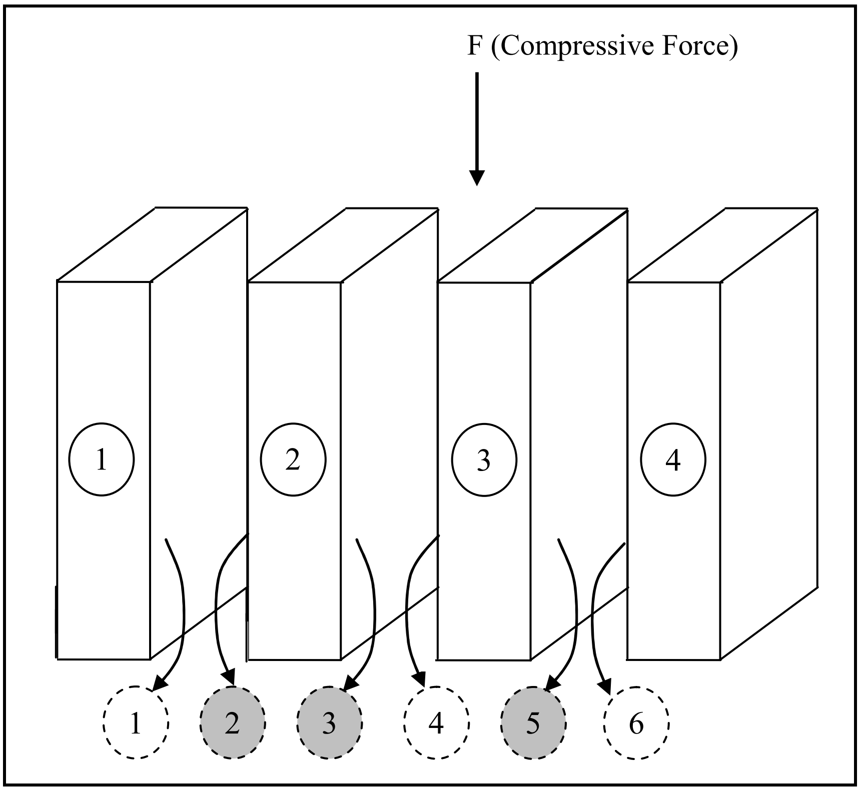

Figure 4.6 Representation of cross sectional pieces and surfaces.

The names of the cross sectional images were coded with 5 indexes referring to their aggregate types, gradations, d_{max} values, replication numbers and cross sectional numbers as follows:

- the first index corresponds to aggregate type (C for *crushed* and N for *natural*),
- the second index corresponds to gradation type (W for *well gradation* and G for *gap gradation*),
- the third index corresponds to d_{max} (25 for d_{max} of 1 in. and 13 for d_{max} of $\frac{1}{2}$ in.),
- the fourth index corresponds to replication number (this index varies between 1 and 5),
- the fifth index corresponds to cross section number to which the image belongs (this index varies between 1 and 6).

Gray scale images for cross sections CG13-2-5 and NG13-4-3 are shown in Figure 4.7 and Figure 4.8, respectively.

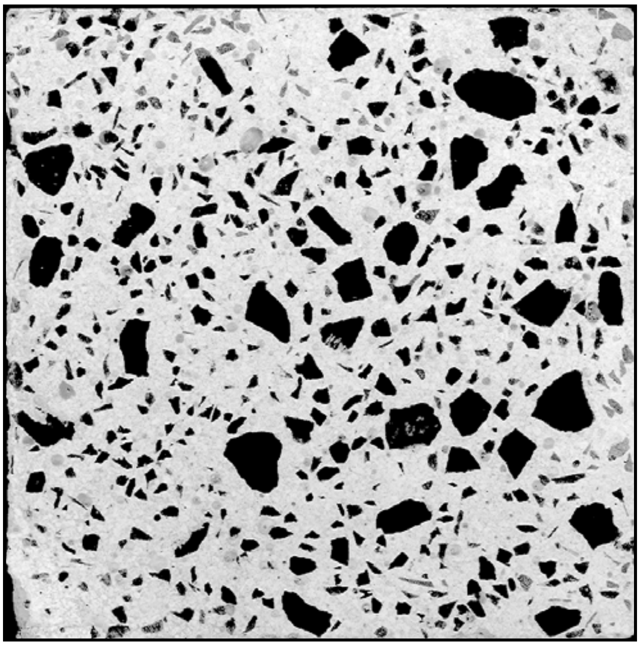

Figure 4.7 A gray scale image for cross section CG13-2-5.

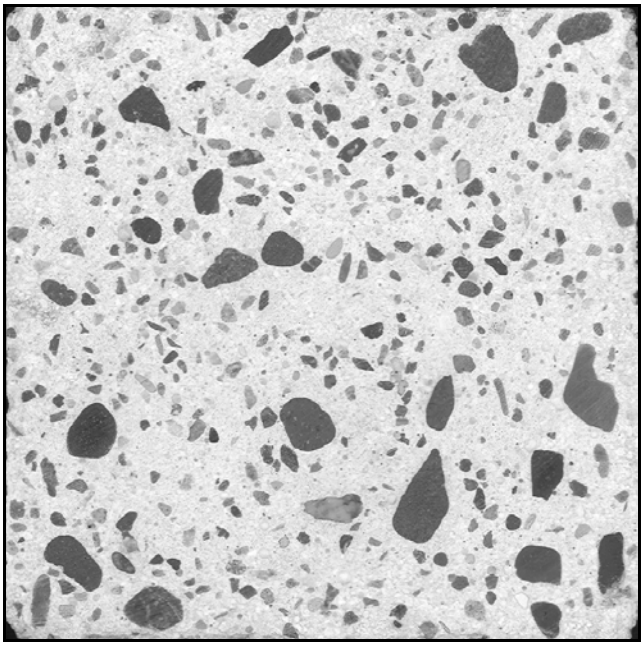

Figure 4.8 A gray scale image for cross section NG13-4-3.

In the analyses of relationships between the compressive strength and the aggregate shape properties, only those images corresponding to the 2nd, 3rd and 5th cross sectional surfaces were considered hence eliminating the duplication of analyses for the overlapped cross sections.

In the following chapter, the procedures used to determine the aggregate shape parameters and the methods of analysis for the aforementioned relationships are discussed.

CHAPTER 5

DATA ANALYSIS

5.1 Introduction

In this chapter, the procedures used for the determination of aggregate shape parameters are introduced. The method utilized for the elimination of particles finer than No.8 sieve (2.38 mm) is explained. The selection of representative shape parameters used in the statistical analyses is discussed accordingly.

5.2 Determination of the Aggregate Shape Parameters

In the first stage of determining the aggregate shape parameters, the thresholding operation was applied in order to convert the grayscale cross sectional images to binary images which contain particle regions with pixel values of 1 and background regions with pixel values of 0. The *aggregate analyzer* program written in LabVIEW (Laboratory Virtual Instrumentation Engineering Workbench) environment was utilized in this application. The user interface of the *aggregate analyzer* program is presented in Figure 5.1.

The *Input Image File Path* box shown in Figure 5.1 demonstrates the file path of the grayscale image to be analyzed. The input grayscale images can be thresholded by manually or automatically. The selection of the threshold method is chosen under the *Manual/Auto Threshold* label by the user.

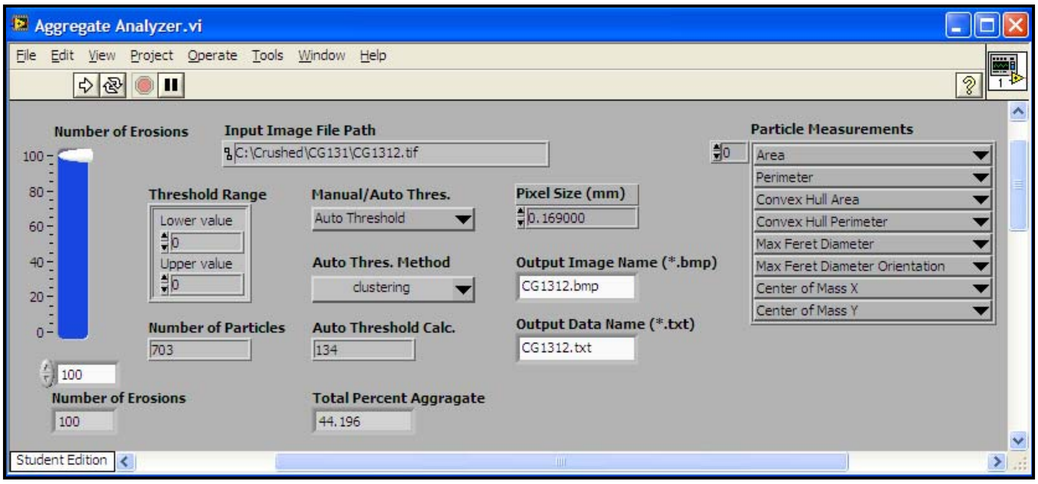

Figure 5.1 User interface of *aggregate analyzer* program.

The *Input Image File Path* box shown in Figure 5.1 demonstrates the file path of the grayscale image to be analyzed. The input grayscale images can be thresholded by manually or automatically. The selection of the threshold method is chosen under the *Manual/Auto Threshold* label by the user.

The manual thresholding can be performed by using a single threshold value or two different threshold values. In the case of single threshold, the user defines the upper threshold limit and enters it into the *Upper Value* box under the *Threshold Range* label and the *Lower Value* box is left zero. For the multiple thresholds, the user defines the upper and lower limits of the threshold range in their corresponding input locations (*Lower Value* and *Upper Value* boxes). In either case of manual thresholding, the threshold upper and lower limits must be defined in their corresponding input boxes before the *aggregate analyzer* is run by the user.

In the automatic thresholding method, the *aggregate analyzer* has five different automatic threshold methods, namely clustering, entropy, metric, moments and inter-class variance. The *aggregate analyzer* program calculates the automatic threshold value according to the selected automatic threshold method before the particle analyses are performed.

The calculated threshold value is displayed to the user in the *Auto Threshold Calculation* box by the *aggregate analyzer* program and the thresholding operation is performed according to this value. In this study, clustering automatic threshold method was applied for all the gray scale digital images. Because of the fact that the thresholding is a subjective process, the resultant binary images may contain unwanted information such as noise particles, particles touching the border of images frames, overlapped particles, and particles with uneven borders. The separation function of the LabVIEW, a type of morphological operation, is used to remove this unwanted information in the thresholded binary images. The number of erosion-dilation cycles used by the separation function is specified under the *Number of Erosions* label before the *aggregate analyzer* is run by the user. The image obtained after the separation operation is called *separated binary image*.

Aggregate analyzer calculates various particle shape characteristics using the separated binary images. The aggregate shape parameters to be calculated are chosen under the *Particle Measurements* label before the program is run by the user. After the analyses of the input image, the separated binary image is also saved into the computer as ".bmp" file by *aggregate analyzer*. The results of particle analyses are also saved as ".txt" file. The filenames for the output ".bmp" and ".txt" files are entered in *Output Image Name* and *Output Data Name* boxes. The *aggregate analyzer* program also displays the calculated number of particles and the percent of aggregate area from the input image in *Number of Particles* and *Total Percent Aggregates* boxes, respectively. Examples of grayscale and separated binary images for each mix design combinations are presented in Appendix A. An example of ".txt" data file for cross section CW25-5-4 is also presented in Appendix B.

Figure 5.2 and Figure 5.3 illustrate the grayscale and the separated binary images for cross sections CW25-2-2 and NW25-1-3. Because of the convention used in the algorithm of *aggregate analyzer*, the aggregates appear in red instead of white in the separated binary images.

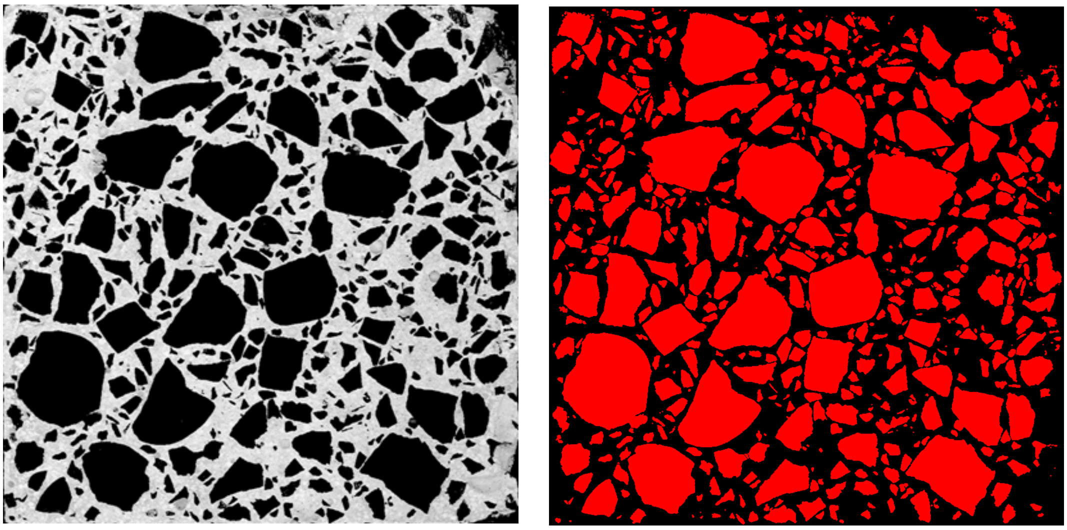

(a) (b)

Figure 5.2 A gray scale and its separated binary image for cross section CW25-2-2.

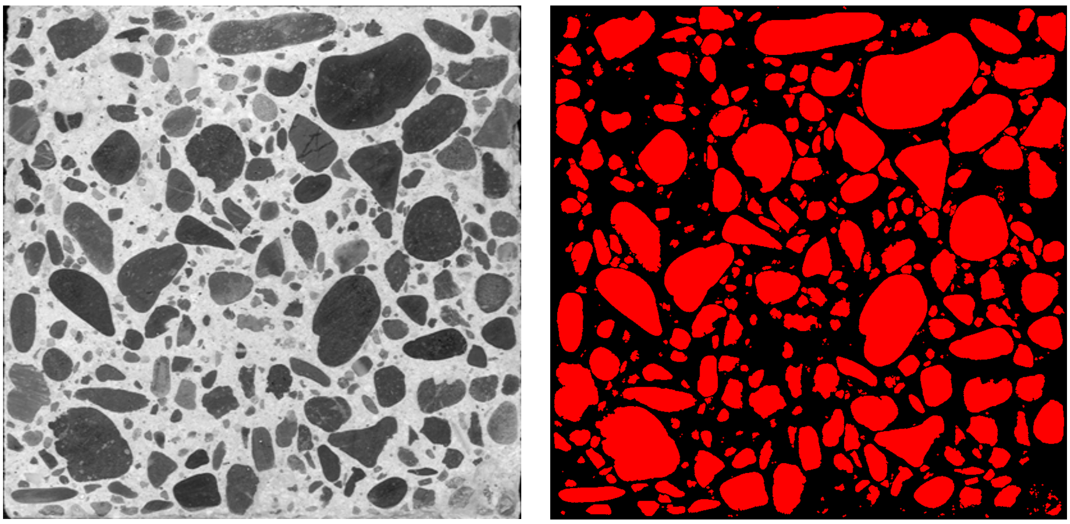

(a) (b)

Figure 5.3 A gray scale and its separated binary image for cross section NW25-1-3.

The following aggregate shape properties were determined in units of pixels by utilizing *aggregate analyzer* throughout this investigation:

- area,
- perimeter,
- convex area,
- convex perimeter,
- maximum Feret diameter,
- maximum Feret diameter orientation (in degrees),
- center of mass X coordinate,
- center of mass Y coordinate.

From the particle shape measurements presented above, the aggregate shape parameters listed in Table 5.1 were computed using a MATLAB script according to their corresponding formulations.

Table 5.1 Particle shape parameters and their corresponding formulations.

Parameter	Formulation
Angularity*	$\text{Angularity} = \left(\frac{\text{Perimeter}_{\text{convex}}}{\text{Perimeter}_{\text{ellipse}}}\right)^2$
Convexity Ratio	$\text{Convexity Ratio} = \frac{\text{Area}}{\text{Convex Area}}$
Fullness Ratio	$\text{Fullness Ratio} = \sqrt{\frac{\text{Area}}{\text{Convex Area}}}$
Roughness	$\text{Roughness} = \left(\frac{\text{Perimeter}}{\text{Perimeter}_{\text{convex}}}\right)^2$
Formfactor	$\text{Formfactor} = \frac{4\pi\text{Area}}{\text{Perimeter}^2}$

* The formulation for perimeter of equivalent ellipse is presented in Equation 3.16.

The elongation ratio, i.e. the ratio of *particle maximum dimension (length)* to *the maximum dimension in the plane perpendicular to the length (width)*, of particles was also calculated in MATLAB environment through the maximum Feret diameter orientation (θ) which is presented in Figure 5.4.

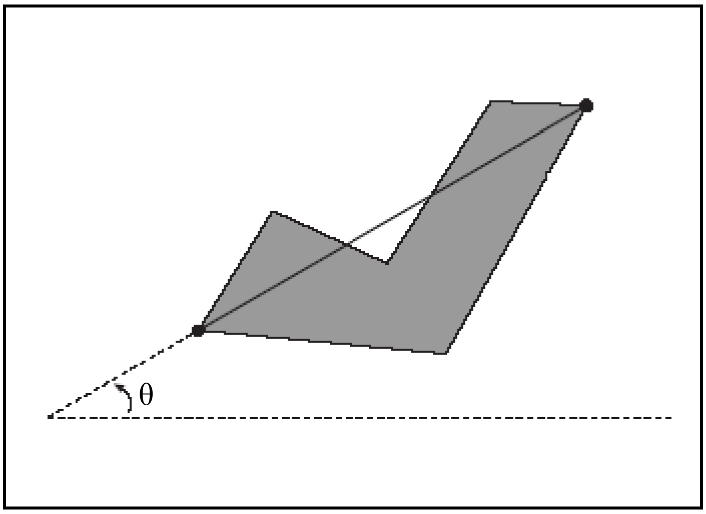

Figure 5.4 Maximum Feret diameter orientation (θ) (After NI Vision).

For that reason, the separated binary images obtained by utilizing *aggregate analyzer* were again analyzed by MATLAB software. By labeling, each aggregate of the separated binary images was rotated θ degree in the MATLAB environment in order to make the maximum Feret diameter parallel to the vertical axis as shown in Figure 5.5. Then, the elongation ratio of each aggregate was calculated in pixels as the ratio of the maximum vertical segment of the particle to the maximum horizontal segment of the particle.

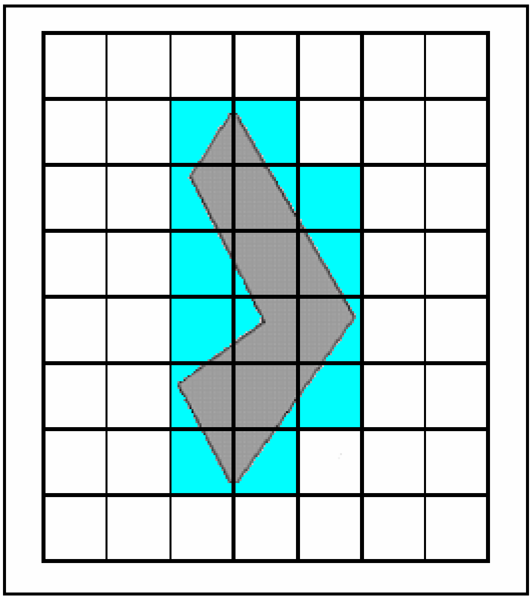

Figure 5.5 Illustration of particle elongation ratio.

It should be noted that LabVIEW runs in row-wise order whereas MATLAB runs in column–wise order when using matrices. For this reason, the separated binary images obtained by the *aggregate analyzer* program should be transposed before analyzing in the MATLAB environment in order to maintain the same order of aggregates listed in the ".txt" output file. Table 5.2 lists the calculated shape parameters from the digital image of cross sections that are used in the analyses of relationships between the compressive strength and the aggregate shape parameters.

Table 5.2 Calculated aggregate shape parameters to be used in analyses.

Particle Shape Property	Parameter
Roundness	Angularity
	Convexity Ratio
	Fullness Ratio
Surface Texture	Roughness
Form	Formfactor
	Elongation Ratio

MATLAB algorithm used for calculating the aggregate shape parameters are given in Table 5.2 of Appendix C.

The shape parameters shown in Table 5.2 were determined from the three cross sectional images of each specimen. The calculated parameters of the three frames belonging to the same concrete specimen were then combined to generate only 40 output data file for the entire specimen set.

Table 5.3 illustrates the values of particle shape parameters for various geometrical shapes shown in Figure 5.6. The minimum and the maximum parameter values are indicted by boldface numbers for each particle.

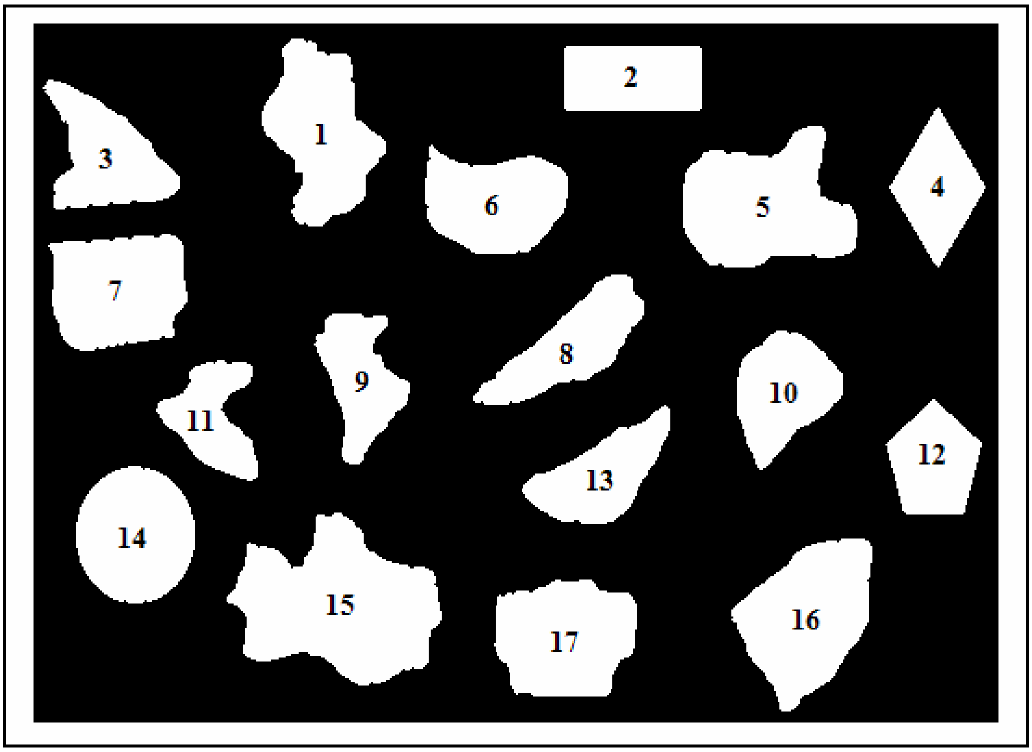

Figure 5.6 Illustration of various particle shapes.

Table 5.3 Values of the particle shape parameters for geometrical shapes shown in Figure 5.6.

Parameters	Particle Number																
	1	**2**	**3**	**4**	**5**	**6**	**7**	**8**	**9**	**10**	**11**	**12**	**13**	**14**	**15**	**16**	**17**
Area	4000	2586	2854	2290	4943	3335	3870	2765	2303	2722	1979	2227	2517	3715	6715	4431	3973
Perimeter	277.42	212.04	246.60	198.90	298.85	230.89	241.03	246.94	222.44	201.40	212.27	180.00	220.35	218.74	365.04	262.31	238.25
Convex Area	4691	2586	3315	2290	5639	3613	3968	2971	2833	2795	2432	2227	2675	3718	7917	4546	4122
Convex Perimeter	262.61	212.04	236.98	198.90	283.83	227.39	238.64	244.76	210.59	200.35	193.52	180.00	219.84	218.44	329.84	260.74	238.08
Maximum Feret Diameter	102.42	81.03	92.46	86.01	100.72	81.39	83.82	108.41	82.46	76.92	69.35	64.29	91.79	74.43	117.05	103.32	82.46
Maximum Feret Diameter Orientation	99.55	155.97	141.15	90.67	155.98	153.75	144.22	37.50	75.96	74.16	118.41	105.33	29.36	96.17	146.85	64.18	39.09
Angularity	1.12	1.08	1.44	1.23	1.27	1.18	1.17	1.06	1.37	1.13	**1.48**	1.12	1.13	**1.01**	1.26	1.11	1.13
Convexity Ratio	0.85	1.00	0.86	1.00	0.88	0.92	0.98	0.93	**0.81**	0.97	**0.81**	1.00	0.94	**1.00**	0.85	0.97	0.96
Fullness Ratio	0.92	**1.00**	0.93	**1.00**	0.94	0.96	0.99	0.96	**0.90**	0.99	**0.90**	**1.00**	0.97	**1.00**	0.92	0.99	0.98
Roughness	1.12	**1.00**	1.08	**1.00**	1.11	1.03	1.02	1.02	1.12	1.01	1.20	**1.00**	**1.00**	**1.00**	**1.22**	1.01	**1.00**
Formfactor	0.65	0.72	0.59	0.73	0.70	0.79	0.84	0.57	0.58	0.84	**0.55**	0.86	0.65	**0.98**	0.63	0.81	0.88
Elongation Ratio	1.94	**2.08**	1.46	1.62	1.22	1.36	**1.08**	2.92	1.61	1.31	1.21	1.28	2.28	1.15	1.26	1.56	1.11

It can be seen that, the variation in angularity ranges from 1.01 to 1.48, convexity ratio from 0.81 to 1.00, fullness ratio from 0.90 to 1.00, roughness from 1.00 to 1.22, formfactor from 0.55 to 0.98 and elongation ratio from 1.08 to 2.08. In spite of the significant change in the particle shapes, the changes in the convexity ratio and fullness ratio seems quite minor as compared to the other particles' shape parameters.

5.2 Elimination of Fine Aggregate Particles

As stated previously, the analyses of relationships between the strength and the shape parameters were performed only for those aggregates retained on No.8. This required the elimination of aggregate portions that are finer than No.8 before conducting the statistical analyses.

Before eliminating the finer aggregates, an effective particle size parameter that best simulates the passing of a particle through a sieve opening needs to be determined so that it can be used to perform a virtual sieving operation. For this purpose, the actual particle size distribution of the specimens was compared with the particle size distributions obtained using a) *area*, and b) *maximum Feret diameter* parameters.

Using the *area* parameter, the total pixel area of each particle was converted into the area in units of square millimeters given the fact that the resolution of the images was known in advance. Then, the area of each particle was compared to the area of sieve openings for a range of standard sieve sizes that were initially used in the laboratory. If the particle area is larger than the area of the sieve opening, the particle is assumed to retain on that sieve, and it is assumed to pass if its area is smaller.

Similarly, in the case of using the *maximum Feret diameter*, the maximum Feret diameter of particles in each specimen was converted into the unit of millimeters. Then, the maximum Feret diameter of each particle was compared to the sieve openings of a range of standard sieves sizes. If the particle maximum Feret diameter is larger than the standard sieve opening, the particle is assumed to retain on that sieve, and it is assumed to pass if its maximum Feret diameter is smaller.

Figure 5.7 illustrates the *actual gradation* and the calculated particle size distributions based on virtual sieving operation using the *area* and the *maximum Feret diameter* parameters.

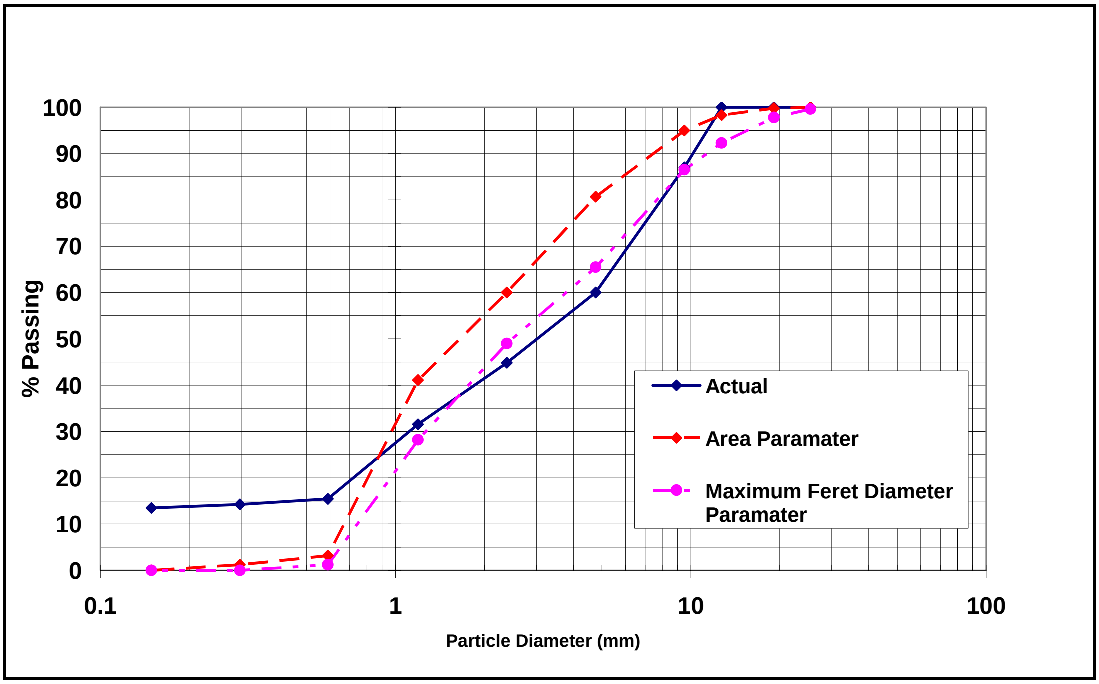

Figure 5.7 A plot of actual gradation curve and calculated particle size distribution curves based on *area* and maximum Feret diameter.

Once the particle size distributions was obtained based on the two parameters, the sum of the squares of the errors between the actual gradation and the estimated particle size distributions were calculated to identify which parameter provides the minimum sum of squares.

The error analysis showed that the calculated particle size distribution according to the *maximum Feret diameter* was better to represent the actual gradation curve for 26 out of 40 specimens.

For this reason, the *maximum Feret diameter* was selected as the best parameter describing the actual gradation curve of the specimens. Thus, the elimination of particles finer than No.8 sieve was carried out according to *maximum Feret diameter* parameter using the following procedure:

The resolution of the separated binary images was at 96 dpi in which a pixel corresponds to 0.256 mm. Since the opening of a No.8 sieve equals to 2.38 mm. which corresponds to approximately 9.3 pixels, particles with a maximum Feret diameter equal to or lower than 9.3 pixels were eliminated from the data file of each specimen.

MATLAB algorithms used for the abovementioned elimination process are presented in Appendix D.

5.3 Selection of the Representative Particle Shape Parameter Values

As a continuation of the process, a single representative particle shape parameter value to be used in the analyses was identified for *angularity*, *convexity ratio*, *fullness ratio*, *roughness*, *formfactor* and *elongation ratio* for each concrete specimen. This identification process was carried out using three different methods.

The two of these methods are based on the idea that the maximum relative frequency of parameter and its corresponding parameter value would have a dominant influence on the compressive strength of the concrete specimens. However, in the third method, the individual areas of aggregate particles with the assumption that, the aggregate particles with a larger surface area would have more influence on the compressive strength. These methods are explained in detail in the further sections.

5.3.1 Method Based on Parameter Maximum Relative Frequency, f_{max}

The first method was based on the relative frequency distribution of the particle shape parameters. The relative frequency histograms of the parameters were plotted by using 20 class intervals and the maximum relative frequency values (f_{max}) were selected from the histograms to use in the data analyses (see Figure 5.8).

5.3.2 Method Based on Parameter Value Corresponding to Maximum Relative Frequency, p_{fmax}

In the second method, the same procedure was applied, but this time the parameter value (p_{fmax}) corresponding to the maximum relative frequency was selected from the histogram as the representative value for the considered shape parameter.

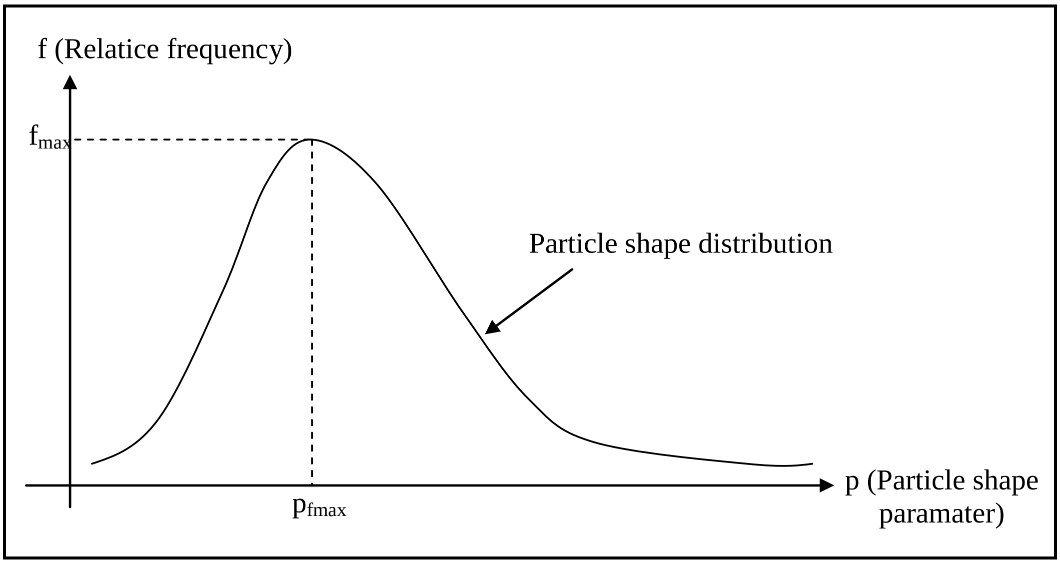

Figure 5.8 Typical relative frequency distribution of a parameter.

The figures Figure 5.9 through Figure 5.14 illustrate the relative frequency histograms of the particle shape parameters for the comparative evaluation of the specimens CW25-2 and NW25-1 whose binary images are presented in Figure 5.2 and Figure 5.3, respectively.

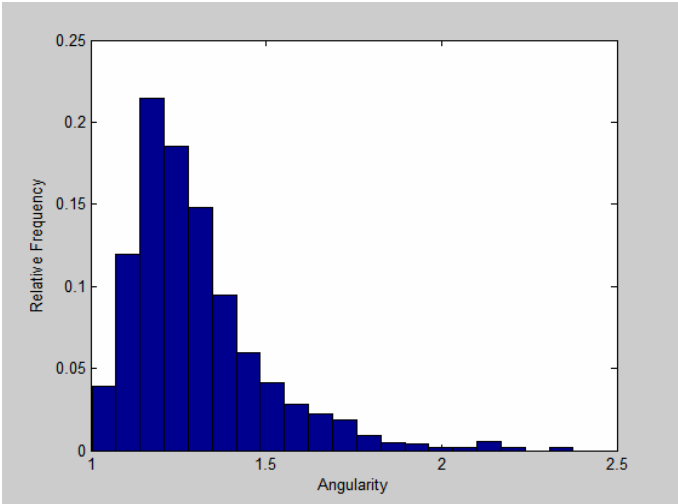

(a) CW25-2

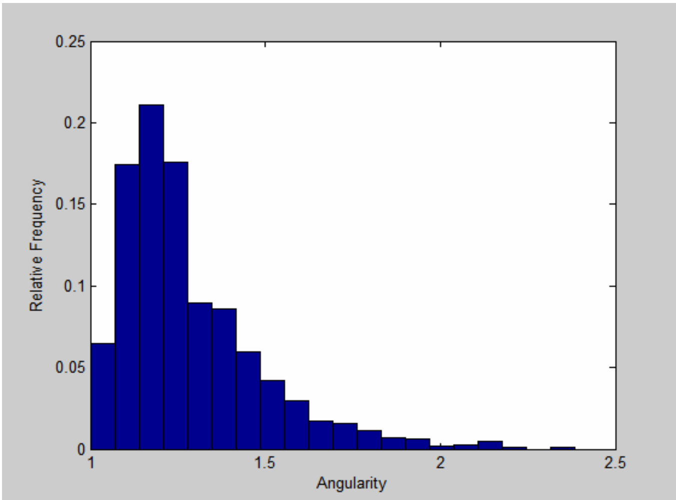

(b) NW25-1

Figure 5.9 Typical relative frequency histogram of *angularity*.

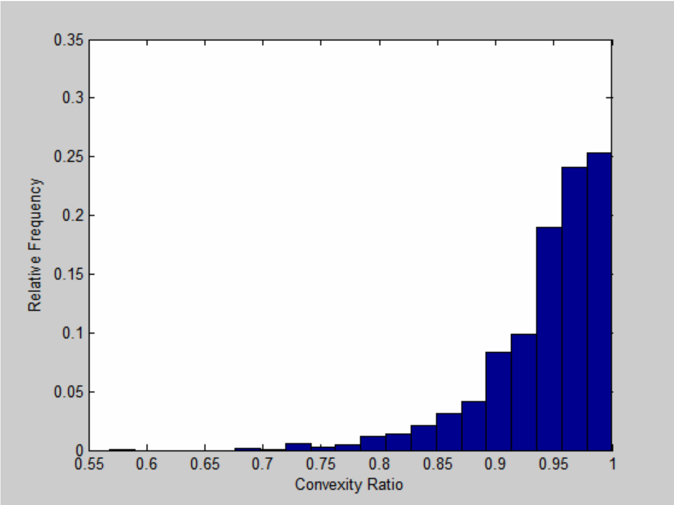

(a) CW25-2

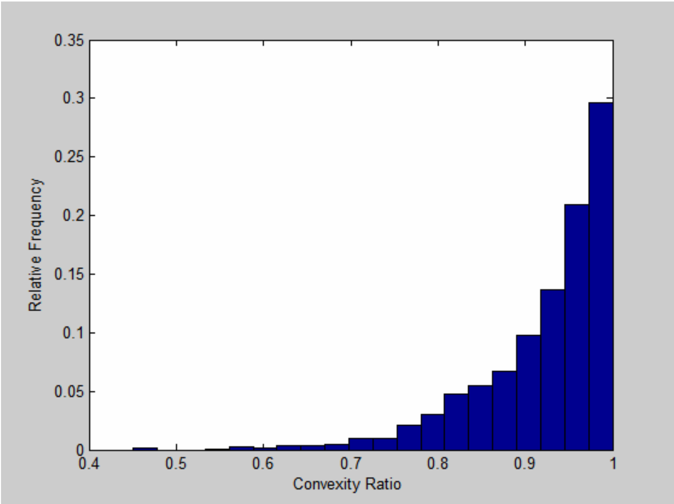

(b) NW25-1

Figure 5.10 Typical relative frequency histogram of *convexity ratio*.

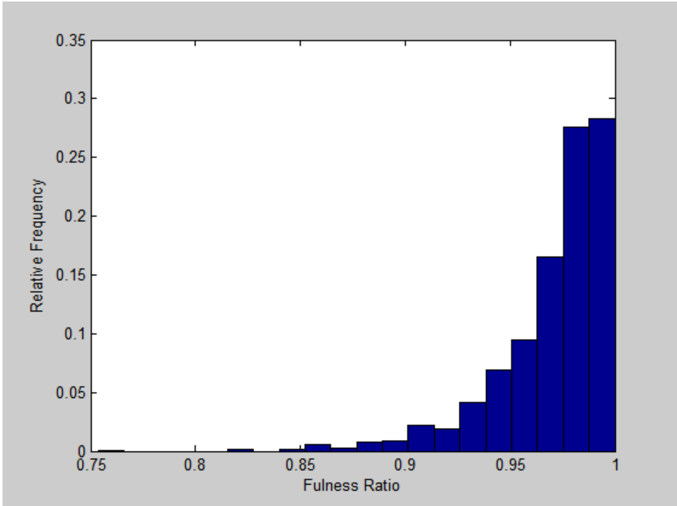

(a) CW25-2

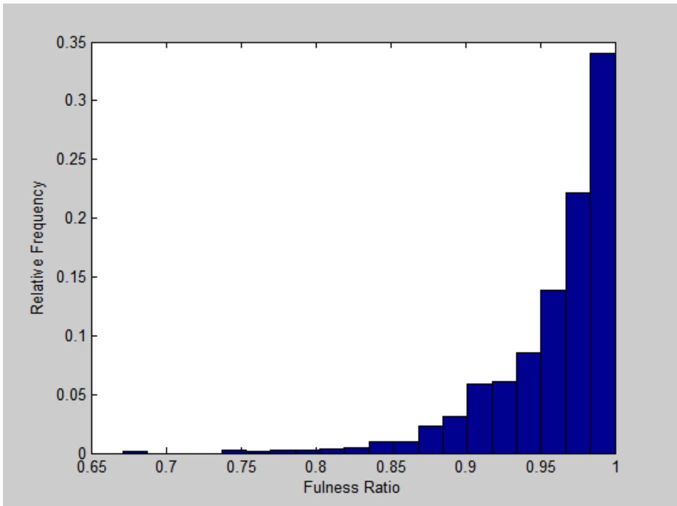

(b) NW25-1

Figure 5.11 Typical relative frequency histogram of *fullness ratio*.

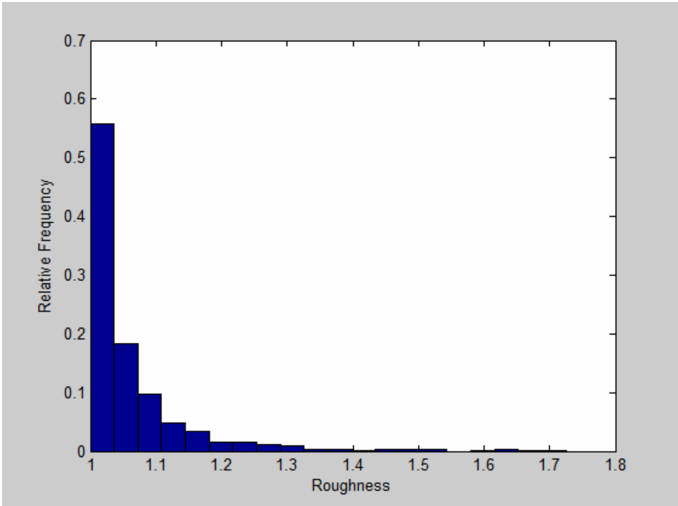

(a) CW25-2

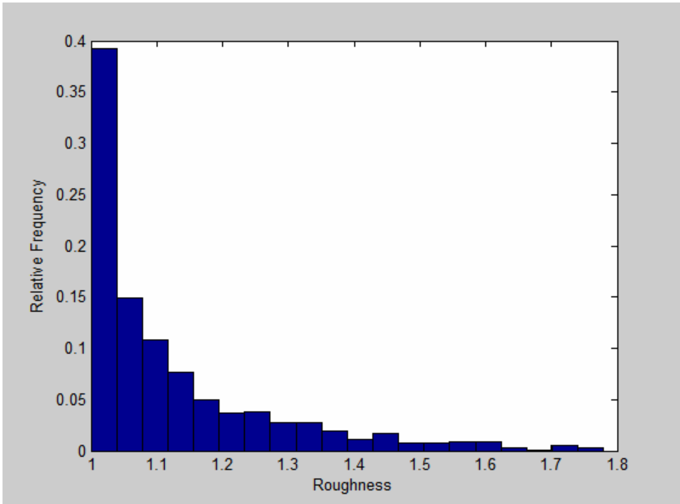

(b) NW25-1

Figure 5.12 Typical relative frequency histogram of *roughness*.

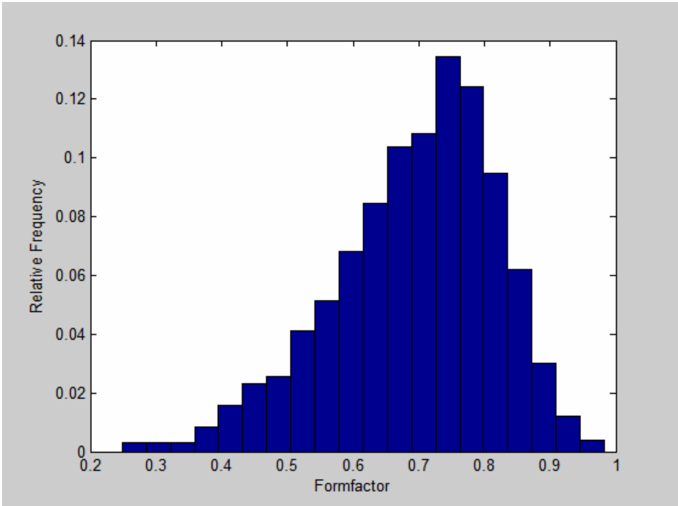

(a) CW25-2

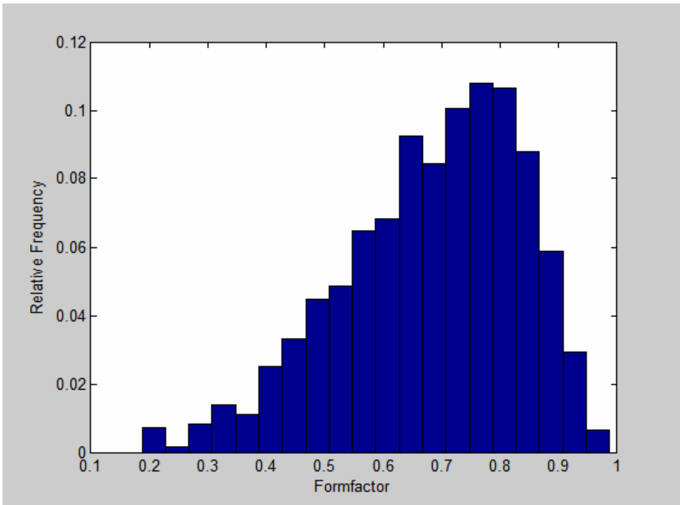

(b) NW25-1

Figure 5.13 Typical relative frequency histogram of *formfactor*.

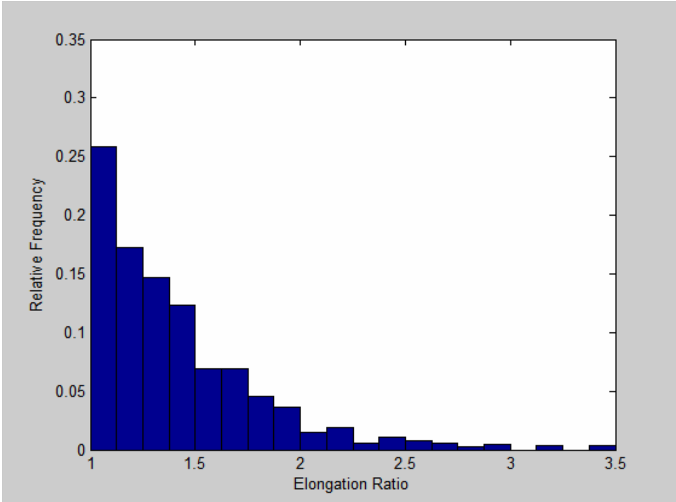

(a) CW25-2

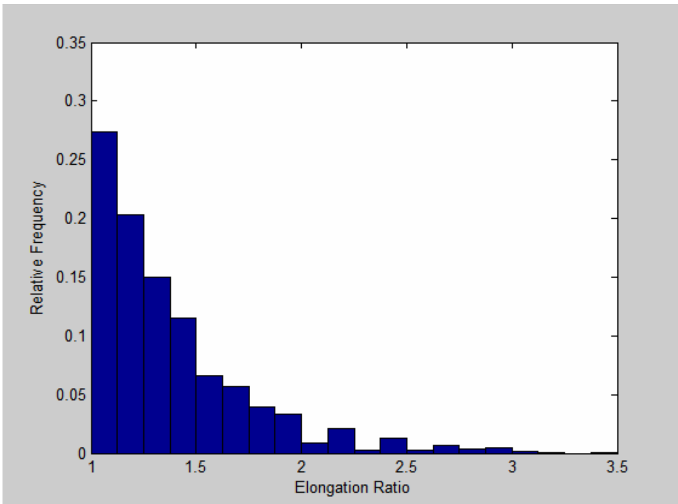

(b) NW25-1

Figure 5.14 Typical relative frequency histogram of *elongation ratio*.

The relative frequency histograms of the particle shape parameters for the specimens which the gray scale and separated binary images presented in Appendix A belongs to, are presented in Appendix E.

5.3.3 Method Based on Weighed Particle Area, A_w

In the third method, the representative particle shape parameter values were determined as the average of the considered parameter values for each aggregate by weighed individual areas as shown in Equation 5.1.

$$\text{Area Weighed Parameter of the Specimen} = \frac{\sum_{i=1}^{n} \text{Area}_i \text{Parameter}_i}{\sum_{i=1}^{n} \text{Area}_i} \tag{5.1}$$

where n = number of the aggregates in specimen; Area_i = area of the i^{th} aggregate and Parameter_i = considered parameter value of the i^{th} aggregate.

MATLAB algorithms used for the determination of the representative particle shape parameters are presented in Appendix F.

The following Table 5.4 through Table 5.10 represents the selected representative particle shape parameters for mixtures according to abovementioned methods.

Tablo 5.4 Selected representative particle shape parameters for mixtures prepared with crushed aggregates according to f_{max}.

Mixture	Specimen	Strength (Mpa)	Angularity	Convexity Ratio	Fullness Ratio	Roughness	Formfactor	Elongation Ratio
CG13	CG13-1	29.5	0.182	0.348	0.398	0.628	0.122	0.231
	CG13-2	32.6	0.216	0.289	0.319	0.597	0.130	0.234
	CG13-3	30.2	0.196	0.263	0.285	0.587	0.114	0.268
	CG13-4	31.9	0.194	0.298	0.341	0.584	0.123	0.258
	CG13-5	29.4	0.206	0.316	0.342	0.624	0.133	0.253
CW13	CW13-1	32.0	0.201	0.270	0.297	0.568	0.130	0.232
	CW13-2	32.2	0.209	0.245	0.266	0.627	0.131	0.279
	CW13-3	30.8	0.193	0.256	0.282	0.613	0.129	0.250
	CW13-4	31.6	0.208	0.228	0.248	0.608	0.131	0.250
	CW13-5	32.3	0.210	0.203	0.220	0.617	0.127	0.219
CG25	CG25-1	26.5	0.187	0.299	0.335	0.597	0.133	0.288
	CG25-2	26.9	0.183	0.335	0.373	0.554	0.126	0.295
	CG25-3	26.6	0.198	0.363	0.407	0.612	0.130	0.271
	CG25-4	25.6	0.187	0.293	0.320	0.562	0.130	0.262
	CG25-5	25.2	0.188	0.258	0.276	0.570	0.121	0.262
CW25	CW25-1	30.1	0.195	0.254	0.283	0.516	0.120	0.235
	CW25-2	29.8	0.214	0.254	0.283	0.559	0.135	0.259
	CW25-3	28.6	0.205	0.270	0.304	0.568	0.139	0.250
	CW25-4	29.9	0.196	0.242	0.261	0.552	0.121	0.260
	CW25-5	26.0	0.209	0.233	0.251	0.560	0.122	0.259

Table 5.5 Selected representative particle shape parameters for mixtures prepared with natural aggregates according to f_{max}.

Mixture	Specimen	Strength (MPa)	Angularity	Convexity Ratio	Fullness Ratio	Roughness	Formfactor	Elongation Ratio
NG13	NG13-1	23.8	0.185	0.302	0.326	0.440	0.105	0.278
	NG13-2	24.8	0.183	0.303	0.349	0.435	0.103	0.233
	NG13-3	24.9	0.222	0.287	0.312	0.439	0.125	0.289
	NG13-4	24.6	0.190	0.316	0.348	0.498	0.103	0.303
	NG13-5	23.5	0.202	0.375	0.404	0.507	0.105	0.294
NW13	NW13-1	26.9	0.214	0.278	0.309	0.453	0.119	0.273
	NW13-2	28.0	0.235	0.370	0.404	0.518	0.124	0.276
	NW13-3	28.5	0.212	0.321	0.355	0.497	0.124	0.275
	NW13-4	28.3	0.221	0.391	0.434	0.513	0.128	0.285
	NW13-5	26.0	0.213	0.413	0.454	0.530	0.128	0.263
NG25	NG25-1	26.7	0.202	0.277	0.297	0.455	0.100	0.292
	NG25-2	24.9	0.200	0.321	0.351	0.480	0.112	0.293
	NG25-3	24.7	0.194	0.300	0.322	0.457	0.108	0.281
	NG25-4	26.1	0.188	0.290	0.330	0.413	0.104	0.275
	NG25-5	24.6	0.205	0.303	0.328	0.444	0.095	0.260
NW25	NW25-1	22.9	0.211	0.297	0.341	0.393	0.108	0.273
	NW25-2	25.9	0.196	0.362	0.409	0.449	0.107	0.291
	NW25-3	28.0	0.224	0.292	0.316	0.422	0.110	0.273
	NW25-4	28.3	0.192	0.309	0.360	0.448	0.109	0.265
	NW25-5	27.6	0.219	0.269	0.284	0.458	0.109	0.246

Tablo 5.6 Selected representative particle shape parameters for mixtures prepared with crushed aggregates according to p_{fmax}.

Mixture	Specimen	Strength (Mpa)	Angularity	Convexity Ratio	Fullness Ratio	Roughness	Formfactor	Elongation Ratio
CG13	CG13-1	29.5	1.173	0.988	0.993	1.018	0.741	1.061
	CG13-2	32.6	1.173	0.990	0.994	1.018	0.757	1.058
	CG13-3	30.2	1.173	0.992	0.996	1.016	0.721	1.063
	CG13-4	31.9	1.170	0.988	0.993	1.020	0.694	1.061
	CG13-5	29.4	1.176	0.990	0.994	1.017	0.747	1.063
CW13	CW13-1	32.0	1.174	0.989	0.994	1.019	0.749	1.060
	CW13-2	32.2	1.168	0.991	0.995	1.019	0.782	1.063
	CW13-3	30.8	1.232	0.990	0.994	1.019	0.740	1.063
	CW13-4	31.6	1.175	0.973	0.985	1.020	0.750	1.063
	CW13-5	32.3	1.175	0.992	0.996	1.019	0.753	1.057
CG25	CG25-1	26.5	1.175	0.990	0.994	1.018	0.736	1.063
	CG25-2	26.9	1.164	0.989	0.994	1.015	0.704	1.063
	CG25-3	26.6	1.238	0.988	0.993	1.020	0.721	1.063
	CG25-4	25.6	1.239	0.990	0.994	1.020	0.738	1.063
	CG25-5	25.2	1.220	0.991	0.995	1.020	0.752	1.063
CW25	CW25-1	30.1	1.245	0.989	0.993	1.019	0.738	1.057
	CW25-2	29.8	1.175	0.989	0.994	1.018	0.744	1.063
	CW25-3	28.6	1.170	0.989	0.994	1.020	0.740	1.061
	CW25-4	29.9	1.234	0.990	0.994	1.020	0.713	1.060
	CW25-5	26.0	1.177	0.990	0.995	1.020	0.753	1.063

Table 5.7 Selected representative particle shape parameters for mixtures prepared with natural aggregates according to p_{fmax}.

Mixture	Specimen	Strength (MPa)	Angularity	Convexity Ratio	Fullness Ratio	Roughness	Formfactor	Elongation Ratio
NG13	NG13-1	23.8	1.107	0.989	0.994	1.019	0.744	1.056
	NG13-2	24.8	1.161	0.987	0.992	1.019	0.686	1.055
	NG13-3	24.9	1.172	0.989	0.994	1.020	0.778	1.059
	NG13-4	24.6	1.164	0.990	0.994	1.020	0.790	1.059
	NG13-5	23.5	1.170	0.988	0.993	1.020	0.777	1.062
NW13	NW13-1	26.9	1.162	0.990	0.995	1.020	0.773	1.061
	NW13-2	28.0	1.171	0.988	0.993	1.018	0.818	1.063
	NW13-3	28.5	1.169	0.989	0.994	1.020	0.775	1.056
	NW13-4	28.3	1.107	0.987	0.992	1.020	0.815	1.059
	NW13-5	26.0	1.168	0.987	0.992	1.019	0.807	1.062
NG25	NG25-1	26.7	1.173	0.990	0.994	1.020	0.822	1.058
	NG25-2	24.9	1.174	0.989	0.994	1.020	0.777	1.063
	NG25-3	24.7	1.101	0.990	0.994	1.020	0.812	1.059
	NG25-4	26.1	1.174	0.988	0.993	1.020	0.811	1.061
	NG25-5	24.6	1.157	0.989	0.994	1.020	0.826	1.050
NW25	NW25-1	22.9	1.176	0.986	0.992	1.020	0.767	1.063
	NW25-2	25.9	1.101	0.986	0.992	1.019	0.851	1.060
	NW25-3	28.0	1.177	0.989	0.994	1.020	0.696	1.061
	NW25-4	28.3	1.150	0.987	0.992	1.020	0.739	1.061
	NW25-5	27.6	1.175	0.991	0.995	1.020	0.804	1.055

Table 5.8 Selected representative particle shape parameters for mixtures prepared with crushed aggregates according to A_w.

Mixture	Specimen	Strength (MPa)	Angularity	Convexity Ratio	Fullness Ratio	Roughness	Formfactor	Elongation Ratio
	CG13-1	29.5	1.275	0.945	0.972	1.046	0.720	1.374
	CG13-2	32.6	1.266	0.940	0.969	1.060	0.713	1.396
	CG13-3	30.2	1.277	0.944	0.971	1.057	0.713	1.374
CG13	CG13-4	31.9	1.270	0.945	0.972	1.057	0.725	1.333
	CG13-5	29.4	1.277	0.946	0.972	1.049	0.717	1.384
	CW13-1	32.0	1.282	0.938	0.968	1.068	0.703	1.376
	CW13-2	32.2	1.292	0.940	0.969	1.050	0.705	1.398
CW13	CW13-3	30.8	1.276	0.942	0.970	1.050	0.711	1.394
	CW13-4	31.6	1.293	0.939	0.969	1.052	0.704	1.385
	CW13-5	32.3	1.289	0.940	0.969	1.055	0.702	1.403
	CG25-1	26.5	1.268	0.939	0.969	1.068	0.717	1.300
	CG25-2	26.9	1.263	0.937	0.968	1.073	0.708	1.350
CG25	CG25-3	26.6	1.266	0.939	0.969	1.069	0.716	1.325
	CG25-4	25.6	1.284	0.933	0.966	1.080	0.702	1.313
	CG25-5	25.2	1.270	0.932	0.965	1.087	0.698	1.356
	CW25-1	30.1	1.282	0.928	0.963	1.095	0.694	1.325
	CW25-2	29.8	1.259	0.939	0.969	1.069	0.716	1.346
CW25	CW25-3	28.6	1.271	0.936	0.967	1.069	0.713	1.327
	CW25-4	29.9	1.279	0.929	0.963	1.086	0.703	1.312
	CW25-5	26.0	1.278	0.927	0.963	1.087	0.696	1.348

Tablo 5.9 Selected representative particle shape parameters for mixtures prepared with natural aggregates according to A_w.

Mixture	Specimen	Strength (MPa)	Angularity	Convexity Ratio	Fullness Ratio	Roughness	Formfactor	Elongation Ratio
NG13	NG13-1	23.8	1.221	0.941	0.970	1.112	0.722	1.358
	NG13-2	24.8	1.235	0.939	0.969	1.100	0.718	1.368
	NG13-3	24.9	1.221	0.941	0.970	1.096	0.727	1.349
	NG13-4	24.6	1.214	0.945	0.971	1.092	0.744	1.306
	NG13-5	23.5	1.231	0.943	0.971	1.088	0.729	1.354
NW13	NW13-1	26.9	1.202	0.951	0.975	1.084	0.741	1.379
	NW13-2	28.0	1.206	0.955	0.977	1.070	0.751	1.363
	NW13-3	28.5	1.206	0.954	0.976	1.081	0.738	1.391
	NW13-4	28.3	1.205	0.953	0.976	1.081	0.746	1.362
	NW13-5	26.0	1.208	0.954	0.976	1.070	0.747	1.388
NG25	NG25-1	26.7	1.186	0.954	0.976	1.089	0.754	1.351
	NG25-2	24.9	1.216	0.947	0.973	1.113	0.719	1.399
	NG25-3	24.7	1.211	0.948	0.973	1.112	0.724	1.361
	NG25-4	26.1	1.206	0.947	0.973	1.112	0.720	1.403
	NG25-5	24.6	1.183	0.949	0.974	1.111	0.741	1.350
NW25	NW25-1	22.9	1.216	0.942	0.970	1.119	0.720	1.334
	NW25-2	25.9	1.191	0.952	0.975	1.099	0.742	1.390
	NW25-3	28.0	1.194	0.951	0.975	1.110	0.735	1.372
	NW25-4	28.3	1.187	0.956	0.978	1.078	0.744	1.429
	NW25-5	27.6	1.175	0.958	0.978	1.088	0.754	1.368

CHAPTER 6

DISCUSSION OF RESULTS

6.1 Introduction

In this chapter, the effects of experimental design parameters on the compressive strength of concrete specimens and the relationships between the shape parameters and the compressive strength were investigated using statistical analyses.

6.2. Effects of Experiment Design Parameters on Compressive Strength

Three-way ANOVA analysis was employed for investigating the effects of experimental design parameters on the compressive strength of concrete specimens at 95% confidence level. The three-factor interaction was not taken into consideration due to complexity in explaining its physical meaning. The results of the ANOVA analysis are presented in the Table 6.1.

Table 6.1 The ANOVA table.

Source	Degrees of Freedom	Fisher Number (F)	p-Value
Aggregate Type	1	62.87	0
Gradation Type	1	22.07	0
Maximum Aggregate Size	1	18.12	0.0002
Aggregate Type x Maximum Aggregate Size	1	18.91	0.0001
Aggregate Type x Gradation Type	1	0.11	0.7457
Gradation Type x Maximum Aggregate Size	1	0.03	0.8557
Error	33	-	-
Total	39	-	-

The following results can be stated by examining the results of ANOVA analysis:

– All the main effects have a significant influence on the compressive strength of the concrete specimens (i.e. $F_{\text{aggregate type}} = 62.87 > F_{0.05,1,33} = 4.17$; $F_{\text{gradation type}} = 62.87 > F_{0.05,1,33} = 4.17$ and $F_{\text{maximum aggregate size}} = 62.87 > F_{0.05,1,33} = 4.17$).

– There is also significant interactions between aggregate type and the maximum aggregate size (i.e. $F_{\text{aggregate type x maximum aggregate size}} = 18.91 > F_{0.05,1,33} = 4.17$).

– The influence of the interactions between aggregate type and the maximum aggregate size is more significant than the main effect of the maximum aggregate size (i.e. The Fisher number of the interaction between aggregate type and maximum aggregate size is greater than that of maximum aggregate size).

6.3 Relationships between Aggregate Shape Parameters and Compressive Strength

The relationships between the aggregate shape parameters *(Angularity, Convexity Ratio, Fullness Ratio, Roughness, Formfactor and Elongation Ratio*) and the compressive strength of the concrete specimens were investigated according to three different methods as introduced in Chapter 5.

For this purpose, the graphs of relationships were plotted between mixtures that have the same gradation type and the same maximum aggregate size. In general, weak correlations were obtained between the aggregate shape parameters and the compressive strength of the specimens. Plots for some of the relationships are presented in the following figures.

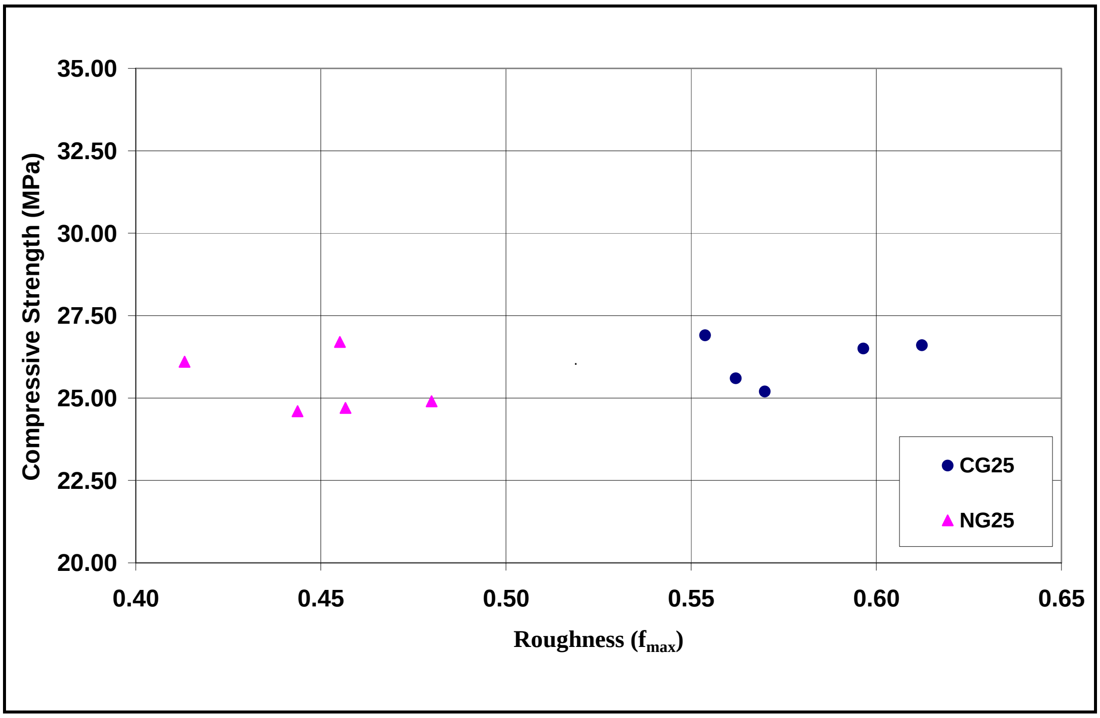

Figure 6.1 Relationship between mixtures CG25 and NG25 for roughness according to f_{max}.

As shown in Figure 6.1, although the compressive strengths of the mixtures CG25 and NG25 vary within the same limits, the mixtures prepared with crushed aggregates have higher maximum relative frequencies for roughness parameter.

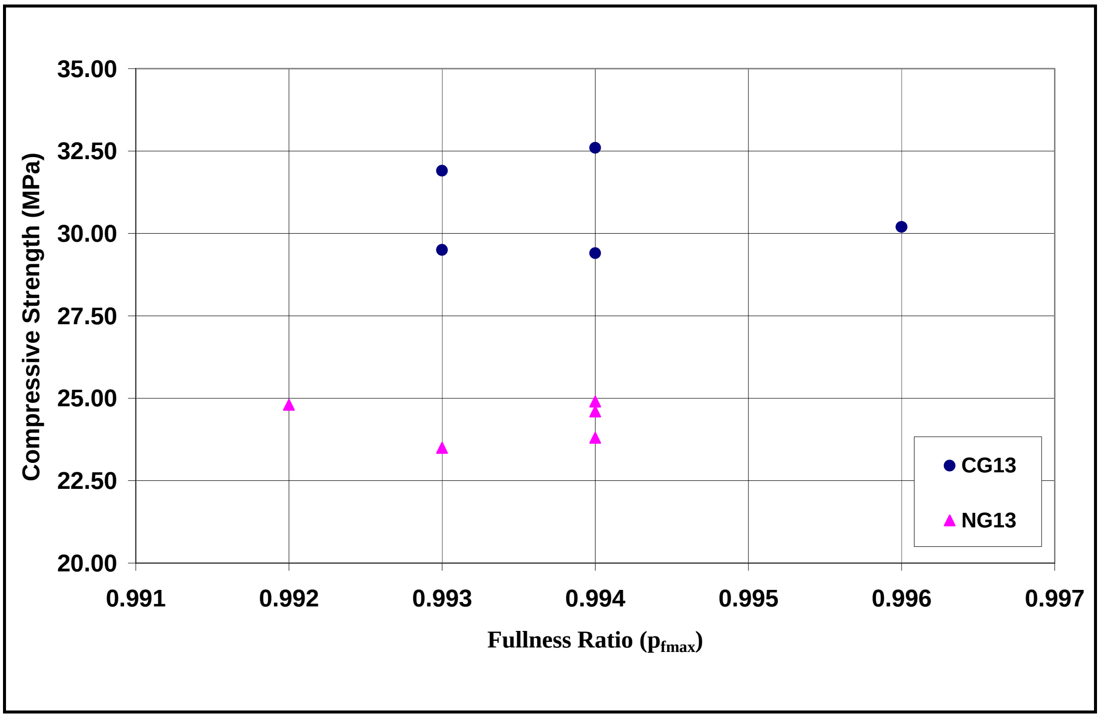

Figure 6.2 Relationship between mixtures CG13 and NG13 for fullness ratio according to p_{fmax}.

In Figure 6.2, fullness ratio parameter varies in a very close range for mixtures CG13 and NG13; however, the mixtures prepared with crushed aggregates have higher compressive strength values.

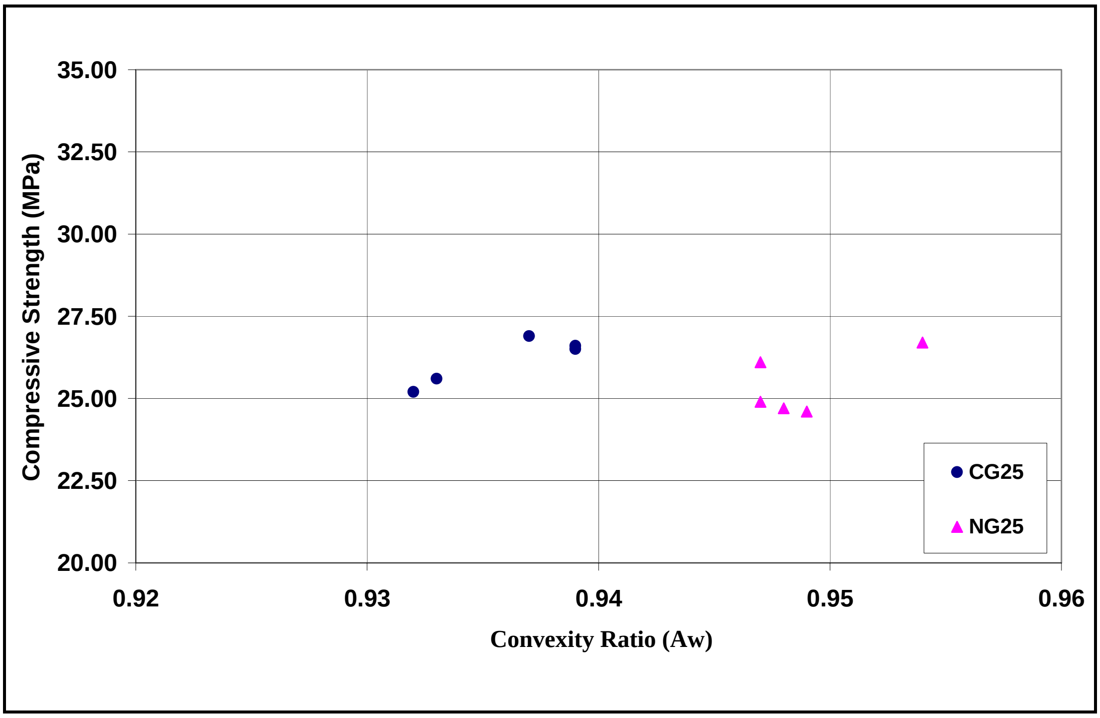

Figure 6.3 Relationship between mixtures CG25 and NG25 for convexity ratio according to A_w.

It is seen in Figure 6.3 that although the compressive strengths of the mixtures CG25 and NG25 vary within the same limits, the mixtures prepared with natural aggregates have slightly higher area weighed convexity ratio parameters.

CHAPTER 7

SUMMARY AND CONCLUSIONS

7.1 Summary

In this study, effects of aggregate shape parameters on compressive strength were investigated using cross sectional digital images of concrete specimens obtained from a flatbed scanner. The design parameters included aggregate shape, gradation and maximum aggregate size varying at two levels in the mix designs of the specimens. As part of the study, an analysis of variance was conducted to determine the significant design parameters on the compressive strength of the test specimens. To extract the particle shape parameters, three cross sectional images taken form each specimen were combined and subsequently analyzed using various digital image processing and analysis techniques. A number of shape parameters were extracted from the cross sectional images and used to determine possible correlations between the shape parameters and the compressive strength of the test specimens. The analyses of the relationships were performed using three derived parameters from the frequency distribution characteristics of the shape parameters. The derived parameters for each shape parameter were defined as the maximum relative frequency, shape parameter corresponding to the maximum relative frequency and shape parameter weighed according to the individual particle areas. Based on the graphical analyses conducted using the derived parameters, several conclusions were obtained in the course of this study.

7.2 Conclusions

- Analysis of variance results indicated that aggregate type has the strongest influence on the compressive strength of the test specimens among the other design variables used.
- The results showed that aggregate gradation ranked the second and the maximum aggregate size the third most significant design parameters for the compressive strength as indicated by the calculated Fisher numbers from the analysis variance table. It was also found that there is a strong interaction effect on the compressive strength between aggregate type and the maximum aggregate size design variables. However, no interaction effects were seen for the interactions between aggregate type and gradation type, and maximum aggregate size and gradation type as observed for the corresponding Fisher number.
- The weak correlations obtained for most of the shape parameters may be because of the interactions effects that were not accounted for in the analyses or the particle distribution characteristics that need to be considered separately in the analyses of the shape parameters.

7.3 Suggestions for Future Studies

The results of the relationships between the shape parameters and the compressive strength suggest that the correlations presented are, in general, weak. The author comments that the particle distribution characteristics within the cross sections should be considered in the analyses of the analyzed relationships. Additional analyses tools should also be developed to find out whether there are interactions effects on the presented relationships.

REFERENCES

- Aschenbrenner, B.C. “A New Method of Expressing Particle Sphericity”, *Journal of Sedimentary Petrology*, Vol. 26, 1956, pp. 15-31.

- ASTM C 127, Standard Test Method for Specific Gravity and Absorption of Coarse Aggregate, ASTM, Philadelphia, 1988.

- ASTM C 128, Standard Test Method for Specific Gravity and Absorption of Fine Aggregate, ASTM, Philadelphia, 1988.

- ASTM C 131, Standard Test Method for Resistance to Degradation of Small-Size Coarse Aggregate by Abrasion and Impact in the Los Angeles Machine, ASTM, Philadelphia, 1989.

- ASTM C 136, Standard Test Method for Sieve Analysis of Fine and Coarse Aggregates, ASTM, Philadelphia, 1992.

- ASTM C 138, Standard Test Method for Unit Weight, Yield, and Air Content (Gravimetric) of Concrete, ASTM, Philadelphia, 1992.

- ASTM C 143, Standard Test Method for Slump of Hydraulic Cement Concrete, ASTM, Philadelphia, 1990.

- ASTM C 192, Standard Practice for Making and Curing Concrete Test Specimens in the Laboratory, ASTM, Philadelphia, 1990.

- ASTM C 702, Standard Practice for Reducing Field Samples of Aggregate to Testing Size, ASTM, Philadelphia, 1987.

- ASTM D 2488, Standard Practice for Description and Identification of Soils (Visual - Manual Procedure), ASTM, West Conshohocken, 2000.

- Barksdale, R. D., Kemp, M.A., Sheffield, W. J. and Hubbard, J. L. "Measurement of Aggregate Shape, Surface Area, and Roughness", *Transportation Research Record*, No. 1301, TRB, National Research Council, Washington, D.C, 1991, pp. 107-116.

- Barksdale, R. D. and Itani, S. Y. "Influence of Aggregate Shape on Base Behavior", *Transportation Research Record*, No. 1227, TRB, National Research Council, Washington, D.C, 1989, pp. 173-182.

- Barrett, P. J. "The Shape of Rock Particles, a Critical Review", *Sedimentology*, Vol. 27, 1980, pp. 291-303.

- Blum, H. "A Transformation for Extracting New Descriptors of Shape", in Whaten-Dunn, W., ed., Models of the Perception of Speech and Visual Form: MIT Press, 1967, pp. 362-280.

- Brodda, R. and Weber, J. W. "Leicht-und Normalbetone mit Ausfallkörnung und stetiger Sieblinie, *Beton*, Vol. 27, No. 9, 1977, pp. 340-342.

- BS 812, Testing Aggregates, British Standards Institution, 1975.

- BS 882, Specification for Aggregates from Natural Sources for Concrete, British Standards Institution, 1992.

- Calabi, L. and Hartnett, W. E. "Shape Recognition, Prairie Fires, Convex Deficiencies and Skeletons", *American Math Monthly*, Vol. 75, 1968, pp. 335-342.

– Castleman, K. R. “Digital Image Processing”, Prentice Hall, USA, 1996.

– Chandan, C., Sivakumar. E., Masad, E. and Fletcher, T. “Application of Imaging Techniques to Geometry Analysis of Aggregate Particles”, *Journal of Computing in Civil Engineering*, Vol. 18, 2004, pp. 75-82.

– Cordon, W. A. and Gillespie, H. A. “Variables in Concrete Aggregates and Portland Cement Paste which Influence the Strength of Concrete”, *ACI Materials Journal*, Vol. 60, 1963, pp. 1029-1050.

– Das, A. “A Revisit to Aggregate Shape Parameters”, *Workshop on Aggregates – flakiness and elongation indices – (WSOA)*, New Delhi, 2006.

– Dewar, J. D., “Computer Modelling of Concrete Mixtures” E & FN Spon, London, 1999.

– Duda, R. and Hart, P., “Pattern Classification and Scene Analysis”, John Wiley & Sons, New York, USA, 1973.

– Efford, N. “Digital Image Processing: A practical introduction with JAVA”, Addison-Wesley, USA, 2000.

– Ehrlich, R., Kennedy, S. T., Crabtree, S. J. and Cannon, R. L. “Petrographic Image Analysis, I. Analysis of Reservoir Pore Complexes”, *Journal of Sedimentary Petrology*, Vol. 54, No. 4, pp. 1365-1378.

– Erdoğan, S. T. and Fowler, D. W. “Determination of Aggregate Shape Properties Using X-ray Topographic Methods and the Effect of Shape on Concrete Rheology”, *Research Report: ICAR 106-1*, International Center for Aggregates Research, 2005.

– Gimp-Savvy.com “The RGB Colorspace” http://gimp.savvy.com/book/node.50.html, Last Access: March, 2007.

– Gonzalez, R. F and Woods R. E. “Digital Image Processing”, Addison Wesley, USA, 1992.

– Gonzalez, R. F and Woods R. E. “Digital Image Processing”, Prentice Hall, USA, 2001.

– Harr, M. E. “Mechanics of Particulate Media”, McGraw-Hill, Inc., New York, USA, 1977.

– Hudson, B. “Modification to Fine Aggregate Angularity Test”, *Proceedings of the 7th ICAR Symposium,* 1999.

– Janoo, V. C. “Quantification of Shape, Angularity, and Surface Texture of Base Course Materials”, *CRREL Special Report No. 98-1*, Cold Regions Research and Engineering, USA, 1998.

– Jähne, B. “Digital Image Processing”, Springer, Germany, 2005.

– Kaplan, M. F. “Flexural and Compressive Strength of Concrete as Affected by the Properties of Coarse Aggregates”, *ACI Materials Journal*, Vol. 55, 1959, pp. 1193-1208.

– Kosmatka, S. “Bleeding”, *ASTM Special Technical Publication*, No. 169C, Philadelphia, USA, 1994, pp. 89-111.

– Krumbein, W. C. “Measurement of Geological Significance of Shape and Roundness of Sedimentary Particles”, *Journal of Sedimentary Petrology*, Vol. 11, 1941, pp. 64-72.

- Krumbein, W. C. “Settling-Velocity and Flume-Behavior of Non-Spherical Particles”, *Transactions of the American Geophysical Union*, 1942, pp. 621-633.

- Kuo, C-Y., Frost, J. D., Lai, J. S. and Wang, L. B. “Three-Dimensional Image Analysis of Aggregate Particles from Orthogonal Projections”, *Transportation Research Record*, No. 1526, TRB, National Research Council, Washington, D.C, 1996, pp. 98-103.

- Kuo, C-Y., Rollings, R. S. and Lynch, L. N. “Morphological Study of Coarse Aggregates Using Image Analysis”, *Journal of Materials in Civil Engineering,* Vol. 10, No. 3, 1998, pp. 135-142.

- Kuo, C-Y. and Freeman, R. B. “Imaging Indices for Quantification of Shape, Angularity, and Surface Texture of Aggregates”, *Transportation Research Board 79th Annual Meeting*, Washington, D.C, January 2000, paper no: 000686.

- Kwan, A. K. H., Mora, C. F. and Chan, H. C. “Particle Shape Analysis of Coarse Aggregate Using Digital Image Processing”, *Cement and Concrete Research*, Vol. 29, 1999, pp. 1403-1410.

- Kwan, A. K. H., Mora, C. F. “Effects of Various Shape Parameters on Packing of Aggregate Particle”, *Magazine of Concrete Research*, Vol. 53, No. 2, 2001, pp. 91-100.

- Lees, G. “The Measurement of Particle Shape and Its Influence in Engineering Materials”, *Journal of British Granite and Whinestone Federation*, London, Vol. 4, No. 2, 1964, pp. 1-22.

- Legg, F. E. Jr. “Concrete Construction Handbook”, ed. Dobrowolski, J., McGraw-Hill, 1998.

- Lerner, B. "Contrast Enhancement"
  http://www.bgu.ac.il/~greg/graphics/stats.front-page.html,
  Last Access: November, 2005.

- Lewis, H. T. Discussion on "Walker, S. and Bloem, D. L., Effects of Aggregate Size on Properties of Concrete, ACI Materials Journal, Vol. 57, 1960, pp. 283-298", *ACI Materials Journal*, Vol. 57, 1961, pp. 1240-1244.

- Macnaughton, M. F. Discussion on "Walker, S. and Bloem, D. L., Effects of Aggregate Size on Properties of Concrete, ACI Materials Journal, Vol. 57, 1960, pp. 283-298", *ACI Materials Journal*, Vol. 57, 1961, pp. 1220-1226.

- Masad E. and Button J. W. "Unified Imaging Approach for Measuring Aggregate Angularity and Texture", *Computer Aided Civil and Infrastructure Engineering*, Vol. 15, 2000, pp. 273-280.

- Masad, E., Button, J. W. and Papagiannakis, T. "Fine Aggregate Angularity: Automated Image Analysis Approach", *Transportation Research Record,* No. 1721, TRB, National Research Council, Washington, D.C., 2000, pp. 66–72.

- Masad, E., Olcott, D., White, T. And Tashman, L. "Correlation of Fine Aggregate Shape Imaging Shape Indices with Aspalt Mixture Performance", *Transportation Research Record,* No. 1757, TRB, National Research Council, Washington, D.C., 2001, pp. 148–156.

- Masad, E. and Sivakumar K. "Advances in the Characterization and Modeling of Civil Engineering Materials Using Imaging Techniques", *Journal of Computing in Civil Engineering*, Vol. 18, January, 2004.

- McAndrew A. "Introduction to Digital Image Processing with MATLAB", Thomson Course Technology, USA, 2004.

- McIntosh, J. D. “The Selection of Natural Aggregates for Various Types of Concrete Work”, *Reinf. Concr. Rev.*, Vol. 4, No. 5, 1957, pp. 281-305.

- Mehta, P. K. and Monteiro P. J. M. “Concrete: Microstructure, Properties and Materials”, McGraw-Hill, New York, USA, 2006.

- Mindess, S., Young, F. J. and Darwin, D. “Concrete”, Prentice-Hall, Pearson Education, Inc., New Jersey, USA, 2003.

- Mora, C. F. and Kwan, A. K. H. “Sphericity, Shape Factor, and Convexity Measurement of Coarse Aggregates for Concrete Using Digital Image Processing”, *Cement and Concrete Research*, Vol. 30, 2000, pp. 351-358.

- Neville, A. M. “Properties of Concrete”, Longman Scientefic & Technical, England, 2003.

- NI Vision Development Module for LabVIEW 8.0.

- Popovics, “Concrete Materials”, Noyes Publications, New Jersey, U.S.A, 1992.

- Quiroga P. N. and Fowler D. W. “The Effects of Aggregates Characteristics on the Performance of Portland Cement Concrete”, *Research Report: ICAR 104-1F* International Center for Aggregates Research, 2003.

- Rao, C., Tutumluer, E. and Kim, I. T. “Quantification of Coarse Aggregate Angularity Based on Image Analysis”, *Transportation Research Board 81st Annual Meeting*, Washington, D.C, January 2002, paper no: 02-3124.

- Rao, C., Pan, T. and Tutumluer, E. “Determination of Coarse Aggregate Surface Texture Using Image Analysis”, *16th ASCE Engineering Mechanics Conference,* University of Washington, Seattle, 2003.

- Rosenfeld, A. and Kak, A. C. "Digital Picture Processing Vol. 2", Acedemic Press, Inc., USA, 1982.

- Russ, J. C. "The Image Processing Handbook", CRC Press, USA, 1999.

- Shacklock, B. W. Discussion on "Newman A. J. and Teychenne D. C., A Classification of Natural Sands and Its Use in Concrete Mix Design, Proc. of a Symposium on Mix Design and Quality Control of Concrete, 1954, pp. 175-193", *Proc. of a Symposium on Mix Design and Quality Control of Concrete*, 1954, pp. 199-200.

- Shah, S. "COSC 6397 Digital Image Processing Lecture Notes", Department of Computer Science, University of Houston, 2005.

- Shilstone, J. M. Sr. "Concrete Mixture Optimization", *Concrete International: Design and Construction*, Vol. 12, No. 6, 1990, pp. 33-39.

- Sneed, E.D. and Folk, R.L "Pebbles in the Lower Colorado River, Texas – A study in Particle Morphogenesis", *Journal of Geology*, Vol. 66, No. 2, 1958, pp. 114-150.

- Terzaghi, K. and Peck, R. B. "Soil Mechanics in Engineering Practice", John Wiley & Sons, Inc., USA, 1958.

- Young, I. T., Peverini, R. L., Verbeek, P. W., and Van Otterloo, P. J. "A New Implementation for the Binary and Minkowski Operators", *Computer Graphics and Image Processing*, Vol. 17, 1981, pp. 189-210.

- Yue, Z.Q., Bekking, W., and Morin, I. "Application of Digital Image Processing to Quantitative Study of Asphalt Concrete Microstructure", *Transportation Research Record*, No. 1492, TRB, National Research Council, Washington, D.C, 1995, pp. 53-60.

- Wadell, H. "Volume, Shape, and Roundness of Rock Particles", *Journal of Geology*, Vol. 40, 1932, pp. 443-451.

- Wadell, H. "Sphericity and Roundness of Rock Particles", *Journal of Geology*, Vol. 41, 1933, pp. 310-331.

- Washa, G. W. "Concrete Construction Handbook", ed. Dobrowolski, J., McGraw-Hill, New York, USA, 1998.

APPENDIX A

GRAY SCALE IMAGES AND THEIR CORRESPONDING SEPARATED BINARY IMAGES

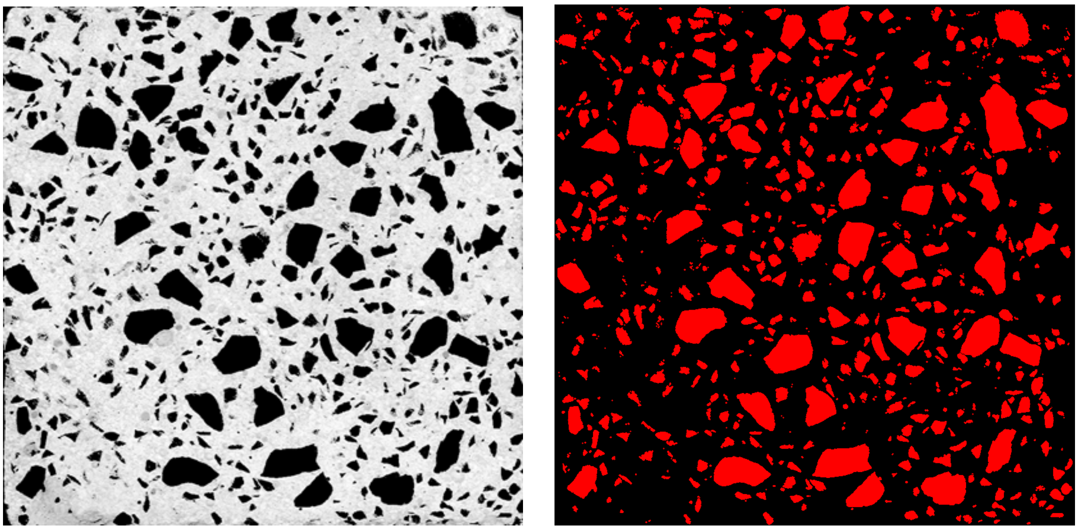

(a) (b)

Figure A.1 A gray scale and its separated binary image for cross section CG13-2-3.

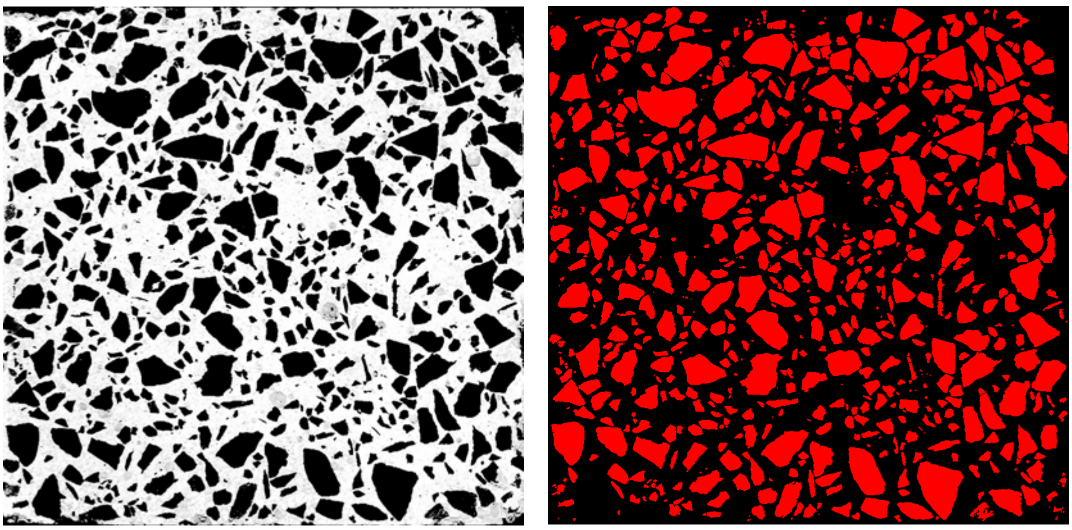

(a) (b)

Figure A.2 A gray scale and its separated binary image for cross section CW13-3-5.

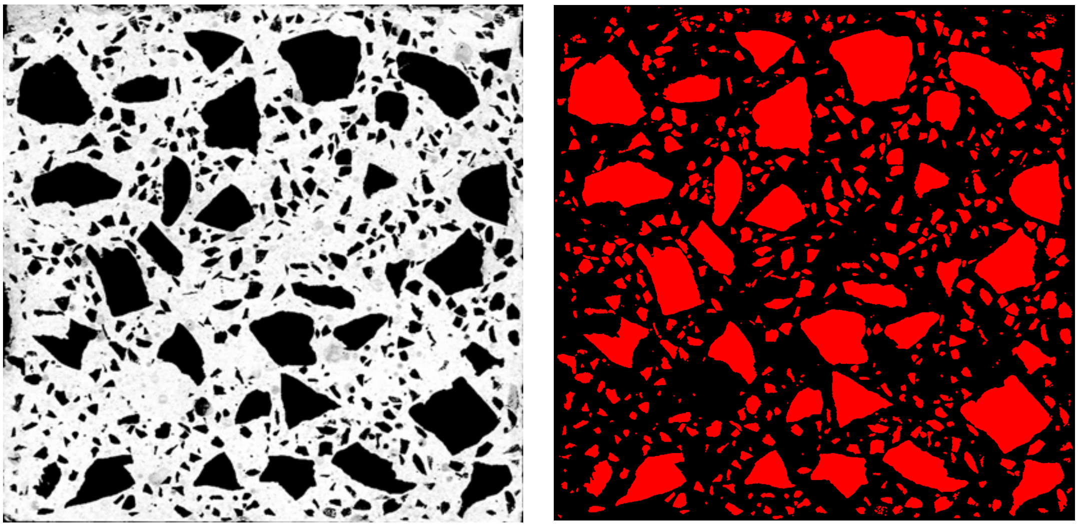

(a) (b)

Figure A.3 A gray scale and its separated binary image for cross section CG25-1-5.

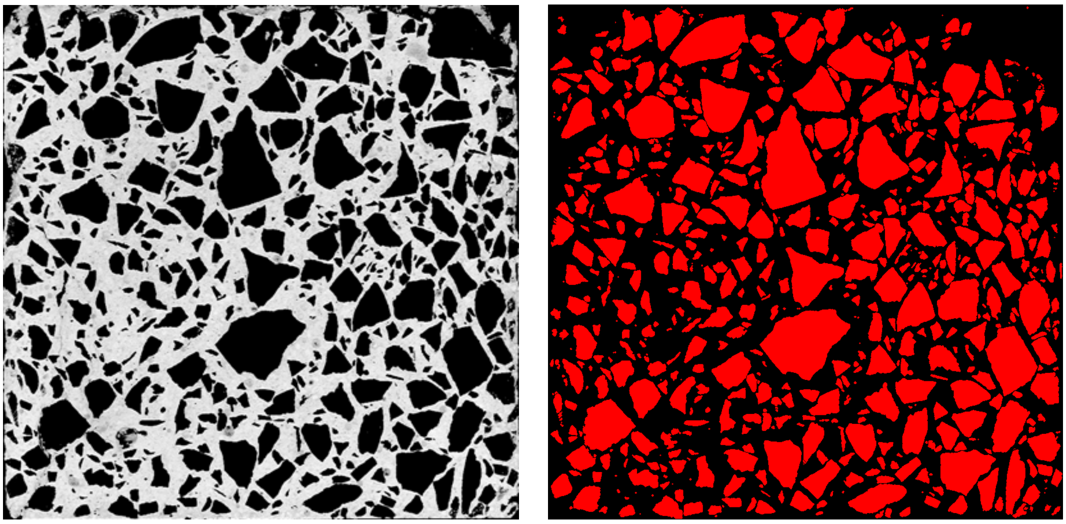

(a) (b)

Figure A.4 A gray scale and its separated binary image for cross section CW25-3-3.

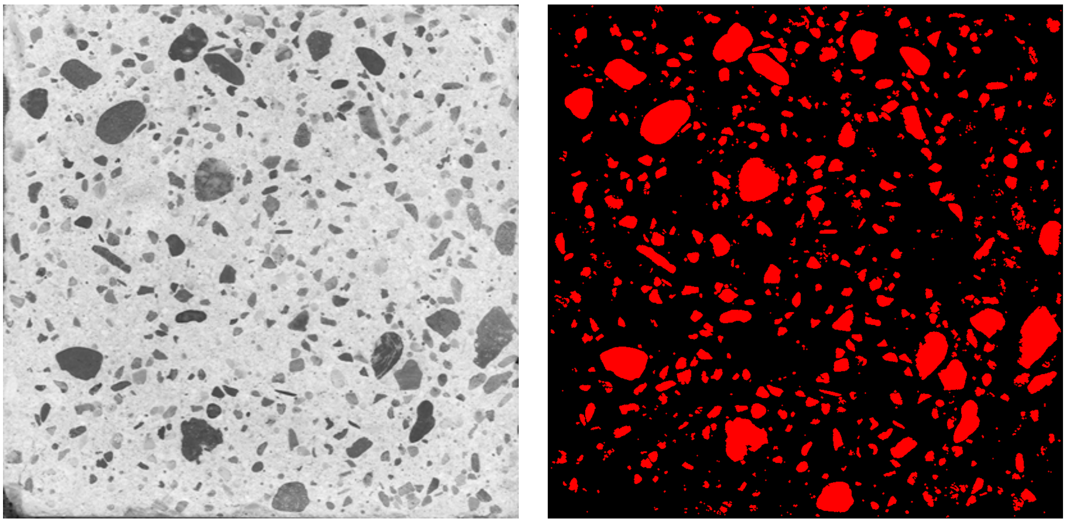

(a) (b)

Figure A.5 A gray scale and its separated binary image for cross section NG13-5-5.

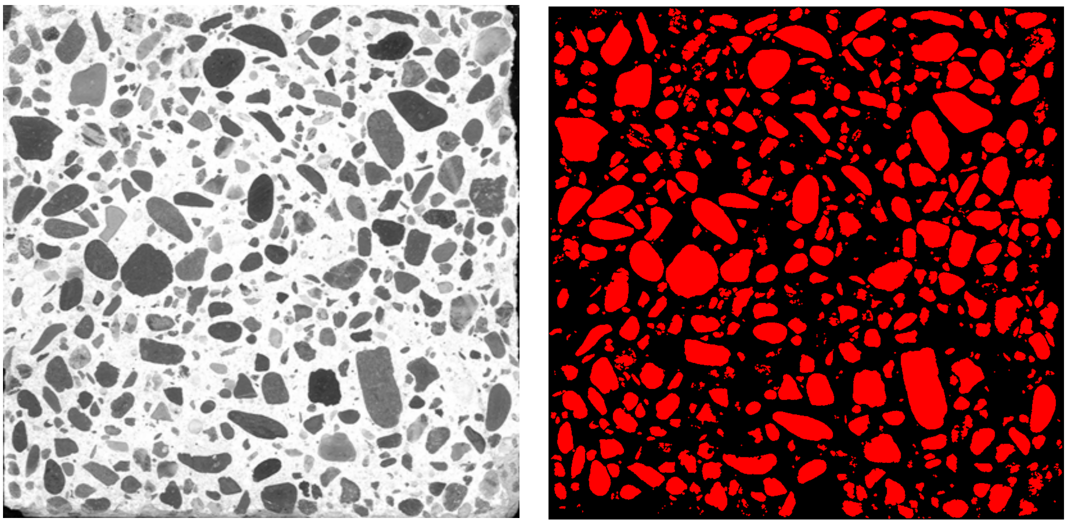

(a) (b)

Figure A.6 A gray scale and its separated binary image for cross section NW13-4-2.

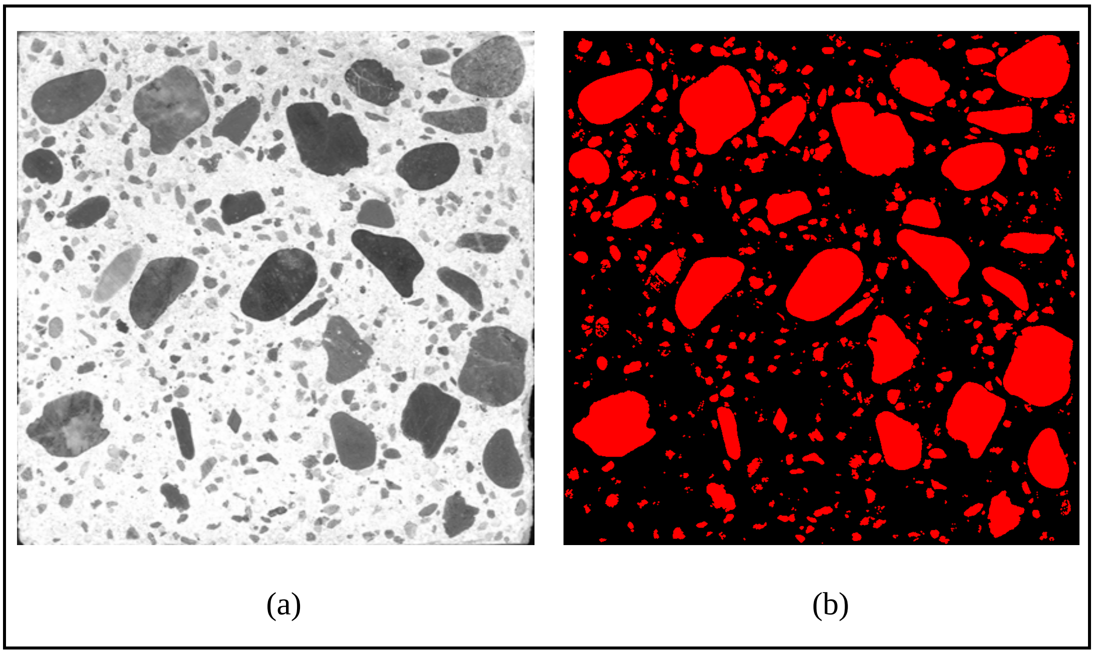

Figure A.7 A gray scale and its separated binary image for cross section NG25-5-3.

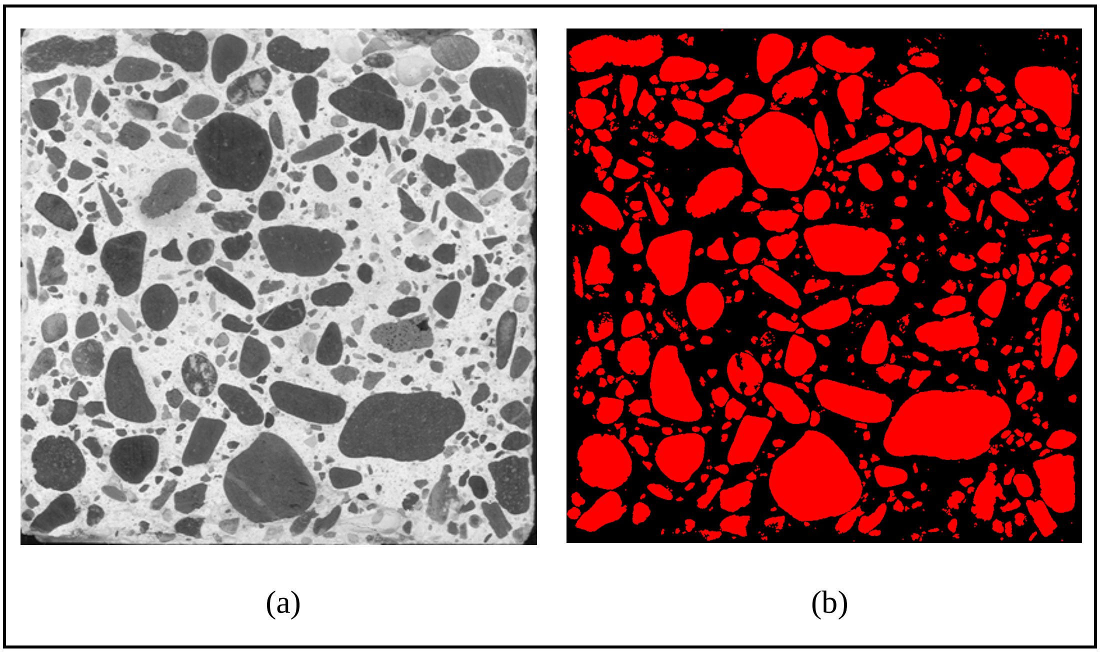

Figure A.8 A gray scale and its separated binary image for cross section NW25-2-3.

APPENDIX B

OUTPUT DATA FILE PRODUCED BY AGGREGATE ANALYZER FOR CROSS SECTION CW25-5-4

Shape parameters of one aggregate piece

Area	Convex Area	Perimeter	Convex Perimeter	Maximum Feret Diameter	Maximum Feret Diameter Orientation	Center of Mass X	Center of Mass Y
.	.	.	.	.	.	.	.
.	.	.	.	.	.	.	.
.	.	.	.	.	.	.	.
.	.	.	.	.	.	.	.
.	.	.	.	.	.	.	.
.					.	.	.
.					.	.	.
.	.	.	.	.	.	.	.
.	.	.	.	.	.	.	.
.	.	.	.	.	.	.	.
130	52.676	132	51.505	22.825	118.811	606.585	86.923
845	117.471	856	116.469	47.011	60.709	473.775	98.612
25	21.208	26	21.208	9.22	12.529	800.88	79.76
206	55.999	206	55.999	20.1	95.711	378.733	88.84
1195	145.948	1294	141.992	59.203	15.68	218.562	97.535
176	68.809	200	66.305	28.231	22.932	745.108	87.92
430	97.532	509	87.137	30.529	31.608	44.291	96.293
1501	157.581	1655	152.265	52.802	52.696	550.558	102.672
392	85.208	408	84.216	34.015	114.305	101.324	100.495
37	27.273	41	24.874	9.487	108.435	20.432	88.351
670	110.448	720	102.899	39.395	156.038	333.33	96.972
860	133.773	917	129.459	52.555	68.806	423.051	112.438
1	2	1	2	1.414	135	16	86
43	27.551	43	27.551	11.705	70.017	784.209	92.884
1250	140.082	1297	136.24	51.4	37.093	641.891	109.082
31	20.055	33	22.38	8.544	159.444	580	94.032
53	30.778	53	30.778	13.153	98.746	509.943	98.83
476	89.295	501	86.63	30.529	31.608	596.483	110.987
59	29.208	59	29.208	10.44	106.699	728.203	102.153
8	10.797	8	10.797	4.123	104.036	620	100.5
3480	231.786	3585	229.558	91.181	21.218	788.134	132.73
74	34.361	74	34.361	14.318	102.095	307.243	107.635
211	60.76	221	61.029	25.08	23.499	67.28	109.687
.	.	.	.	.	.	.	.
.	.	.	.	.	.	.	.

***A total of 713 aggregate particles was found for cross section CW25-5-4.**

APPENDIX C

MATLAB ALGORITHM FOR THE CALCULATION OF AGGREGATE SHAPE PARAMETERS

```
% This algorithm calculates particle shape parameters, namely, angularity, convexity ratio,
% fullness ratio, roughness, formfactor and elongation ratio, for each particle in separated
% binary images. Then, the particle shape parameters of the images that belong to the
same   % concrete specimen are combined and stored.

% This algorithm uses output data files and separated binary images of the aggregate
analyzer. % The output .txt files and separated binary images of the aggregate analyzer
were numbered %  from 1 to 120 as follows:

%   1  to   15  corresponds to CG13 %
%  16  to   30  corresponds to CW13 %
%  31  to   45  corresponds to CG25 %
%  46  to   60  corresponds to CW25 %
%  61  to   75  corresponds to NG13 %
%  76  to   90  corresponds to NW13 %
%  91  to  105  corresponds to NG25 %
% 106  to  120  corresponds to NW25 %

%   1  to   3  corresponds to CG13-1 %
%   4  to   6  corresponds to CG13-2 %
%   7  to   9  corresponds to CG13-3 %
% 10 to  12  corresponds to CG13-4 %
% 12 to  15  corresponds to CG13-5 %

% 1 corresponds to CG13-1-2 %
% 2 corresponds to CG13-1-2 %
% 3 corresponds to CG13-1-3 %

clear all
clc

% Load the output data files of the LabVIEW aggregate analyzer %
for specimen=1:40
    parameters=[];
    for section=[3*specimen-2 3*specimen-1 3*specimen]
        datafile=load(sprintf('%i.txt',section));

        % datafile(:,1)=Area %
        % datafile(:,2)=Perimeter %
        % datafile(:,3)=Convex Hull Area %
        % datafile(:,4)=Convex Hull Perimeter %
        % datafile(:,5)=Maximum Feret Diamater %
        % datafile(:,6)=Maximum Feret Diameter Orientation %
        % datafile(:,7)=Center of Mass X %
        % datafile(:,8)=Center of Mass Y %
```

```
  % Load the output separated binary images of the LabVIEW aggregate analyzer %
   im=imread(sprintf('%i.bmp',section));

  % Calculation of the elongation ratio parameter. %
   im=im';
   bw=bwlabel(im,4);
   particle=regionprops(bw,'all');
   number_of_particles=max(size(datafile));
   elongation_ratio=[];

   for  i=1:number_of_particles
        imr=imrotate(particle(i).Image,datafile(i,6));
        dim1=max(sum(imr));
        dim2=max(sum(imr'));
        particle_elongation=max(dim1,dim2)/min(dim1,dim2);
         elongation_ratio=[elongation_ratio;particle_elongation];
  end

  datafile(:,9)=elongation_ratio;

  % Angularity=(Convex Hull Perimeter/Perimeter of Equivalent Ellipse)^2 %

 datafile(:,10)=power(rdivide(datafile(:,4),2*power(rdivide(times(1+power(datafile(:,6),2),...
                   pi*datafile(:,1)),2*datafile(:,6)),0.5)),2);

  % Roughness=(Perimeter/Convex Hull Perimeter)^2 %
  datafile(:,11)=power(rdivide(datafile(:,2),datafile(:,4)),2);

  % Convexity Ratio=Area/Convex Hull Area %
  datafile(:,12)=rdivide(datafile(:,1), datafile(:,3));

  % Fullness Ratio=square(Convexity) %
  datafile(:,13)= power(datafile(:,12),0.5);

  % Formfactor=4*pi*Area/Perimeter^2 %
  datafile(:,14)=rdivide(4*pi*datafile(:,1),power(datafile(:,2),2));

  % Combination of the parameters of the images that belong to the same specimen. %
  parameters=[parameters; datafile];
end

fout=sprintf('parameters%3d.txt',specimen);
save(fout, 'parameters', '-ascii');
end
```

APPENDIX D

MATLAB ALGORITHM FOR THE ELIMINATION OF PARTICLES FINER THAN NO.8

```
% This algorithm eliminates the particles finer than No.8 sieve. %
% This algorithm uses the output .txt file of the algorithm given in Appendix C. %

clear all
clc

best_parameter=[];
% pixel size in separated binary images %
pixel = 25.4/96;

for specimen=1:40
    parameters=load(sprintf('parameters%3d.txt',specimen));

    % Determination of particle shape parameter that will be best characterize the actual
   % particle size distribution of the specimen.
   [specimen,minp,gradations,total_error]=particle_distributions(parameters,specimen,pixel);

   best_parameter=[best_parameter; minp];

   % Elimination of the particles finer than No.8 sieve. %
   eliminated_parameters=particle_removing(parameters,pixel,minp);

   fout=sprintf('eliminated_parameters%3d.txt',specimen);
   save(fout, 'eliminated_parameters', '-ascii');
 end

%%%%%%%%%%%%%%%%%%%%%%%%%%%%%%%%%%%%%%%%%%%%%%%%%%%%%

% particle_distributions function generates particle size distributions according to area and
% maximum feret diameter parameters. In addition, it determines the particle shape
% parameter that will be best characterize the actual particle size distribution of the
% considered specimen.

function [specimen,minp,gradations,total_error]=particle_distributions(parameters,...
                                                            specimen,pixel);

error=[];

% ASTM standard sieve sizes used for preparation of the specimens. %
% No = [  1in;     3/4in.;  1/2in.;  No.3/8;  No.4;  No.8;  No.16;  No.30;   No.50;  No.100] %
sieves=[ 25.4;    19.1;    12.7;    9.50;     4.76;  2.38;     1.19;     0.59;   0.297;     0.149];

[number_of_aggregates  number_of_parameter]=size(parameters);
```

```
% Generation of the particle size distribution according to "area" parameter. %
particle_area=parameters(:,1);
area_gradation=area_distribution(particle_area,pixel,number_of_aggregates,sieves);

% Generation of the particle size distribution according to "maximum feret diameter"
% parameter.
maximum_feret_diameter=parameters(:,5);
maximum_feret_diameter_gradation=maximum_feret_diameter_distribution...
                                              (maximum_feret_diameter,sieves,pixel,...
                                               number_of_aggregates);

% Actual particle size distributions of the specimens. %
if      (specimen<6)||((specimen>20)&&(specimen<26));
        actual=[100.0; 100.0; 100.00; 86.40; 86.40; 66.60; 43.70; 16.00; 13.9; 12.6];

elseif ((specimen>5)&&(specimen<11))||((specimen>25)&&(specimen<31));
        actual=[100.0; 100.0; 100.00; 87.0;  60.00; 44.80; 31.50; 15.40; 14.2; 13.5];

elseif ((specimen>10)&&(specimen<16))||((specimen>30)&&(specimen<36));
        actual=[100.0;  86.5;  69.70; 69.70; 69.70; 51.00; 33.10; 11.40;  9.8;  9.8];

else   ((specimen>15)&&(specimen<21))||((specimen>35)&&(specimen<41));
        actual=[100.0;  85.0;  72.00; 60.00; 45.00; 33.00; 23.00; 11.00; 10.1;  9.5];
end

gradations=[actual, area_gradation, maximum_feret_diameter_gradation];
[number_of_sieves  number_of_gradation]=size(gradations);

% Error between actual particle size distribution and particle size distribution according to
% area and maximum feret diameter parameters.
for n=1: number_of_sieves
   error_area=(gradations(n,1)-gradations(n,2))^2;
   error_maximum_feret_diameter=(gradations(n,1)-gradations(n,3))^2;
   error=[error; error_area, error_maximum_feret_diameter];
end
total_error=sum(error);

% If minp=1, the area is the parameter that will be best characterize the actual particle size
% distribution of the specimen. On the other hand if minp=2, the maximum feret diameter is
% the parameter that will be best characterize the actual particle size distribution of the
% specimen.
minp=find(total_error==min(total_error));
return

%%%%%%%%%%%%%%%%%%%%%%%%%%%%%%%%%%%%%%%%%%%%%

% area_gradation function generates the particle size distribution according to area
% parameter.

function area_gradation= ...
                                    area_distribution(particle_area,pixel,number_of_aggregates,sieves);

area_gradation=[];
retained=[];
```

```
number_of_sieves=length(sieves);
 for i=1:number_of_sieves
   if i<number_of_sieves
      number_of_retained_aggregates=length(find(particle_area(:,:)<(sieves(i)/pixel)^2&...
                                          particle_area(:,:)>(sieves(i+1)/pixel)^2));

      retained=[retained; number_of_retained_aggregates];
   else
      number_of_retained_aggregates=length(find(particle_area(:,:)<(sieves(i)/pixel)^2));
      retained=[retained; number_of_retained_aggregates];
   end
end

for j=1:number_of_sieves
   retained_percentage=100*sum(retained(j:number_of_sieves,:))/(number_of_aggregates);
   area_gradation=[area_gradation; retained_percentage];
end
return

%%%%%%%%%%%%%%%%%%%%%%%%%%%%%%%%%%%%%%%%%%%%%%%

% maximum_feret_diameter_gradation function generates the particle size distribution
% according to maximum feret diameter parameter.

function maximum_feret_diameter_gradation=maximum_feret_diameter_distribution...
                                                   (maximum_feret_diameter,sieves,pixel,...
                                                   number_of_aggregates);

maximum_feret_diameter_gradation=[];
retained=[];
number_of_sives=length(sieves);

for i=1:number_of_sives
   if i<number_of_sives;
      number_of_retained_aggregates=length(find(maximum_feret_diameter(:,:)<...
                                         (sieves(i)/pixel)&maximum_feret_diameter(:,:)>...
                                         (sieves(i+1)/pixel)));

      retained=[retained;number_of_retained_aggregates];
   else
   number_of_retained_aggregates=length(find(maximum_feret_diameter(:,:)<(sieves(i)...
                                          /pixel)));
   retained=[retained;number_of_retained_aggregates];
   end

for j=1:number_of_sives
   retained_percentage=100*sum(retained(j:number_of_sives,:))/number_of_aggregates;
   maximum_feret_diameter_gradation=[maximum_feret_diameter_gradation;...
                                           retained_percentage];
end
return

%%%%%%%%%%%%%%%%%%%%%%%%%%%%%%%%%%%%%%%%%%%%%%%
```

```
% particle_removing function eliminates the parameters of the particles finer than No.8
% sieve.

% Since the maximum feret diameter was better to represent actual particle size distribution
% of the specimens, the elimination process was carried out according to maximum feret
% diameter parameter.

function removed_parameters=particle_removing(parameters,pixel,minp)


[number_of_aggregate number_of_parameter]=size(parameters);
mirror=parameters;
flag=0;


for index=1:number_of_aggregate
   row=parameters(index,:);
      if row(5)<(2.38/pixel);
        mirror(index-flag,:)=[];
        flag=flag+1;
      end
end


removed_parameters=mirror;
return

%%%%%%%%%%%%%%%%%%%%%%%%%%%%%%%%%%%%%%%%%%%%%
```

APPENDIX E

RELATIVE FREQUENCY HISTOGRAMS OF PARTICLE SHAPE PARAMETERS

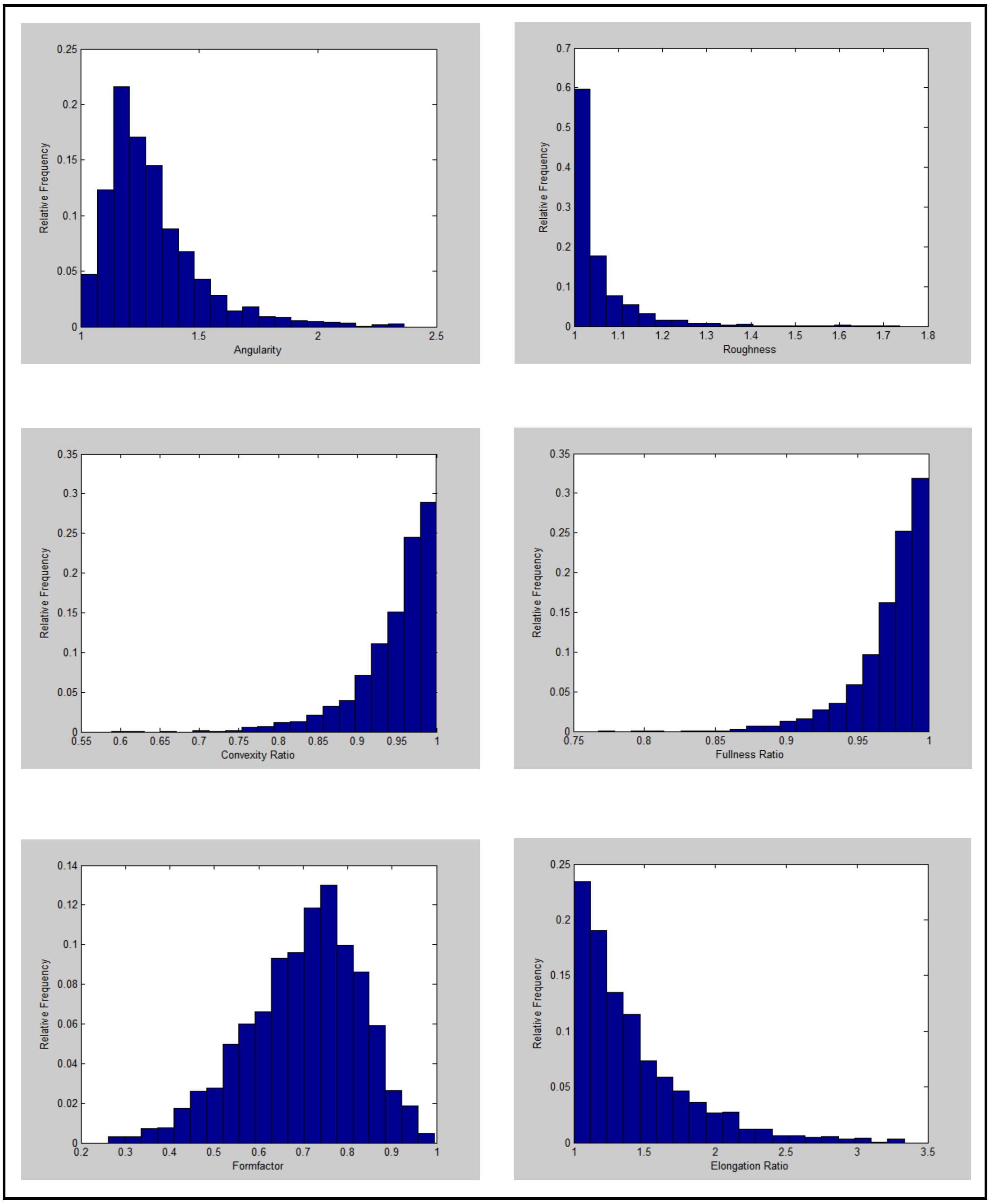

Figure E.1 Relative frequency histograms of parameters for specimen CG13-2.

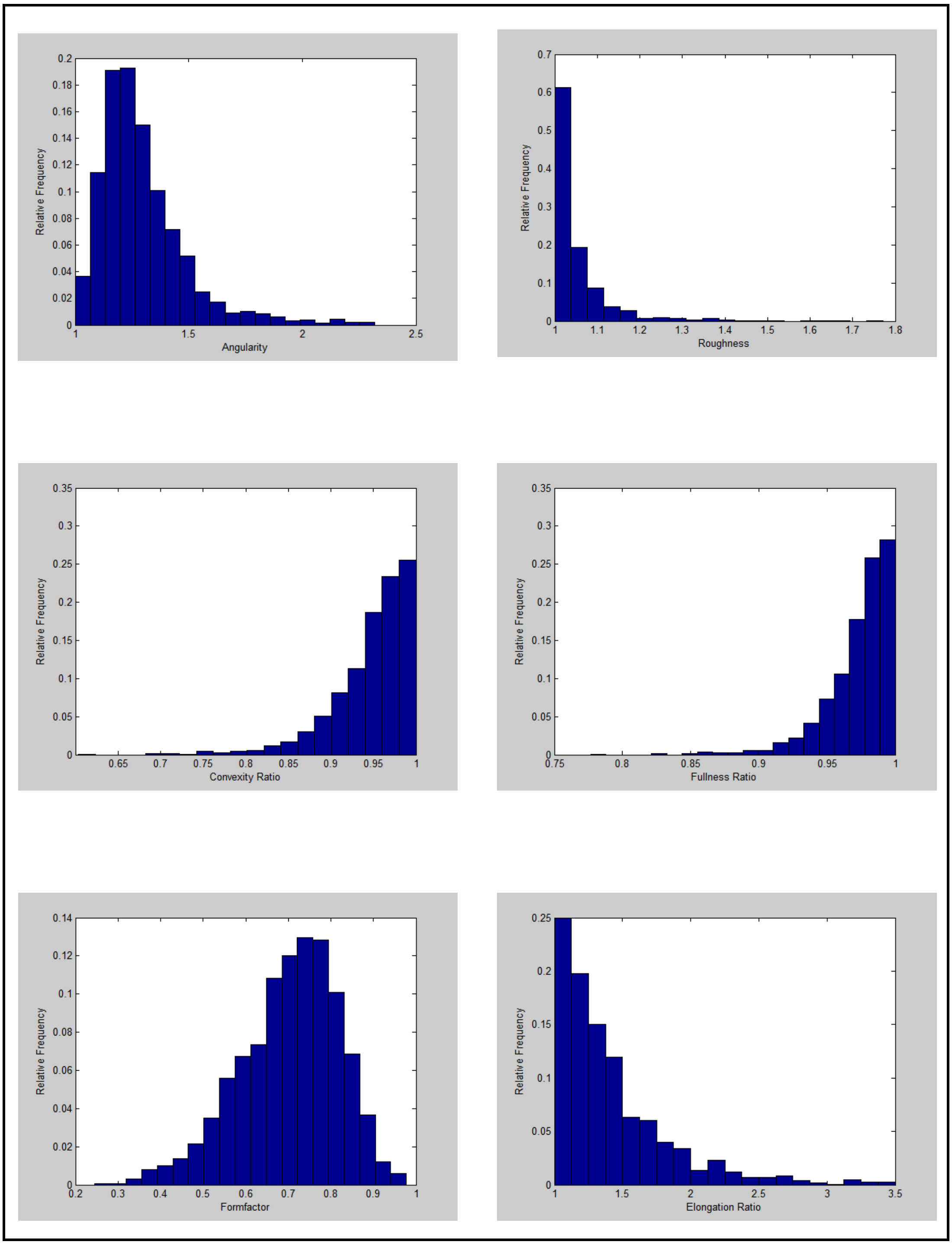

Figure E.2 Relative frequency histograms of parameters for specimen CW13-3.

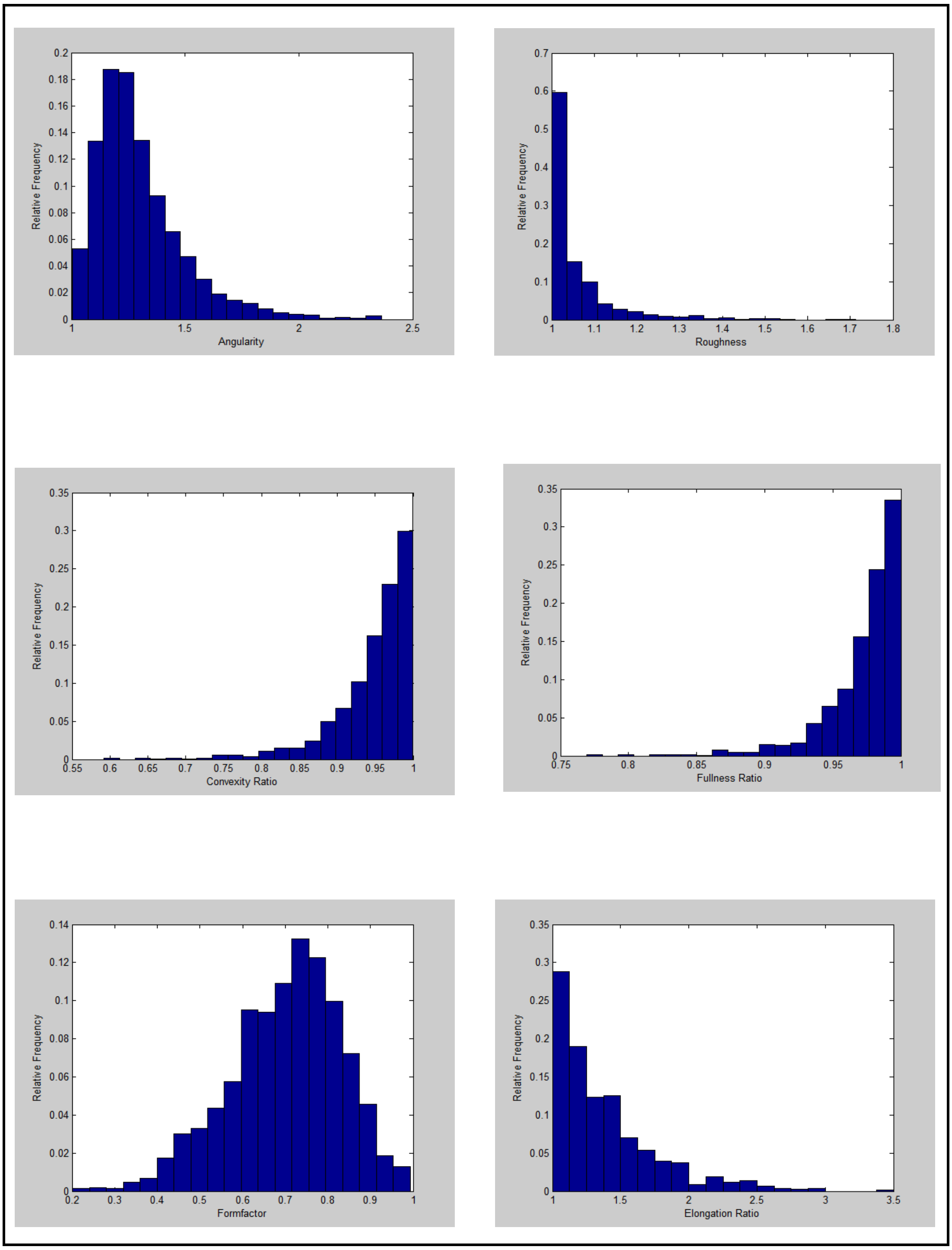

Figure E.3 Relative frequency histograms of parameters for specimen CG25-1.

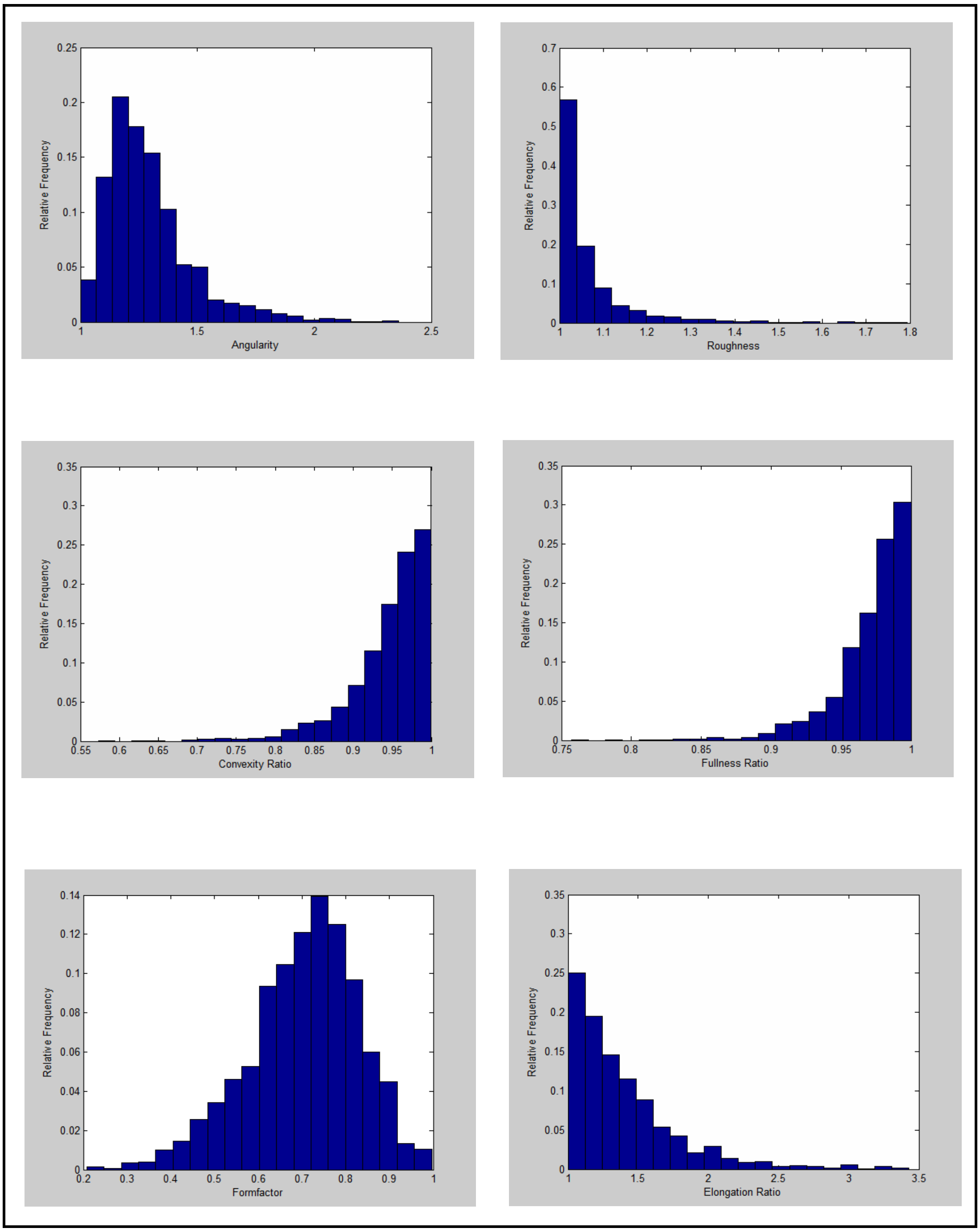

Figure E.4 Relative frequency histograms of parameters for specimen CW25-3.

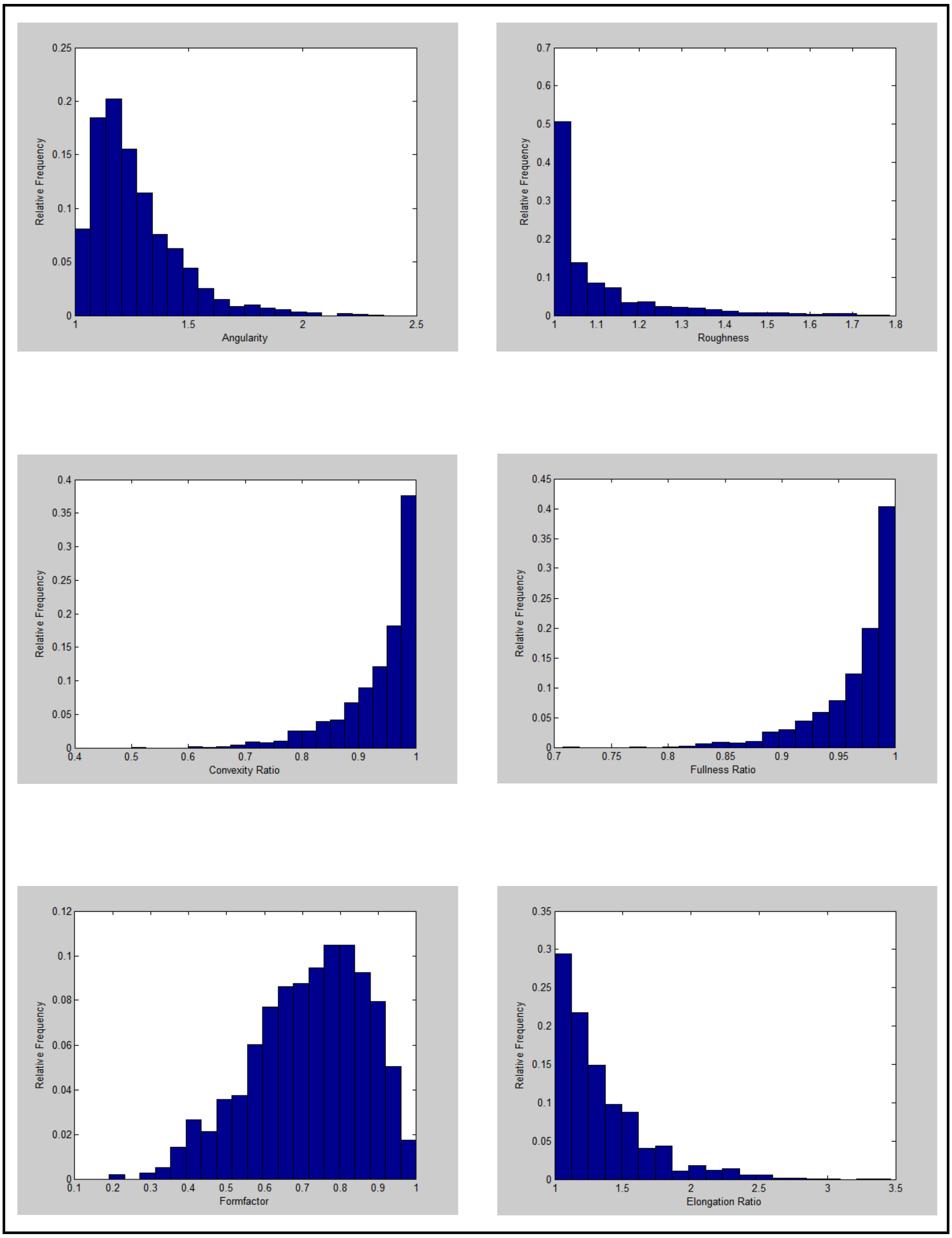

Figure E.5 Relative frequency histograms of parameters for the specimen NG13-5.

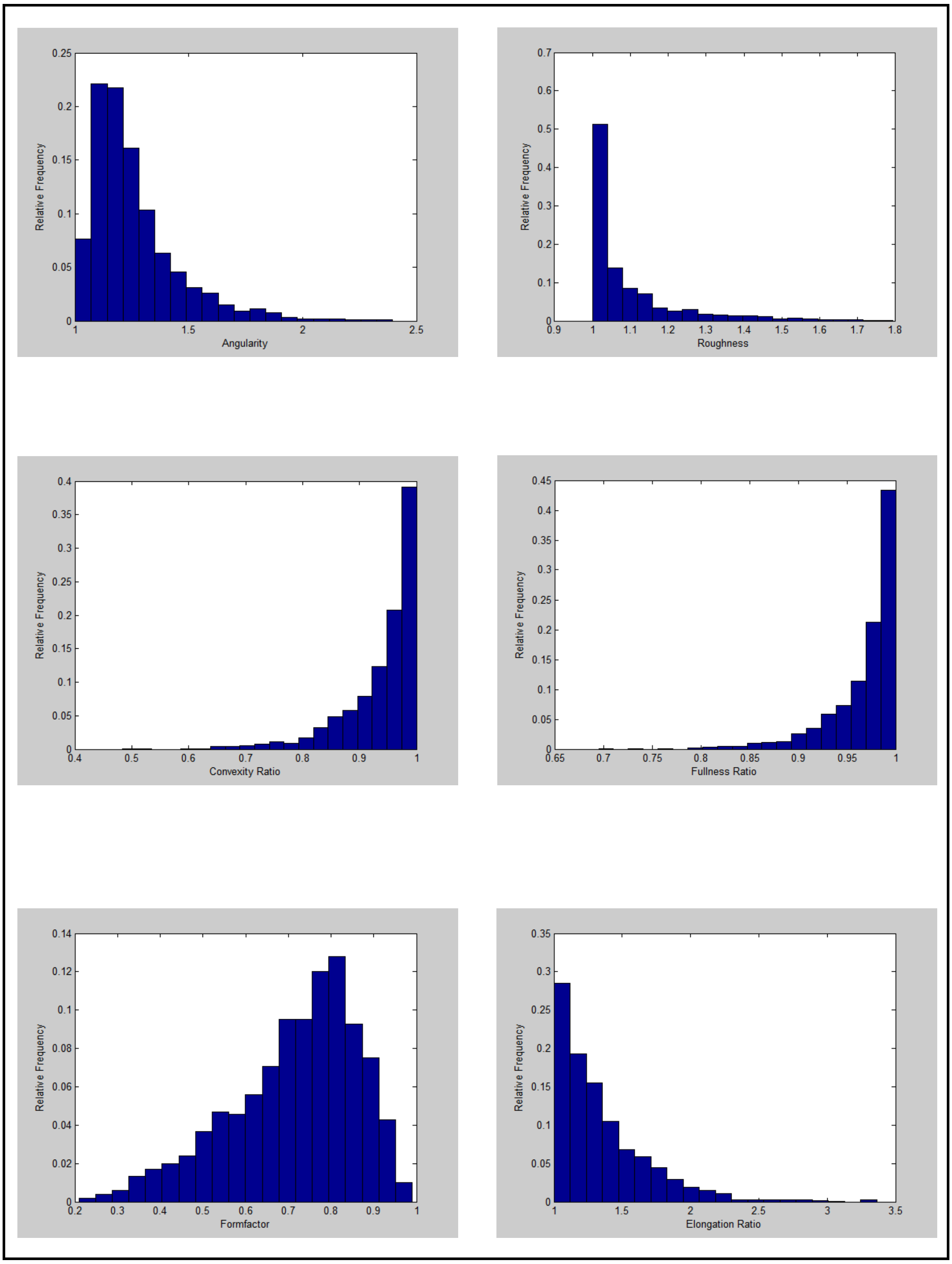

Figure E.6 Relative frequency histograms of parameters for specimen NW13-4.

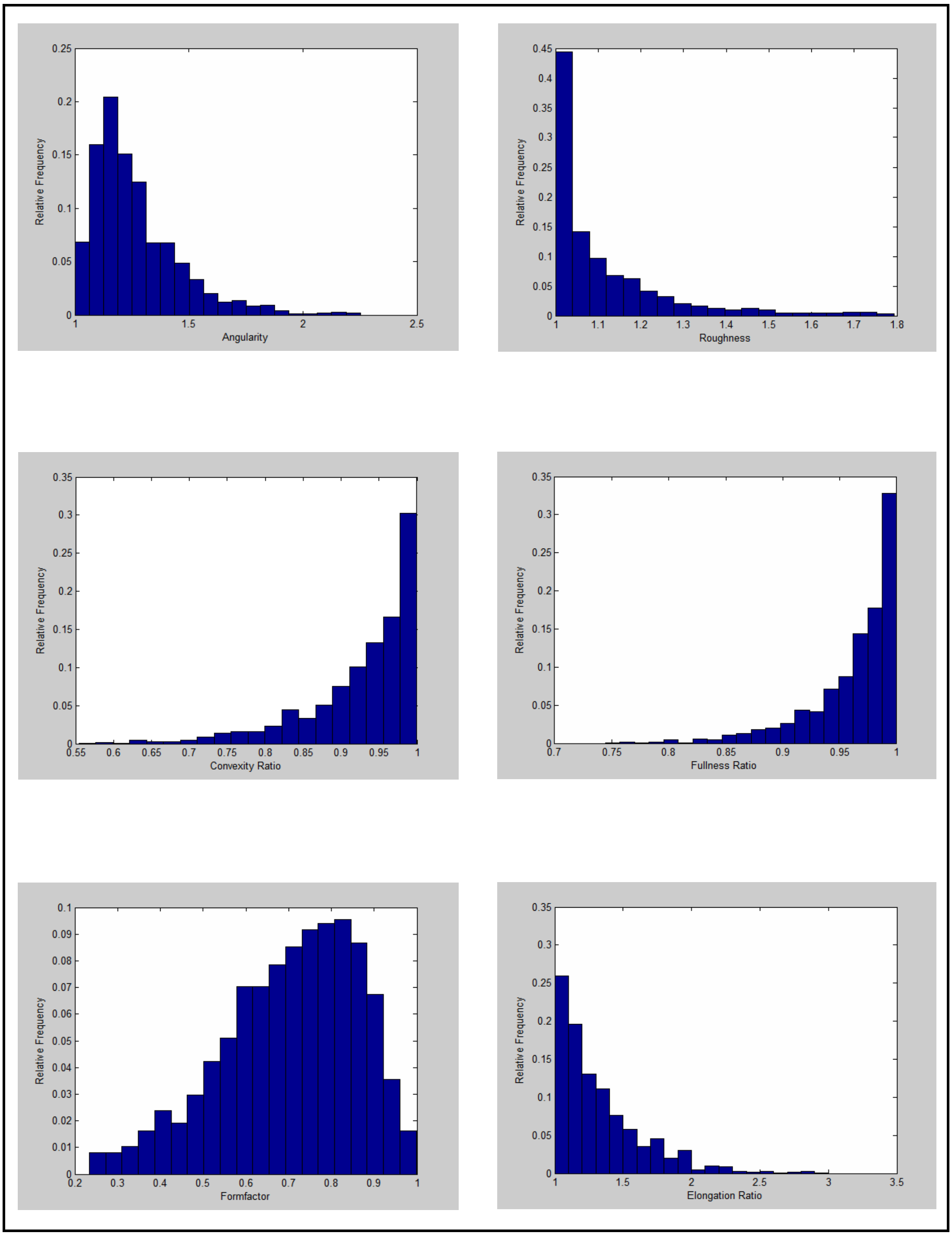

Figure E.7 Relative frequency histograms of parameters for specimen NG25-5.

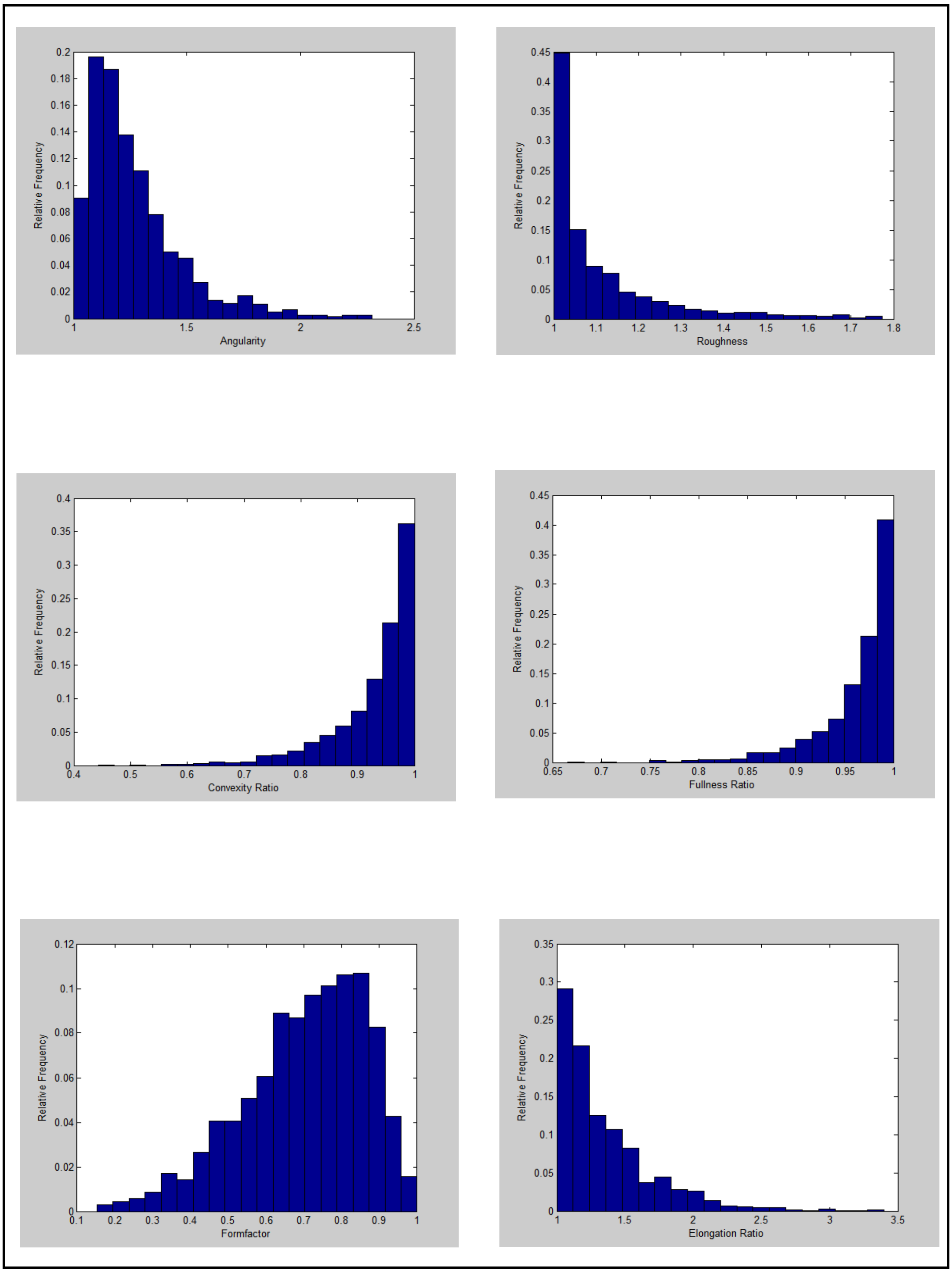

Figure E.8 Relative frequency histograms of parameters for specimen NW25-2.

APPENDIX F

MATLAB ALGORITHM FOR THE SELECTION OF REPRESENTATIVE PARTICLE SHAPE PARAMETERS

```
% This algorithm determines the representative particle shape parameters for specimens
% according to following methods:

% - The method based on parameter maximum relative frequency %
% - The method based on parameter value corresponding to maximum relative frequency %
% - The method based on weighed particle area %

% This algorithm uses the output .txt file of the algorithm given in Appendix D. %

clear all
clc

Relative_Frequency=[];
Parameter_Value=[];
Area_Weighed;

   % eliminated_parameters(:,1)=Area %
   % eliminated_parameters(:,2)=Perimeter %
   % eliminated_parameters(:,3)=Convex Hull Area %
   % eliminated_parameters(:,4)=Convex Hull Perimeter %
   % eliminated_parameters(:,5)=Maximum feret Diameter %
   % eliminated_parameters(:,6)=Maximum Feret Diameter Orientation %
   % eliminated_parameters(:,7)=Center of Mass X %
   % eliminated_parameters(:,8)=Center of Mass Y %
   % eliminated_parameters(:,9)=Elongation Ratio %
   % eliminated_parameters(:,10)=Angularity %
   % eliminated_parameters(:,11)=Roughness %
   % eliminated_parameters(:,12)=Convexity Ratio %
   % eliminated_parameters(:,13)=Fullness Ratio %
   % eliminated_parameters(:,14)=Formfactor %

for specimen=1:40
    parameters=load(sprintf('eliminated_parameters%3d.txt',specimen));


   %Parameters to be used in analysis%
   analysis_parameters = [eliminated_parameters(:,9:14)];

   % Determination of the representative particle shape parameters for the method based
   % on parameter maximum relative frequency and  the method based on parameter value
   % corresponding to maximum relative frequency.
   [selected_maximum_relative_frequency  selected_parameter_value]= ...
                        representative_parameter_selection(specimen, analysis_parameters);

   Relative_Frequency=[specimen, selected_maximum_relative_frequency];
   Parameter_Value=[specimen, selected_parameter_value];
```

```
    % Determination of the representative particle shape parameters for the method based
    % on weighed particle area.
    area_method_parameters=[eliminated_parameters(:,1), eliminated_parameters(:,9:14)];


    [selected_area_weighed_parameters]=weighed_area(area_method_parameters);
    Area_Weighed=[Area_Weighed; area_weighed_parameters]
end

save Relative_Frequency.txt    'Relative_Frequency'    '-ascii'
save Parameter_Value.txt       'Parameter_Value'       '-ascii'
save Area_Weighed.txt  'Area_Weighed'  '-ascii'

%%%%%%%%%%%%%%%%%%%%%%%%%%%%%%%%%%%%%%%%%%%%%

% representative_parameter_selection function determines the representative particle
% shape parameters for the method based on parameter maximum relative frequency and
% the method based on parameter value corresponding to maximum relative frequency.

function
[selected_maximum_relative_frequency  selected_parameter_value]=...
                    representative_parameter_selection(specimen, analysis_parameters);

selected_maximum_relative_frequency=[];
selected_parameter_value=[];
number_of_class_intervals=20;

% Determination of the representative parameters particle shape parameters. %
% analysis_parameters(:,1)=Elongation Ratio %
% analysis_parameters(:,2)=Angularity %
% analysis_parameters(:,3)=Roughness %
% analysis_parameters(:,4)=Convexity Ratio %
% analysis_parameters(:,4)=Fullness Ratio %
% analysis_parameters(:,6)=Formfactor %

for i=1:6
     considered_parameter= analysis_parameters (:,i);

    % Relative frequency histogram of the considered parameter. %
     [number_of_relative_parameters_per_interval  position_of_class_interval_center]=...
                              rhist(considered_parameter, number_of_class_intervals,i);

    % Determination of the particle shape parameter value according to method based on
    % parameter maximum relative frequency.
    max_relative_frequency=max(number_of_relative_parameters_per_interval);

    % Determination of the particle shape parameter value according to method based on
    % parameter value corresponding to maximum relative frequency.
    position=find(number_of_relative_parameters_per_interval==...
                              max(number_of_relative_parameters_per_interval));

    parameter_value= position_of_class_interval_center(position(1));

    selected_maximum_relative_frequency=[selected_maximum_relative_frequency...
                              max_relative_frequency];
```

```
    selected_parameter_value=[selected_parameter_value  parameter_value];

end
return

%%%%%%%%%%%%%%%%%%%%%%%%%%%%%%%%%%%%%%%%%%%%%


% rhist function generates the relative frequency distributions of the considered parameters.



function [number_of_relative_parameters_per_interval  position_of_class_interval_center]...
                                                = rhist(considered_parameter, number_of_class_intervals,i)

[m,n] = size(considered_parameter);

% Frequency %
[nn,x]=hist(considered_parameter, number_of_class_intervals); % frequency
% Relative frequency %
nn = nn./m;

% Relative frequency histogram %
bar(x,nn,[min(considered_parameter (:)) max(considered_parameter (:))],'hist');
ylabel('Relative Frequency')

if      i==1;
         xlabel('Elongation Ratio');
elseif i==2;
          xlabel('Angularity');
elseif i==3;
         xlabel('Roughness');
elseif i==4;
         xlabel('Convexity Ratio');
elseif i==5;
         xlabel('Fullness Ratio');
else  i==6;
         xlabel('Formfactor');
end

number_of_relative_parameters_per_interval=nn;
position_of_class_interval_center=x;
return

%%%%%%%%%%%%%%%%%%%%%%%%%%%%%%%%%%%%%%%%%%%%%


% weighed_area function determines the representative particle shape parameters for the
% method based on weighed particle area.


function [selected_area_weighed_parameters]=weighed_area(area_method_parameters);

selected_area_weighed_parameters=[];

[number_of_particles  number_of_parameters]=size(area_method_parameters);
```

```
for i=2: number_of_parameters
    area_weighed_parameter_value=sum(times(area_method_parameters (:,1),...
                                             area_method_parameters (:,i)))...
                                             /sum(area_method_parameters (:,1));
   selected_area_weighed_parameters=[selected_area_weighed_parameters ...
                                        area_weighed_parameter_value];
    end
    return

%%%%%%%%%%%%%%%%%%%%%%%%%%%%%%%%%%%%%%%%%%%%%
```